



**HAL**  
open science

# Non-invasive personalisation of cardiac electrophysiological models from surface electrograms

Sophie Giffard-Roisin

► **To cite this version:**

Sophie Giffard-Roisin. Non-invasive personalisation of cardiac electrophysiological models from surface electrograms. Other. COMUE Université Côte d'Azur (2015 - 2019), 2017. English. NNT : 2017AZUR4092 . tel-01771476v2

**HAL Id: tel-01771476**

**<https://inria.hal.science/tel-01771476v2>**

Submitted on 7 Dec 2017

**HAL** is a multi-disciplinary open access archive for the deposit and dissemination of scientific research documents, whether they are published or not. The documents may come from teaching and research institutions in France or abroad, or from public or private research centers.

L'archive ouverte pluridisciplinaire **HAL**, est destinée au dépôt et à la diffusion de documents scientifiques de niveau recherche, publiés ou non, émanant des établissements d'enseignement et de recherche français ou étrangers, des laboratoires publics ou privés.

UNIVERSITE COTE D'AZUR  
DOCTORAL SCHOOL STIC  
SCIENCES ET TECHNOLOGIES DE L'INFORMATION  
ET DE LA COMMUNICATION

# PHD THESIS

to obtain the title of

**PhD of Science**

**Specialty : Automatic, Signal and Image Processing**

Defended by

Sophie GIFFARD-ROISIN

## Non-invasive Personalisation of Cardiac Electrophysiological Models from Surface Electrograms

Thesis Advisors:

Maxime SERMESANT, Nicholas AYACHE, Hervé DELINGETTE

prepared at Inria Sophia Antipolis, ASCLEPIOS Team

Defended on 11 December 2017

**Jury :**

<i>President :</i>	Reza RAZAVI	-	KCL (London)
<i>Reviewers :</i>	Rémi DUBOIS	-	IHU LIRYC (Bordeaux)
	Olaf DOESSEL	-	KIT (Karlsruhe)
<i>Advisor :</i>	Nicholas AYACHE	-	Inria (Sophia-Antipolis)
<i>Co-advisor :</i>	Hervé DELINGETTE	-	Inria (Sophia-Antipolis)
<i>Co-supervisor :</i>	Maxime SERMESANT	-	Inria (Sophia-Antipolis)



---

## Non-invasive Personalisation of Cardiac Electrophysiological Models from Surface Electrograms

### Abstract:

The objective of this thesis is to use non-invasive data (body surface potential mapping, BSPM) to personalise the main parameters of a cardiac electrophysiological (EP) model for predicting the response to cardiac resynchronization therapy (CRT). CRT is a clinically proven treatment option for some heart failures. However, these therapies are ineffective in 30% of the treated patients and involve significant morbidity and substantial cost. The precise understanding of the patient-specific cardiac function can help to predict the response to therapy. Until now, such methods required to measure intra-cardiac electrical potentials through an invasive endovascular procedure which can be at risk for the patient.

We developed a non-invasive EP model personalisation based on a patient-specific simulated database and machine learning regressions. First, we estimated the onset activation location and a global conduction parameter. We extended this approach to multiple onsets and to ischemic patients by means of a sparse Bayesian regression. Moreover, we developed a reference ventricle-torso anatomy in order to perform a common offline regression and we predicted the response to different pacing conditions from the personalised model. In a second part, we studied the adaptation of the proposed method to the input of 12-lead electrocardiograms (ECG) and the integration in an electro-mechanical model for a clinical use. The evaluation of our work was performed on an important dataset (more than 25 patients and 150 cardiac cycles). Besides having comparable results with state-of-the-art ECG imaging methods, the predicted BSPMs show good correlation coefficients with the real BSPMs.

**Keywords:** ECG Imaging, Personalisation, Cardiac Electrophysiology Model, Machine learning, Simulated database, Inverse problem.

---

## Remerciements

Je tiens tout d'abord à remercier chaleureusement Maxime Sermesant, Nicholas Aycha et Hervé Delingette pour m'avoir encadrée tout au long de cette aventure. Trois superviseurs complémentaires qui m'ont permis de garder une vision d'ensemble de la thèse (merci Nicholas!), de me questionner pour m'améliorer (merci Hervé!) et surtout de me motiver et de proposer sans cesse des idées nouvelles (merci Maxime!).

Je tiens à remercier les membres de mon jury de thèse, et particulièrement mes rapporteurs Rémi Dubois et Olaf Doessel qui ont eu la gentillesse de prendre le temps de lire ce manuscrit.

Je remercie bien sûr toute l'équipe du projet européen VP2HF avec qui j'ai eu le plaisir de travailler tout au long de la thèse, lors de réunions toujours conviviales aux quatre coins du continent. J'ai ainsi pu collaborer directement avec le monde médical, améliorer ma compréhension téléphonique de l'anglais 'british', et surtout découvrir le 'shuffleboard' des pubs norvégiens, espèce de curling de table sur sable. Je remercie Reza Razavi, grand coordinateur du projet, mais aussi Tom Jackson et Jessica Webb, les cardiologues les plus disponibles de tous les temps et à qui je dois tout. Je ne remercierai jamais assez l'équipe de modélisation cardiaque de King's College (Jack Lee, Simone Rivolo et surtout Lauren Fovargue) avec qui nous avons travaillé pendant plusieurs années à cette étude prospective clinique, dans un esprit toujours agréable malgré les délais parfois très courts!

Ensuite, un grand merci à cette équipe Asclepios (ou devrais-je dire Epione maintenant!) qui, comme le disait justement un ancien -Loïc pour ne pas le nommer- "les doctorants changent, mais l'esprit de colonie de vacances reste"! Tout d'abord, merci aux anciens de la "vieille génération" de m'avoir tout appris: l'installation de Sofa, la course à pied, l'utilisation du cluster, les conférences, auron... Je remercie aussi fortement ceux de ma génération et des suivantes pour tous ces moments de détente passés à jouer au ping-pong, au beach volley, à randonner ou à skier. J'ai une pensée particulière pour mes co-bureaux Rocio et Nicolas. Merci Rocio de m'avoir si bien accueillie lorsque je n'étais qu'une petite stagiaire, et surtout merci d'être restée si longtemps! Enfin, je n'oublie pas Isabelle pour son travail sans failles mais aussi pour sa bonne humeur au déjeuner!

Je voudrais bien sûr remercier ces amis devenus des frères et des sœurs avec qui j'ai partagé ma vie à la villa Ondine et qui ont su me faire sentir si bien à Antibes. Si bien que je ne pourrais faire autrement que d'y revenir de temps en temps!

Enfin, merci aux Giffard, aux Roisin et surtout aux Giffard-Roisin pour les déménagements, les réparations de vélo et le soutien moral. Un énorme merci à Vincent qui est arrivé dans ma vie au début de cette thèse et qui a réussi à la rendre si agréable et ambitieuse à la fois.

# Contents

<b>1</b>	<b>Context and State-of-the-Art</b>	<b>1</b>
1.1	Introduction . . . . .	1
1.1.1	Motivation . . . . .	1
1.1.2	Main Contributions . . . . .	2
1.1.3	Manuscript Organization . . . . .	3
1.2	Clinical context . . . . .	6
1.2.1	Generalities on the Heart . . . . .	6
1.2.2	Heart Failure and Cardiac Resynchronization Therapy . . . . .	8
1.2.3	Cardiac Electrical Measures . . . . .	10
1.3	State-of-the-art . . . . .	13
1.3.1	Electrophysiological Cardiac Modelling . . . . .	13
1.3.2	ECG Imaging and Inverse Problem . . . . .	15
1.3.3	Cardiac EP Personalisation . . . . .	17
1.3.4	Reference Ventricle-Torso Anatomy in ECGI . . . . .	17
1.3.5	Data Driven and Machine Learning for Cardiac EP Personalisation . . . . .	18
1.4	Conclusion . . . . .	22
<b>I</b>	<b>Personalisation of a Cardiac Model from Body Surface Potential Mapping (BSPM)</b>	<b>23</b>
<b>2</b>	<b>Activation Onset Location and Global Conductivity Estimation from BSPM</b>	<b>25</b>
2.1	Introduction . . . . .	26
2.1.1	Cardiac EP Model Personalisation . . . . .	26
2.1.2	The Forward Problem of Electrocardiography . . . . .	27
2.1.3	The Inverse Problem of Electrocardiography . . . . .	27
2.1.4	Proposed Approach . . . . .	28
2.1.5	Outline of the Chapter . . . . .	29
2.2	Materials and Methods . . . . .	29
2.2.1	Clinical Data . . . . .	29
2.2.2	Simulating BSPM data: EP Forward Model . . . . .	30
2.2.3	Personalising a Cardiac EP Model from BSPM . . . . .	32
2.3	Personalisation Experiments and Results . . . . .	36
2.3.1	Evaluation on PVC Benchmark Clinical Dataset . . . . .	36
2.3.2	Evaluation on Five Implanted CRT Patients . . . . .	37
2.3.3	Prediction of Stimulation Results from Personalised Model . . . . .	43
2.4	Discussion . . . . .	43
2.4.1	Quantifying the Impact of a Precise Myocardial Geometry . . . . .	43

2.4.2	Modelling Scar Tissue: Its Impact on our Personalisation . . .	45
2.4.3	Future Works . . . . .	45
2.5	Conclusion . . . . .	46
<b>3</b>	<b>Sparse Bayesian Non-linear Regression for Multiple Onsets Estimation in Non-invasive Cardiac Electrophysiology</b>	<b>47</b>
3.1	Introduction . . . . .	48
3.2	Materials and Methods . . . . .	49
3.2.1	Clinical Data . . . . .	49
3.2.2	Non-invasive Personalisation of a Cardiac EP Model . . . . .	49
3.2.3	Dimensionality Reduction of the Myocardial Shape . . . . .	49
3.2.4	Parameter Estimation using Relevance Vector Regression . . .	51
3.3	Application to the Personalisation of a Simultaneous Biventricular Pacing . . . . .	51
3.3.1	Simultaneous Biventricular Pacing Personalisation . . . . .	51
3.3.2	Results . . . . .	53
3.3.3	Evaluation on 3 Other Patients . . . . .	55
3.4	Discussion . . . . .	55
3.5	Conclusion . . . . .	56
<b>4</b>	<b>Learning Relevant ECGI Simulations on a Reference Anatomy for Personalised Predictions of CRT</b>	<b>57</b>
4.1	Introduction . . . . .	58
4.1.1	EP Model-based Inverse Problem of Electrocardiography . . .	58
4.1.2	Reference Anatomy in ECGI . . . . .	59
4.1.3	Contributions . . . . .	59
4.1.4	Outline of the Chapter . . . . .	60
4.2	Materials and Methods . . . . .	60
4.2.1	Clinical Data . . . . .	60
4.2.2	BSPM Reference Anatomy . . . . .	62
4.2.3	Offline Simulated Common Database . . . . .	63
4.2.4	Relevance Vector Regression for SR Sequence Personalisation	65
4.3	Personalisation Results and Pacing Predictions . . . . .	69
4.3.1	Projections on the Reduced Shape Space . . . . .	69
4.3.2	Estimated Sinus Rhythm Activation Maps . . . . .	69
4.3.3	Pacing Predictions Results . . . . .	71
4.4	Discussion . . . . .	74
4.4.1	Reference Anatomy . . . . .	74
4.4.2	Estimating conduction velocity from activation times . . . . .	75
4.4.3	Estimating the uncertainty . . . . .	75
4.4.4	AV node Activation . . . . .	76
4.5	Conclusion . . . . .	76

<b>II</b>	<b>Applications and Translation to Clinics</b>	<b>77</b>
<b>5</b>	<b>From BSPM to 12-lead ECG : Personalisation Using Routinely Available Data</b>	<b>79</b>
5.1	Introduction . . . . .	80
5.2	Estimation of Purkinje Activation from 12-lead ECG . . . . .	80
5.2.1	Purkinje System and General Context . . . . .	80
5.2.2	Materials and Methods . . . . .	81
5.2.3	Intermittent Left Bundle Branch Block Study . . . . .	83
5.2.4	Cardiac Resynchronization Therapy Study . . . . .	85
5.2.5	Electrode Location Perturbation . . . . .	86
5.2.6	Conclusion of the Purkinje Estimation . . . . .	86
5.3	Activation Onset Localisation from 12-lead ECG . . . . .	88
5.3.1	Clinical Data . . . . .	88
5.3.2	Results on Activation Onset Localisation . . . . .	88
5.3.3	Conclusion of the Activation Onset Localisation . . . . .	88
5.4	Conclusion . . . . .	89
<b>6</b>	<b>Personalisation in a CRT Clinical Prospective Study</b>	<b>91</b>
6.1	Introduction . . . . .	92
6.2	VP2HF Project . . . . .	92
6.2.1	Motivation . . . . .	92
6.2.2	Goals . . . . .	92
6.2.3	European Partners Involved . . . . .	92
6.3	CRT Clinical Prospective Study and Modelling Pipeline . . . . .	93
6.3.1	CRT Clinical Prospective . . . . .	93
6.3.2	Modelling Pipeline . . . . .	93
6.4	Electrophysiological Personalisation as part of a Modelling Pipeline . . . . .	94
6.5	First Results and Patients Modelling Reports . . . . .	96
6.6	Discussion . . . . .	97
6.7	Conclusion . . . . .	97
<b>7</b>	<b>Pre-clinical Electro-mechanical Model Personalisation on Canine Data</b>	<b>103</b>
7.1	Introduction . . . . .	104
7.2	Models and Methods . . . . .	104
7.2.1	Geometry Processing . . . . .	105
7.2.2	Electro-Mechanical Modelling: SOFA Software . . . . .	106
7.3	Parameter Estimation . . . . .	107
7.3.1	Sensitivity Study . . . . .	107
7.3.2	Mechanical Parameters Calibration: Unscented Transform Algorithm . . . . .	108
7.4	Results . . . . .	108
7.4.1	Clinical Data . . . . .	108

---

7.4.2	Current Results . . . . .	109
7.4.3	Discussion and Improvements . . . . .	109
7.5	Conclusion . . . . .	111
<b>8</b>	<b>Conclusion</b>	<b>113</b>
8.1	Contributions Summary . . . . .	113
8.2	Publications and Awards . . . . .	114
8.2.1	Publications . . . . .	114
8.2.2	Awards . . . . .	116
8.3	Perspectives . . . . .	116
8.3.1	Clinical Perspectives . . . . .	116
8.3.2	Methodological Perspectives . . . . .	117
<b>A</b>	<b>Electro-Mechanical Personalisation for Image Simulations</b>	<b>121</b>
A.1	A Pipeline for the Generation of Realistic 3D Synthetic Echocardiographic Sequences: Methodology and Open-Access Database . . . . .	122
A.2	Generation of Ultra-realistic Synthetic Echocardiographic Sequences To Facilitate Standardization Of Deformation Imaging . . . . .	123
A.3	A Framework for the Generation of Realistic Synthetic Cardiac US and MRI Sequences from the same Virtual Patients . . . . .	124
<b>B</b>	<b>Applications of the Mitchell-Schaeffer Electrical Cardiac Model</b>	<b>127</b>
B.1	Smoothed Particle Hydrodynamics for Electrocardiography Modeling: an Alternative to Finite Element Methods . . . . .	128
B.2	A Rule-Based Method to Model Myocardial Fiber Orientation for Simulating Ventricular Outflow Tract Arrhythmias . . . . .	129
	<b>Bibliography</b>	<b>131</b>

# Context and State-of-the-Art

---

## Contents

---

<b>1.1 Introduction</b>	<b>1</b>
1.1.1 Motivation	1
1.1.2 Main Contributions	2
1.1.3 Manuscript Organization	3
<b>1.2 Clinical context</b>	<b>6</b>
1.2.1 Generalities on the Heart	6
1.2.2 Heart Failure and Cardiac Resynchronization Therapy	8
1.2.3 Cardiac Electrical Measures	10
<b>1.3 State-of-the-art</b>	<b>13</b>
1.3.1 Electrophysiological Cardiac Modelling	13
1.3.2 ECG Imaging and Inverse Problem	15
1.3.3 Cardiac EP Personalisation	17
1.3.4 Reference Ventricle-Torso Anatomy in ECGI	17
1.3.5 Data Driven and Machine Learning for Cardiac EP Personalisation	18
<b>1.4 Conclusion</b>	<b>22</b>

---

## 1.1 Introduction

### 1.1.1 Motivation

Heart Failure (HF) is a major health issue in Europe affecting 6 million patients and growing substantially because of the ageing population and improving survival following myocardial infarction. The poor short to medium term prognosis of these patients means that treatments such as cardiac resynchronisation therapy can have substantial impact [Sutton 2003]. However, these therapies are ineffective in 30% of the treated patients and involve significant morbidity and substantial cost.

To this end, the precise understanding of the patient-specific cardiac function can help predict the response to therapy and therefore select the potential candidates and optimise the therapy. The anatomical, mechanical and electrophysiological (EP) functions can be evaluated by clinical images and signal recordings.

We call them invasive data when the procedure lead to some health damage for example by intra-cardiac electrical measures through endovascular procedure. At a diagnostic or patient-selection stage the non-invasive data are a preferable alternative. Magnetic resonance (MR) imaging, computed tomography (CT) and echocardiography are non-invasive imaging procedures able to capture the anatomical, mechanical and physiological cardiac functions. The electrocardiogram (ECG) and the body surface potential mapping (BSPM) are meanwhile able to non-invasively capture the electrical activation from the surface of the torso.

In order to assist cardiologists, the scientific community is developing tools for automatically identifying the patient anatomy, physiology but also the electro-mechanical (EM) function. From BSPM electrical data, the ECG imaging field aims at reconstructing the local cardiac electrical patterns either on the heart surface or on the transmural cardiac muscle [Pullan 2010]. This ill-posed inverse problem is usually solved by regularized techniques for the stability of the solutions. However, it is often at the cost of a reduced accuracy and non-physiologically plausible electrical propagations.

The integration of medical data into some cardiac physiological electro-mechanical models (for such models see [Strumpf 1990, Bestel 2001, Pollard 2003]) has also lead to patient-specific modelling able to better understand the personalised cardiac function. The goal is to estimate the main model parameters in order to fit to the patient-specific data. The model personalisation is also able to provide some predictive information. [Sermesant 2012] proposed to personalize an electro-mechanical model of the heart to predict the response to CRT. The method requires to measure intra-cardiac electrical potentials through an invasive endovascular procedure.

The aim of this thesis is to provide a non-invasive approach to cardiac EP model personalisation, thus bridging the gap between ECG imaging and model personalisation.

### 1.1.2 Main Contributions

We worked on a non-invasive cardiac electrophysiological (EP) model personalisation using body surface potential mapping (BSPM) data. We also studied the model personalisation using 12-lead ECG data and its integration in an electromechanical (EM) model for a clinical use. Our developed methodologies propose an ECG imaging (ECGI) inverse approach based on model simulation and machine learning. Moreover, we provided some inter-patient comparison and an outcome prediction of therapies. The main contributions of the thesis are:

- A straightforward and efficient coupled forward BSPM model based on the cardiac Mitchell-Schaeffer model and on a current dipole formulation;

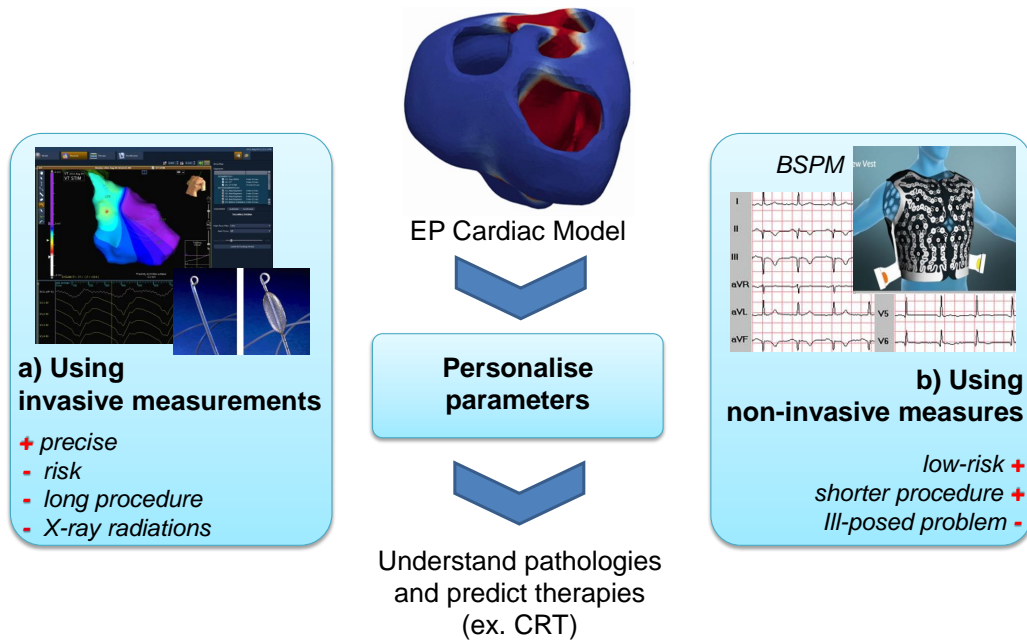


Figure 1.1: The goal of electrophysiological (EP) cardiac model personalisation is to understand pathologies and predict therapies. We aim at replacing invasive EP measures (a) by non-invasive ones (b).

- The development of a machine learning-based personalisation of the main cardiac EP parameters from BSPM acquired clinically, such as onset activation locations and heterogeneous conduction velocity, from a large simulated database.
- The development of a reference ventricle-torso anatomy able to perform a common and offline regression and to provide an interpatient analysis.
- A prediction of the patient-specific response to different pacing configurations.
- An evaluation on an important and diverse dataset (more than 25 patients and 150 heart beats), including different types of imaging data (MRI, CT scan), different types of electrical data (BSPM, 12-lead ECG, QRS duration), different pathologies (dyssynchrony, ischemy, premature ventricular complex) and different electrical stimulations (sinus rhythm, pacemakers).
- An adaptation to 12-lead ECG data and an integration of simple personalisation methods into pre-clinical and clinical electromechanical studies.

### 1.1.3 Manuscript Organization

After a survey of the clinical context of cardiac EP and of the state-of-the-art of non-invasive EP model personalisation, the manuscript is divided into two main

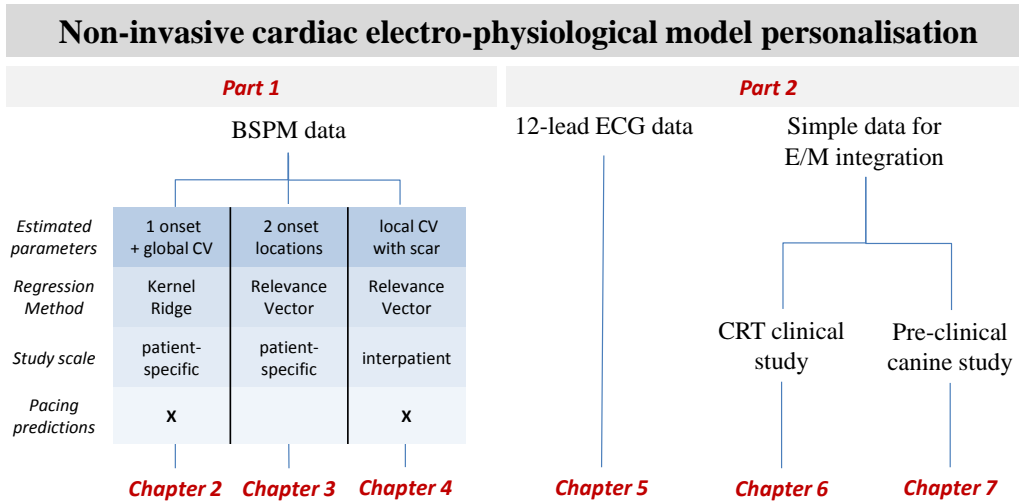


Figure 1.2: Manuscript organization of the 6 main chapters. *BSPM*: body surface potential mapping; *E/M*: electro-mechanical; *CV*: conduction velocity; *CRT*: cardiac resynchronization therapy.

parts. The former (chapters 2, 3 and 4) includes the BSPM personalisation methodology, its improvements on more complex cases and its evaluation on real data. The latter (chapters 5, 6 and 7) deals with the applications using some simplified electrical data (as the 12-lead ECG or the QRS duration) and the integration into a real-time clinical study and some EM model personalisations. Figure 1.2 summarizes the manuscript organization. Each chapter can be read independently, even if we suggest a linear reading. More specifically, the chapters are organized as followed:

Chapter 1 is a background on the cardiac anatomy and function, on the cardiac electrophysiology, its pathologies and its measures. Moreover, a state-of-the-art on EP modelling, ECGI, cardiac model personalisation and machine learning techniques is presented.

### Part I:

In Chapter 2, we develop a method for the EP personalisation from BSPM able to estimate the activation onset location and the global conductivity parameter. The current dipole formulation able to simulate the torso signals efficiently is explained and compared to a standard forward method. This chapter is based on a published TBME journal paper [Giffard-Roisin 2017b].

Chapter 3 is an extension of Chapter 2 to non-linear situations such as multiple onsets and includes uncertainty quantification. The learning method is based on a relevance vector regression and a myocardial shape dimension reduction. This chapter is based on a published FIMH conference proceedings

paper [Giffard-Roisin 2017a].

In Chapter 4, the non-linear method of Chapter 3 is used for solving the inverse problem on ischemic patients. A reference ventricle-torso geometry enables to perform an inter-patient study and to reduce the personalisation computation time. Finally, the prediction of different pacings is evaluated. This chapter is based on a journal paper in preparation.

### Part II:

In Chapter 5 we investigate how to personalise the EP cardiac model using only 12-lead ECG data. First, we propose a new framework for the evaluation of conduction parameters (linked to the fast conduction Purkinje system) from 12-lead ECG in the case of dyssynchronous patients. Secondly, an extension of Chapter 2 to 12-lead ECG is presented. This chapter is mostly based on a published STACOM workshop (held in conjunction with the MICCAI conference) proceedings paper [Giffard-Roisin 2016].

Chapter 6 is dedicated to the integration of a simpler version of EP personalisation into a non-invasive clinical prospective study, where the EM modelling helps the clinicians to select CRT candidates. This study was part of the European project VP2HF (<http://www.vp2hf.eu/>).

In Chapter 7, we evaluated an EM cardiac model by comparing the simulated ventricular motion with the true motion of hearts imaged by tagged MRI. Even if some invasive data were needed, pre-clinical studies with very accurate data are essential for building correct methods. As part of an EM challenge, this chapter is based on a published STACOM workshop (held in conjunction with the MICCAI conference) proceedings paper [Giffard-Roisin 2014].

Finally, Chapter 8 proposes a general conclusion and perspectives on clinical and methodological aspects.

### Appendices A and B:

This PhD has also led to other collaborations that are partly linked to the thesis subject. Two appendices are gathering first the applications of the EM personalisation to image simulations in Appendix A (2D and 3D echocardiography [Alessandrini 2015b, Alessandrini 2015a], MRI [Zhou 2017]) and second some applications of our electrical cardiac model in Appendix B (for a comparison to a mesh-free model [Lluch Alvarez 2017] and for a cardiac fiber orientation study [Doste 2017]).

## 1.2 Clinical context

### 1.2.1 Generalities on the Heart

#### 1.2.1.1 Anatomy

The heart is the pump providing oxygenated blood to the organs and in parallel sending de-oxygenated blood to the lungs. It is composed of four chambers; two atria and two ventricles, see Figure 1.3a. The right atrium and ventricle provide blood to the lungs while the left side, with a stronger muscle, is providing blood to the organs. The left ventricle (LV) and the right ventricle (RV) are separated by an intraventricular muscle, called septum. The inferior part of the heart is called the apex. The ventricles cavities are closed by valves separating the ventricles from the atria. Finally, the pulmonic and aortic valves allow blood to leave the ventricles via the arteries.

An entire cardiac cycle lasts approximately one second and is divided into two stages: the systole during which the ventricles are contracting, and the diastole during which the ventricles relax.

The ventricular muscular wall is called myocardium and has an inner surface (endocardium) and an outer surface (epicardium), see Figure 1.3b. The surrounding membrane is called the pericardium. The myocardium is composed of myocyte cells or muscle fibers whose direction varies across the myocardium (Figure 1.3c). The mean elevation angle (obliquity with respect to the plane of the section) varies approximately from  $-70^\circ$  in the epicardium to  $+70^\circ$  in the endocardium. This organization optimizes the contraction.

#### 1.2.1.2 Cardiac Electrical Conduction System

The cardiac contraction is driven by an electrical wave spreading through the myocardium and depolarizing each cell; first the atria and then the ventricles. The ventricular depolarization is fast (less than 100ms) and synchronous between the left and the right side. Because of the particular fiber organization of the myocardial cells, the electrical propagation is anisotropic.

The resting polarized state of a myocyte consists in a difference of approximately 90mV between the intracellular and extracellular medium. When a stimulus occurs, the transmembrane potential is modified with respect to the gradient of ionic concentrations. The concentrations of different ions (sodium, calcium and potassium) and their flow through the membrane are responsible of particular cell state changes. The evolution of the transmembrane potential called action potential is composed of 3 phases: the depolarization phase, the plateau phase and the repolarization phase (see Figure 1.4a).

The cardiac rhythm is driven by the sinoatrial node capable of spontaneously generating electrical signals. In a normal sinus rhythm, the stimulus reaches the ventricles from the atrioventricular node through the His bundle where the network splits into two branches, the left bundle and the right bundle (see Figure 1.4b). The

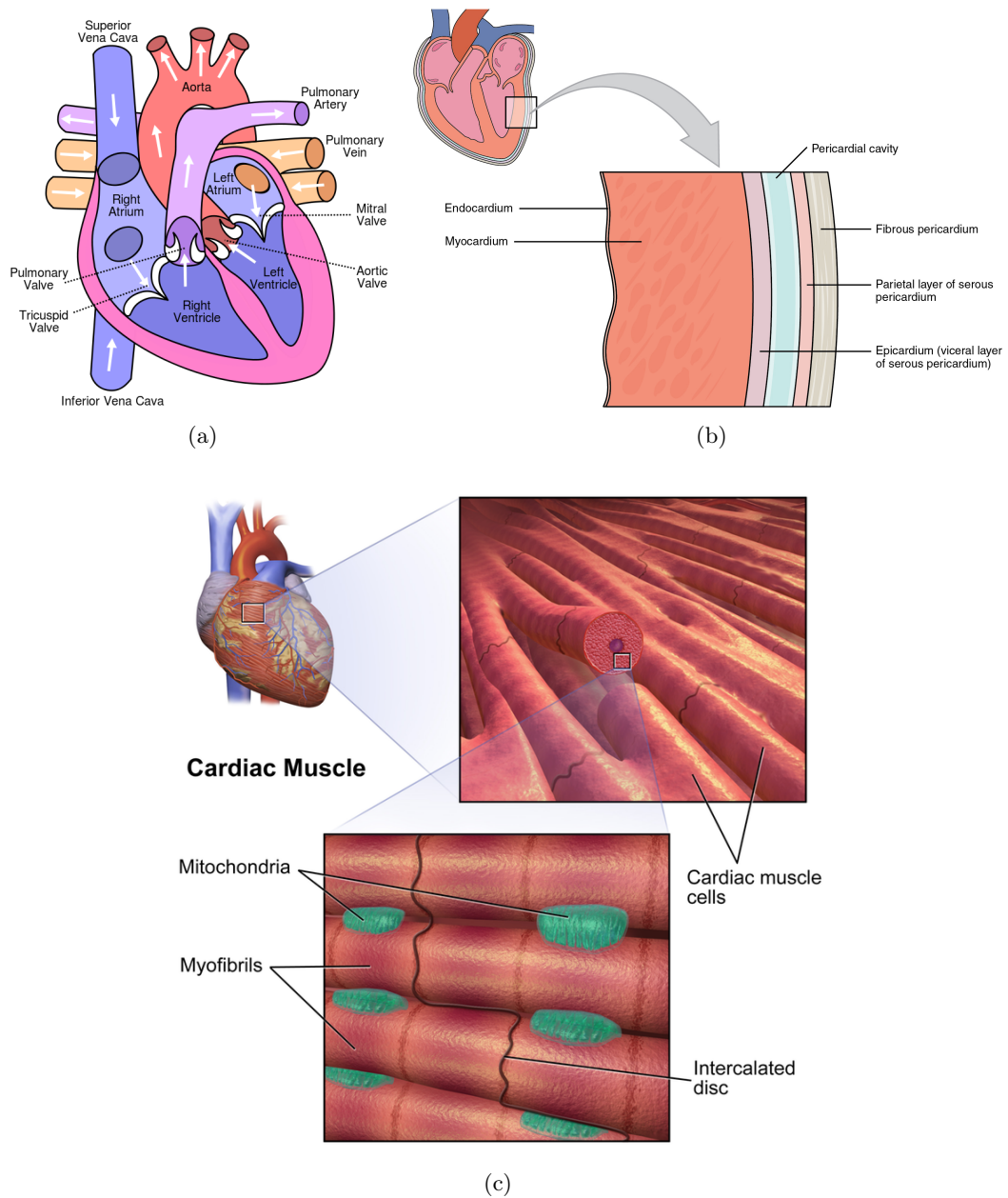


Figure 1.3: (a) The 4 chambers of the human heart (b) Membranes and layers of the heart wall (c) Cardiac cells organized in fibers. From [www.commons.wikimedia.org](http://www.commons.wikimedia.org)

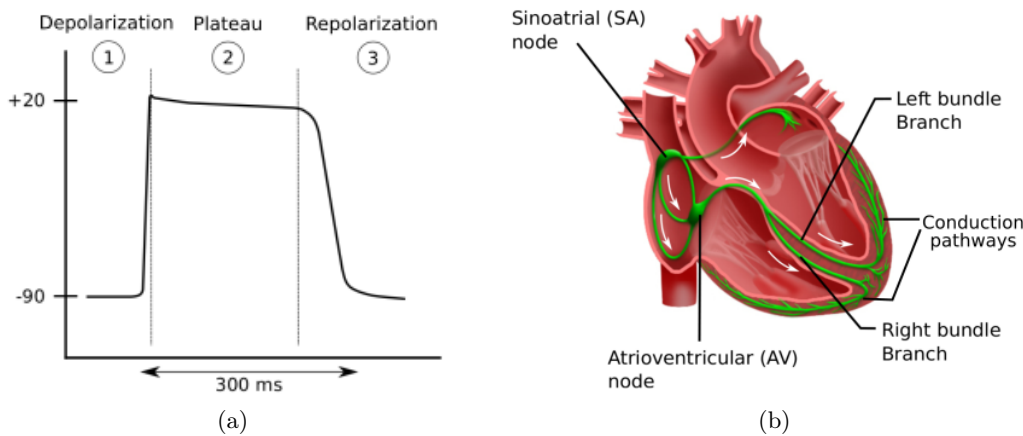


Figure 1.4: (a) Action potential response of a cardiac cell in mV (from Talbot, *Interactive Patient-specific Simulation of Cardiac Electrophysiology*, 2014). (b) Electrical conduction system of the heart (from hopkinsmedicine.org)

bundle branches are connected to a fast conduction system called Purkinje fibers, composed of specialised heart muscle cells. The Purkinje fibers are located just beneath the endocardium and are able to conduct quickly and efficiently: typical conduction velocity ranges from 2 to 3m/s while it ranges from 0.3 to 0.4m/s for myocardial cells [Durrer 1970].

## 1.2.2 Heart Failure and Cardiac Resynchronization Therapy

### 1.2.2.1 Heart Failure

Heart failure (HF) includes all pathologies leading an insufficient amount of blood being pumped for the body's needs. The two main types are the systolic HF (lack of contraction) and the diastolic HF (lack of relaxation of the ventricles). It can be brought on by many conditions, including:

- **Coronary artery disease** or ischemic heart disease occurs when the arteries that supply blood to the myocardium become hardened and narrowed.
- **Cardiomyopathy** is more generally a damage on the myocardium that can be caused by artery or blood flow problems, infections, alcohol or drug abuse.
- **Heart attack** occurs when a coronary artery is suddenly blocked, stopping the blood flow in the myocardium.
- **Overwork of the heart** includes high blood pressure, heart valve disease, diabetes or heart defects.

Coronary artery disease or other cardiomyopathies can lead to myocardial infarction, i.e. myocardial cell death. The necrotic zone called infarct or scar does not contract nor conduct anymore, leading to abnormal heart beating patterns.

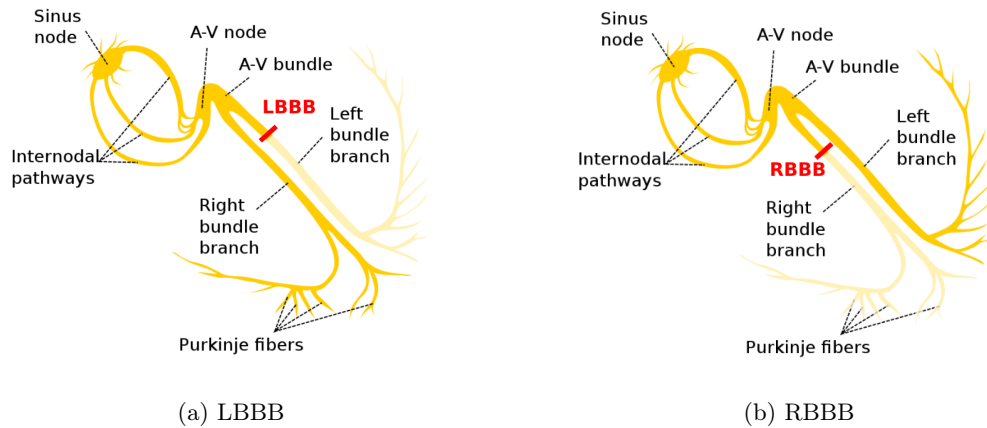


Figure 1.5: (a) Left bundle branch block (b) Right bundle branch block. A defect in a major bundle causes a dysfunction of the underlying fast conduction system.

### 1.2.2.2 Ventricular Dyssynchrony

Heart failure is also correlated to electrical conduction pathologies, such as ventricular dyssynchrony. Ventricular dyssynchrony consists in a difference of contraction timings of the ventricles. A large difference can considerably reduce the heart efficiency. We distinguish three types of ventricular dyssynchrony: the atrioventricular dyssynchrony, the interventricular dyssynchrony and the intraventricular dyssynchrony. The interventricular dyssynchrony occurs when there is a delay between the right and the left ventricular depolarizations. The intraventricular dyssynchrony results in a disordinated contraction between the left ventricular segments.

One of the main causes are dysfunctions in the conduction system, for example bundle branch blocks. Left (LBBB) and right (RBBB) bundle branch blocks are interventricular dyssynchronies caused by a defect in one of the main bundle branches (Figure 1.5). Since the electrical impulse no longer uses the fast system, it may propagate through the muscle in a slower way and with a different direction.

### 1.2.2.3 Cardiac Resynchronization Therapy

An important treatment to ventricular dyssynchrony is the cardiac resynchronization therapy (CRT). It consists in the implantation of a cardiac device that sends an electrical and periodic impulse to the myocardium in order to resynchronize the contraction. Depending on the pathology and on the device, one or more leads are placed in contact to the myocardium in different locations. A standard CRT pacemaker is composed of three leads: one in the right atrium, one in the right ventricle and one on the left ventricle (Figure 1.6). The last one is usually inserted in the coronary sinus vein and will pace from the outside (or epicardium) of the myocardium. This lead placement is often the most delicate part of the procedure. It is controlled by radiography and electrocardiogram. Delays and timings between

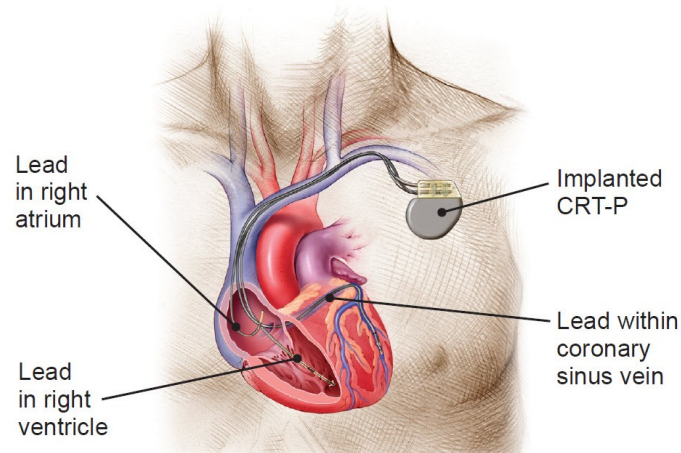


Figure 1.6: Implanted CRT-pacemaker system with three leads, from <http://www.bostonscientific.com>.

pacings can be adapted to every patient.

However, these therapies are ineffective in 30% of the treated patients and involve significant morbidity and substantial cost.

### 1.2.3 Cardiac Electrical Measures

#### 1.2.3.1 Electrocardiogram

The electrical activation is routinely non-invasively measured by the electrocardiogram (ECG) on the body surface.

The 12-lead ECG using only 9 or 10 torso electrodes is widely used because of its efficiency and reduced cost. They contain the Einthoven standard limb leads and the Goldberger and Wilson augmented leads which measure the potential differences between selected electrodes. The overall magnitude and direction of the heart's electrical depolarization is then captured at each moment of the cardiac cycle. The electrode placements follow some specific guidelines using the chest anatomy, see Figure 1.7a.

The signal recorded reflects the depolarization and repolarization phases as shown in Figure 1.7b: the atria depolarization (P wave), the ventricular depolarization (QRS complex) and the ventricular repolarization (T wave). The atria repolarization is hidden as it usually occurs during the QRS complex. By analyzing the different leads, cardiologists are able to determine a large number of cardiac pathologies. A typical marker of conduction pathology is the QRS complex duration, indicating the total ventricular depolarization time. If it is over 120ms, it suggests disruption of the heart's conduction system.

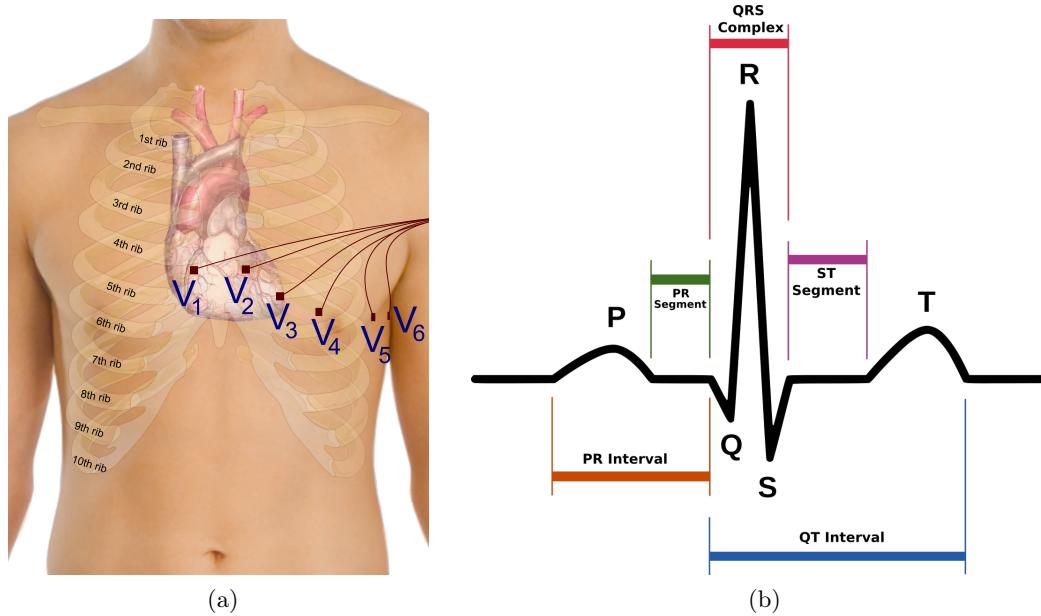


Figure 1.7: (a) Precordial electrode placement in ECG. They are complemented with an electrode on each arm and one or two electrodes on the legs. (b) Standard sinus rhythm electrocardiogram, composed of the atria depolarization (P wave), the ventricular depolarization (QRS complex) and the ventricular repolarization (T wave). From [www.commonswiki.org](http://www.commonswiki.org)

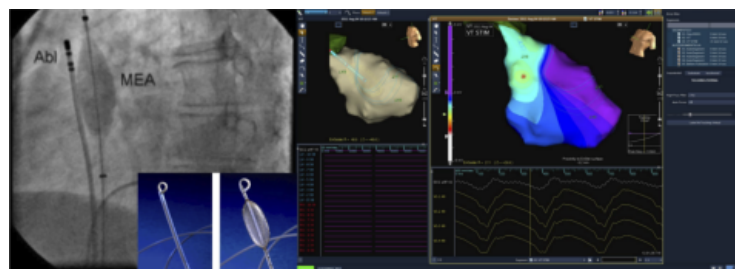


Figure 1.8: EnSite navigation system: with (left) fluoroscopic images, (middle) the deflated and inflated balloon, (right) and the electroanatomical mapping (Images from KCL, London)



Figure 1.9: CardioInsight device for body surface potential mapping. (ECVUE, CardioInsight Technologies Inc., Cleveland, Ohio)

### 1.2.3.2 Intra-cardiac Electrical Mapping

In order to have a better insight of the depolarization wave, an invasive procedure can provide an electrical mapping of the LV endocardial or epicardial potentials. The signals are recorded using two different mapping approaches: a contact mapping (consisting in moving a catheter along the wall to capture electrical signals) or a non-contact mapping (using a balloon floating inside the chamber and measuring remotely the surrounding electrical activity). An example using the Ensite navigation system is presented in Figure 1.8. EnSite NavX technology displays activation timing and voltage data to help the physician identify arrhythmias, to create chamber models and to guide catheter navigation. The uncertainty in the acquisition arises mainly from registration issues.

The optical mapping method consists in perfusing the heart with a fluid containing voltage-sensitive dye. The change in transmembrane potential is recorded by fluorescence spectra. Optical mapping is very precise but is only dedicated to *ex vivo* experiments.

### 1.2.3.3 Body Surface Potential Mapping

The invasive endovascular procedure is long and can be risky for the patient. Recently, some non-invasive devices are extending the electrical mapping from body surface potentials (BSPM). BSPM uses up to 256 sensors on both sides of the torso, as the CardioInsight<sup>1</sup> jacket now commercially available (Figure 1.9). If the technology is comparable to the 12-lead ECG, the goal is to estimate endocardial, epicardial or transmural potentials of the myocardium. It has the potential to replace invasive measurements by inversely reconstructing the cardiac potentials. A state-of-the-art on the inverse problem of ECG imaging is proposed on section 1.3.2.

<sup>1</sup>ECVUE, CardioInsight Technologies Inc., Cleveland, Ohio

## 1.3 State-of-the-art

### 1.3.1 Electrophysiological Cardiac Modelling

#### 1.3.1.1 Categories of Electrophysiological Models

The electrophysiology (EP) of the heart (see section 1.2.1.2) can be modelled in order to reproduce its behaviour, to understand the mechanisms and pathologies or to predict the response to treatments. There are several types of EP models describing the action potential:

- biophysical models [Ten Tusscher 2004]: These complex models includes the different ionic concentrations at the cellular scale. They are able to reproduce and simulate very precisely the cardiac cell behavior, but can be computationally demanding.
- Eikonal models developed by [Keener 1991]: they are simplistic models corresponding to non-linear partial differential equations of the activation time. Their efficiency has been proven, however these models cannot accurately account for complex physiological states.
- phenomenological models as [Aliev 1996, FitzHugh 1961, Mitchell 2003]: they have an intermediate complexity and are derived from the biophysical models. They involve less parameters but still capture the action potential shape and its propagation at the organ scale.

Cardiac EP models can be classified as bidomain or monodomain depending on the considered electrical potentials.

#### 1.3.1.2 Mitchell-Schaeffer Model

The Mitchell-Schaeffer model [Mitchell 2003] is a phenomenological model with 2 variables and 6 parameters. A bi-domain and a monodomain version have both been developed. In our work, we used a monodomain version of the Mitchell-Schaeffer model as implemented in [Talbot 2013].

The Mitchell-Schaeffer model has two variables, the transmembrane potential  $v$  and  $z$  a secondary variable controlling the repolarization phase. Their evolution is governed by:

$$\begin{cases} \partial_t v = \operatorname{div}(D\nabla v) + \frac{zv^2(1-v)}{\tau_{in}} - \frac{v}{\tau_{out}} + J_{stim} \\ \partial_t z = \begin{cases} \frac{1-z}{\tau_{open}} & \text{if } v < v_{gate} \\ \frac{-z}{\tau_{close}} & \text{if } v > v_{gate} \end{cases} \end{cases} \quad (1.1)$$

The parameters  $\tau_{open}$  and  $\tau_{close}$  define the gate opening and closing depending on the change-over voltage  $v_{gate}$ , and the parameters  $\tau_{in}$  and  $\tau_{out}$  control the depolarisation upstroke and repolarization downstroke.  $J_{stim}(t)$  is the stimulation current applied

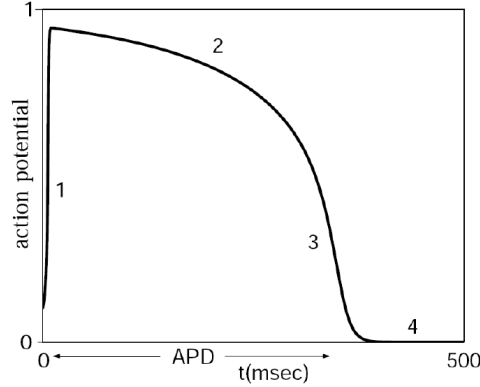


Figure 1.10: Transmembrane potential as described in [Mitchell 2003] with the following phases: (1) depolarization (2) plateau phase (3) repolarisation (4) rest potential.

in the pacing area. The diffusion term is defined by a 3x3 anisotropic diffusion tensor:

$$D = d \cdot \text{diag}(1, r, r) \quad (1.2)$$

where  $d$  is the tissue electrical diffusivity. The anisotropy ratio  $r$  enables conduction velocity in the fibre direction to be larger than in the transverse plane (typically  $r = (1/2.5)^2$ ).

The diffusivity  $d$  (in  $m^2s^{-1}$ ) can be expressed as a conductivity  $\sigma$  (in  $S/m$ ) from:

$$\sigma = C_m \beta d \quad (1.3)$$

with  $C_m$  the membrane capacitance and  $\beta$  the surface-to-volume ratio. The local conductivity  $\sigma$  can be written in terms of intracellular and extracellular conductivities:

$$\sigma = \frac{\sigma^i \sigma^e}{\sigma^i + \sigma^e} \quad (1.4)$$

The reduction of the monodomain model implies  $\sigma^i = \lambda \sigma^e$  for some scalar  $\lambda$  resulting in a linear relationship between  $\sigma$  and  $\sigma^i$ . Finally, the diffusion  $d$  is linked to the conduction velocity  $c$  in  $m/s$  by  $c = k\sqrt{d}$ .

From an onset activation location, the evolution of the transmembrane potential is computed at each node of a tetrahedral mesh of the myocardium using the finite element method. In Figure 1.10 is represented the transmembrane potential as described in [Mitchell 2003], where we can see a good agreement with the action potential of a cardiac cell as in Figure 1.4a.

### 1.3.1.3 Cardiac Electro-mechanical Modelling

The electrical depolarisation wave activates the mechanical contraction at a microscopic scale, while the repolarization drives the relaxation. That is why the cardiac

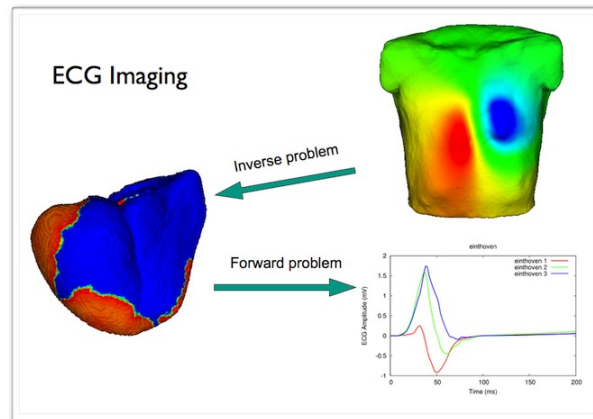


Figure 1.11: Inverse and forward problems in ECG imaging, From *Danila Potyagaylo*, <https://www.ibt.kit.edu/english/1026.php>

EP model is often inserted in a 3D electro-mechanical (EM) model, either as a pre-processing step or as coupled mechanisms. This way, it is possible to evaluate the resulting cardiac motion and the volume of ejected blood. The mechanical models are mainly dependent on the contraction and stiffness parameters of the myocardium tissue. In 2006, the electrical model from [FitzHugh 1961] was coupled with a simple constitutive contraction law in [Sermesant 2006]. In [Talbot 2013], the Mitchell-Schaeffer model is a pre-processing step to the Bestel-Clement-Sorine (BCS) mechanical modelling [Chapelle 2012]. The latter ensures to take into account the microscopic scale phenomena of the contraction as well as laws of thermodynamics. In [Sermesant 2012, Marchesseau 2013], the Eikonal EP model was also weakly coupled to the same BCS model. A strong EM coupling, where the EP propagation at time  $t$  depends on the current contracted shape, was experimented in [Giffard-Roisin 2014] with Eikonal and BCS models.

## 1.3.2 ECG Imaging and Inverse Problem

### 1.3.2.1 Forward Problem of Cardiac Electrocardiography

The estimation of the ECG data from the cardiac potentials is usually called the *forward* problem of electrocardiography (in opposition to the *inverse* problem, see Figure 1.11). The two classical numerical approaches are based either on the Boundary Element Method (BEM) or the Finite Element Method (FEM). They both propagate the epicardial heart action potentials to the surface of the body by taking into account the distance, the null current across the body surface, and the different properties of the tissues in between.

Forward models differ also by their incorporation of heterogeneous conductivity regions associated with various organs within the torso. By taking into account the physical properties of the different tissues, the computed ECG account for more

complex current pathways. In [Keller 2010], Keller et al. demonstrate the importance of the torso inhomogeneity by ranking the influence of the different tissue conductivities on forward-calculated ECGs. Ramanathan et al. [Ramanathan 2001] showed, however, that at a first order approximation the torso inhomogeneities are not necessary for non-invasive reconstructions. Some techniques rely neither on BEM nor on FEM and assume a homogeneous and infinite torso domain using a dipole formulation [Chávez 2015]. While neglecting the null current flow constraint at the body surface, it has been shown to be efficient on simulated experiments.

### 1.3.2.2 Inverse Problem of Cardiac Electrocardiography

BSPM data has been widely used in the last decades to directly compute the cardiac action potentials by solving an ill-posed inverse problem: finding the transfer matrix linking the torso potentials to the cardiac potential sources [Dössel 2000, Pullan 2010]. If most of the methods are only estimating the potential on the surface of the heart (e.g. [Huiskamp 1988, Ghosh 2009]), transmural-based methods have been investigated in the last few years but are computationally more demanding [Messnarz 2004, Jiang 2009]. Rather than estimating directly the transmembrane potentials, the 3DCEI technique [Liu 2006, Han 2011, Han 2013, Han 2015] solves the inverse problem by estimating the equivalent current density.

Aside from standard regularization techniques, some inverse problem studies have been investigated imposing constraints in temporal and spatial domains [Messnarz 2004, Yu 2015] or trying to take advantage of the space/time coupling of the electrical wave propagation [Oster 1992, Chávez 2015]. Some methods are also looking into integrating physiological and model-based priors in a Bayesian framework [Rahimi 2016, Wang 2011]. The work by Li and He [Li 2001] solves the inverse problem by means of heart-model parameters (onset activation location) and was further extended [He 2002] and validated on rabbits [Zhang 2005] and swines [Liu 2008, Liu 2012]. A preliminary step is based on prior knowledge using artificial neural network and an optimization algorithm refining the parameters. Lastly, the fastest route algorithm [Van Dam 2009, van Dam 2013] is used for a preliminary exhaustive ECGI estimation from a simplified EP modelling.

ECG imaging is already commercially available for some clinical applications, as the CardioInsight Technologies software [Ramanathan 2003] which was also used in recent ECGI studies [Dubois 2015]. Moreover, a consortium on ECG imaging was recently developed, leading to some shared databases, shared methodological tools and shared publications [Aras 2015, Coll-Font 2016b].

ECG imaging can help in understanding dyssynchrony and selecting CRT candidates : [Varma 2007] and [Ghosh 2011] worked on characterizing the EP substrate and electrical dyssynchrony on HF patients undergoing CRT while [Dawoud 2016] investigated regional electromechanical uncoupling in patients referred for CRT.

### 1.3.3 Cardiac EP Personalisation

The estimation of patient-specific parameters of a cardiac EP model is crucial for understanding the pathologies and predicting the response to therapies. The model personalisation usually deals with local parameters, such as conductivities or onset activation locations.

#### 1.3.3.1 Cardiac EP Personalisation from Invasive Data

The first EP model personalisations were using invasive data measures such as presented in section 1.2.3.2. [Relan 2011b] used optical mapping in an ex vivo study to personalize local diffusivity parameters. Personalisation using intra-cardiac potential mapping was investigated by [Relan 2011a, Wallman 2014, Konukoglu 2011], also including epicardial recordings. In [Konukoglu 2011], the integration of uncertainty estimation was also studied.

#### 1.3.3.2 Cardiac EP Personalisation from Non-invasive Data

Calibration using non-invasive data was recently studied: [Zettinig 2014] used two features from the 12-lead ECG to recover 3 electrical diffusivity parameters using a polynomial regression. The method is novel and efficient, but it suffers from the fact that the earliest activation site was fixed but actually unknown, and only two features (QRS complex duration and electrical axis) may not be sufficient to describe the cardiac activation. The estimation of heterogeneous myocardial conduction using a Bayesian framework has been explored by [Dhamala 2017a], but the other parameters such as the onset are supposed to be known. The problem of uncertainty in the field of non-invasive cardiac EP model parameter estimations is has also raised interests [Dhamala 2017b].

Finally, the estimation of cardiac activation patterns from motion imaging data was investigated with the use of a database of synthetic image sequences [Prakosa 2014]. Using also imaging data (delayed enhanced MRI), [Cabrera-Lozoya 2017] worked on locating cardiac ablation targets to guide radiofrequency ablation by simulating patient-specific intracardiac electrograms.

### 1.3.4 Reference Ventricle-Torso Anatomy in ECGI

The personalisations of EP cardiac model parameters from BSPM data rely on time-consuming patient-specific computation. Moreover, the patient-specificity is at the expense of an inter-patient study where information from different patients could be compared. Because of the natural similarity of the anatomical structures between patients, a common framework could be exploited.

One study showed the importance of the interindividual variability (averaged standard deviation) of electrocardiograms (ECG) on 25 healthy subjects [Hoekema 1999]. A large part of this variability is due to the heart position and orientation relative to electrodes. In terms of geometry, the larger variations are

found for the heart long axis angle. Another study showed that ECG imaging is sensitive to global anatomical parameters such as the heart orientation and location with regard to the lead positions [Huiskamp 1989]. The use of a reference anatomy model, able to represent every patient, is thus a difficult task. Hoekema et al. [Hoekema 1999] showed that by only moving the electrodes in a frontal plane to a common reference, the interindividual variability is not reduced because the heart orientation is not preserved. Another study created a patient-specific adapted torso model by stretching and squeezing a standard torso model according to the measures [Lenkova 2012]. They concluded that it was crucial to adapt both the outer shape of the torso model and the position of electrodes according to reality. Yet, it has been also shown that some adapted ventricle-torso standard model were able to get good ECGI results while excluding local geometrical details [Wang 2010, Rahimi 2015]. To the best of our knowledge, the goals of these geometrical models were only to simplify the anatomical modelling process. Yet, a study has recently tackled the interindividual variability by separating the factors of variation throughout a deep network using a denoising autoencoder on a large ECG dataset [Chen 2017b] for learning the ventricular tachycardia origin. Inter-subject variations coming from cardiac EP differences and geometry differences are however not separable, so a personalised EP model could not be estimated.

### 1.3.5 Data Driven and Machine Learning for Cardiac EP Personalisation

In order to tackle model personalisation, several approaches of data-driven algorithms exist. On the one hand, sequential algorithms are estimating the error between the simulation results and the real data at each time step to correct the values of the parameters. On the other hand, variational techniques are minimizing a functional in order to approximate the extreme function that makes the functional attain the minimum value. Machine learning techniques are handling problems with a similar criterion as variational approaches, but without estimating the gradient of the criterion. As no large patient-specific database exists, they can only rely on simulated patient-specific samples covering the parameter space.

#### 1.3.5.1 Sequential Data Assimilation

The Unscented Kalman filter (UKF) [Julier 1997] is a sequential data assimilation algorithm. The algorithm, derived from the Unscented Transform and the Kalman filter, is used to linearize a function of a random variable through a linear regression between  $n$  points drawn from the prior distribution of the random variable. The UKF consists of the iteration of the following three steps: selection of some sigma points where the function is evaluated, model forecast and data assimilation.

For the EP personalisation problem, sequential methods suffer from the fact that the state of the system at time  $t$  highly depends on the state at time  $t - 1$  so correcting the parameter values during the simulation might be inefficient, while

identifying the initial activation site is nearly impossible. As a solution, [Wang 2011] and [Talbot 2015] used static versions of the UKF where the algorithm iterates through a complete cardiac cycle and thus acting more like the variational approaches.

A recent study has also developed a new sequential estimation method for making an atrial EP model patient-specific from simulated invasive measures [Collin 2015]. They have tackled the problem of complex EP wave shapes such as fibrillation by incorporating a correction term based on topological gradients. This way, it is possible to act only in active regions on the propagation front.

### 1.3.5.2 Variational Data Assimilation

The large variety of variational or optimization methods has been used in all problems that can be described by a functional  $f$  to minimize (or maximize), corresponding to some criterion or error, and a set of available parameter values. Variational techniques impose to have the whole sequence of data before trying to optimize the parameters. The minimum of a function can be found by taking steps proportional to the negative of the gradient (procedure known as the gradient descent), however many problems are described with non-differentiable functionals. We will describe in the following sections some derivative-free optimization techniques.

### 1.3.5.3 Evolution Strategy

In this scope, the evolution strategy optimization technique uses natural problem-dependent representations, where mutation and selection are the search operators. These operators are applied in a loop (each iteration is called generation) until a criterion is met. At each generation, new individuals (candidate solutions  $x$ ) are generated by variation, usually in a stochastic way, of the current parental individuals. They are sampled according to a multivariate normal distribution, and pairwise dependencies between the variables in the distribution are represented by a covariance matrix. The covariance matrix adaptation (CMA) is a method to update the covariance matrix of this distribution. The CMA evolution strategy (CMA-ES) [Hansen 2006] has been used in cardiac mechanical personalisation by [Molléro 2016] because it is derivative-free and suited for non-convex continuous optimization problems. The concept of directional optimization in the CMA-ES on a 2D problem is shown in Figure 1.12.

### 1.3.5.4 Regression Analysis

The multivariate regression analysis is an intuitive machine learning continuous process for estimating relationships between variables. Regression analysis estimates the conditional expectation of the dependent variable given the independent variables. The estimated target is a function of the independent variables called the regression function. Many regression techniques have been developed, among the familiar ones are the linear regression and the ordinary least square regression. In

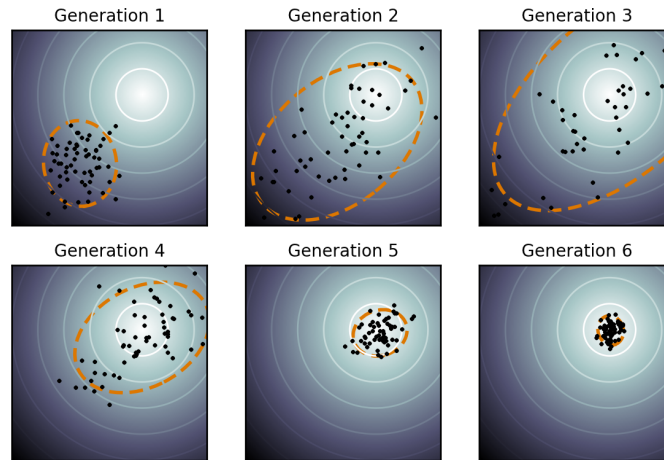


Figure 1.12: Concept of directional optimization in the covariance matrix adaptation evolution strategy (CMA-ES). The spherical optimization landscape is depicted with solid lines of equal  $f$ -values. The population (dots) shows how the distribution of the population (dotted line) changes during the optimization. On this simple problem, the population concentrates over the global optimum within a few generations. From [www.commonswiki.org](http://www.commonswiki.org)

the polynomial regression the relationship between the independent variable  $x$  and the dependent variable  $y$  is modelled as an  $n$ th degree polynomial in  $x$ . It was used in [Zettinig 2014] for parameter estimation from two features of the 12-lead ECG.

The ridge regression is a regularized least square method which is suited for a reasonable number of training examples. In the kernel ridge regression, we consider a non linear mapping  $x \rightarrow \Phi(x)$  into a higher-dimensional but linear feature space. The *kernel trick* consists in only calculating the equivalent kernel  $K(x_i, x_j) = \Phi(x_i) \cdot \Phi(x_j)$  without computing  $\Phi(x)$ . It is suited for complex non-linear relationships between variables. The predicted target  $y$  for a new test point  $x$  is then estimated using:

$$y = \mathbf{y}(K + \frac{1}{\gamma} \mathbf{I}_n)^{-1} \kappa(x)$$

where  $\mathbf{y}$  is the matrix of the sampled targets  $y_i$ ,  $\gamma$  is the coefficient balancing the smoothness and the adherence to the data and the  $i$ -th coordinate of the vector  $\kappa(x)$  is defined as  $(\kappa(x))_i = K(x_i, x)$ .

### 1.3.5.5 Bayesian Inference

In machine learning, many methods are employing statistical inference which consists in deducing properties of the underlying probability distribution by analysis of the data. Particularly, Bayesian inference proposes to update the probability as more information becomes available. It derives the posterior probability from the prior probability and the likelihood function using a statistical model for the

observed data. This is done by application of the Bayes's theorem:

$$P(H|E) = \frac{P(E|H) \cdot P(H)}{P(E)}$$

where  $P(H)$  the prior probability is the estimate of the probability of the hypothesis  $H$  before the data  $E$  is observed;  $P(H|E)$  is the posterior probability of  $H$  given  $E$ ;  $P(E|H)$  the likelihood is the probability of observing  $E$  given  $H$  and  $P(E)$  is the marginal likelihood. Graphical models are a way of depicting how random variables relate to one another, such as Markov Random Fields [Clifford 1990]. These techniques enable to take into account every piece of data information, including uncertainty or probability distributions. The solution is also given as a probability which interprets a confidence in the result. Because many complex models cannot be processed in closed form by Bayesian analysis, some connections are made with simulation-based Monte-Carlo techniques [Robert 2004] or Polynomial chaos [Wiener 1938].

In the EP model personalisation, [Konukoglu 2011] is based on an inference method combining polynomial chaos and compressed sensing, [Zettinig 2014] employs polynomial regression into a statistical framework and [Wallman 2014, Dhamala 2017a] rely on a Bayesian inference model. The uncertainty on the results was estimated by [Dhamala 2017b] using Gaussian Process-Based Markov Chain Monte Carlo.

### 1.3.5.6 Relevance Vector Machine

The relevance vector machine (RVM) method [Tipping 2003] performs sparse kernel regression or classification based on a sparsity inducing prior on the weight parameters within a Bayesian framework. Unlike the commonly used Elastic-Net or Lasso approaches (based on L1 Norm a.k.a Laplace prior), the RVM method does not require to set any regularization parameters through cross-validation. Instead, it automatically estimates the noise level in the input data and performs a trade-off between the number of basis (complexity of the representation) and the ability to represent the signal. Furthermore, unlike support vector machine regression or Elastic-Net, it provides a posterior probability of each estimated quantity which is reasonably meaningful if that quantity is similar to the training set.

The RVR estimates the weights  $\mathbf{w}$  so that we can predict  $y$  for an unknown input  $\mathbf{x} \in R^L$  if we suppose a non-linear relationship between  $\mathbf{x}$  and  $y$  as  $y = \mathbf{w}^T \Phi(\mathbf{x})$  where  $\Phi$  is a non-linear mapping. We consider our dataset of input-target pairs  $\{\mathbf{x}_k, t_k\}_{k=1}^K$  where we assume that each target  $t_i$  represents the true model  $y_i$  with an addition of noise  $\varepsilon_i \sim P(0, \sigma^2)$ :

$$t_i = \mathbf{w}^T \Phi(\mathbf{x}_i) + \varepsilon_i \quad (1.5)$$

The complexity of the learned relationship between  $\mathbf{x}$  and  $y$  is constrained by limiting the growth of the weights  $\mathbf{w}$ . This is done by imposing a zero-mean Gaussian prior

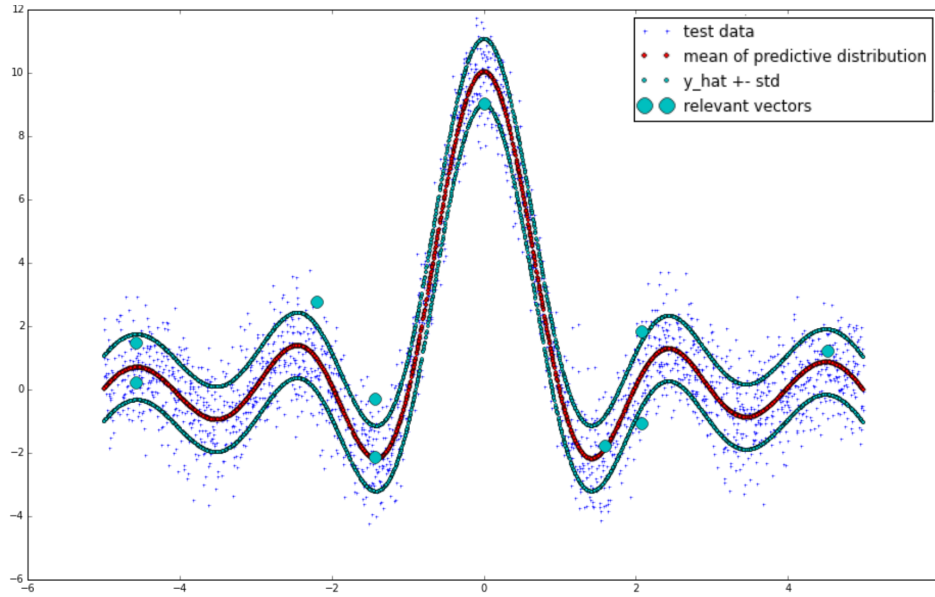


Figure 1.13: Relevance vector regression: 1D example (sinc function). From [github.com/AmazaspShumik/sklearn-bayes](https://github.com/AmazaspShumik/sklearn-bayes)

over the  $w_i$ 's:

$$P(w_i) = \mathcal{N}(0, \alpha_i^{-1}) \quad (1.6)$$

where the  $\alpha_i$  are hyperparameters modifying the strength of each weight prior.  $\alpha = \{\alpha_i\}_{i=1}^K$  and  $\sigma$  are estimated from a marginal likelihood maximisation [Bishop 2000] via an efficient sequential addition and deletion of candidate basis functions (or relevant vectors). Because the optimal values of many  $\alpha_i$  are infinite, the RVR only selects the BSPM input set that can best explain the activation map in the training set, thus limiting the risk of overfitting. RVM regression only performs multivariate regression of a single output scalar value but not of a vector value (unlike kernel ridge regression for instance). However, multivalued versions have been recently proposed [Le Folgoc 2017].

We can see in Figure 1.13 the result of the relevance vector regression on a 1D example of the sinc function with 5000 Gaussian noisy data points. The relevant vectors retained for the regression are in light blue: only 10 are needed. Moreover, we can see the standard deviation of the predictive distribution, which gives an estimation of the uncertainty on the result.

## 1.4 Conclusion

In this chapter, we presented a background on the cardiac anatomy and function, the cardiac electrophysiology, its pathologies and its measures. We also summarized the research on cardiac EP modelling, on ECGI and on cardiac EP model personalisation with their machine learning techniques.

## Part I

# Personalisation of a Cardiac Model from Body Surface Potential Mapping (BSPM)



# Activation Onset Location and Global Conductivity Estimation from BSPM

---

## Contents

---

<b>2.1</b>	<b>Introduction</b>	<b>26</b>
2.1.1	Cardiac EP Model Personalisation	26
2.1.2	The Forward Problem of Electrocardiography	27
2.1.3	The Inverse Problem of Electrocardiography	27
2.1.4	Proposed Approach	28
2.1.5	Outline of the Chapter	29
<b>2.2</b>	<b>Materials and Methods</b>	<b>29</b>
2.2.1	Clinical Data	29
2.2.2	Simulating BSPM data: EP Forward Model	30
2.2.3	Personalising a Cardiac EP Model from BSPM	32
<b>2.3</b>	<b>Personalisation Experiments and Results</b>	<b>36</b>
2.3.1	Evaluation on PVC Benchmark Clinical Dataset	36
2.3.2	Evaluation on Five Implanted CRT Patients	37
2.3.3	Prediction of Stimulation Results from Personalised Model	43
<b>2.4</b>	<b>Discussion</b>	<b>43</b>
2.4.1	Quantifying the Impact of a Precise Myocardial Geometry	43
2.4.2	Modelling Scar Tissue: Its Impact on our Personalisation	45
2.4.3	Future Works	45
<b>2.5</b>	<b>Conclusion</b>	<b>46</b>

---

This chapter is based on the following paper:

**Non-Invasive Personalisation of a Cardiac Electrophysiology Model from Body Surface Potential Mapping**, *Sophie Giffard-Roisin, Thomas Jackson, Lauren Fovargue, Jack Lee, Hervé Delingette, Reza Razavi, Nicholas Ayache and Maxime Sermesant*. IEEE Transactions on Biomedical Engineering, 2017.

## 2.1 Introduction

Heart Failure (HF) is a major health issue in Europe affecting 6 million patients and growing substantially because of the ageing population and improving survival following myocardial infarction. The poor short to medium term prognosis of these patients means that treatments such as cardiac resynchronisation therapy can have substantial impact [Sutton 2003]. However, these therapies are ineffective in 30% of the treated patients and involve significant morbidity and substantial cost. To this end, the precise understanding of the patient-specific cardiac function can help predict the response to therapy and therefore select the potential candidates and optimise the therapy.

In [Sermesant 2012], Sermesant et al. proposed to personalize an electro-mechanical model of the heart to predict the response to CRT. The method requires to measure intra-cardiac electrical potentials through an invasive endovascular procedure which can be risky for the patient, and which is not suitable at a patient selection stage. The aim of this article is to extend this approach to non-invasive body surface potential mapping (BSPM), which uses up to 256 sensors on both sides of the torso, as the CardioInsight<sup>1</sup> jacket now commercially available. This has the potential to replace invasive measurements however the ability to estimate parameters and predict activation from such data still needs to be evaluated.

### 2.1.1 Cardiac EP Model Personalisation

Restricting our study to the ventricles, there are several types of EP models describing the action potential [Pollard 2003]; from complex ones (biophysical models) to very simplistic ones (Eikonal models). In this study we used the Mitchell-Schaeffer model [Mitchell 2003] which is a phenomenological model of intermediate complexity with 2 variables and 6 parameters with a biophysical interpretation. From an onset activation location, the evolution of the transmembrane potential is computed at each node of a tetrahedral mesh of the myocardium using the finite element method.

The estimation of patient-specific parameters of a cardiac EP model is crucial for understanding of pathologies and predicting the response to therapies. The model personalisation usually deals with local parameters. [Relan 2011b] used optical mapping in an ex-vivo study to evaluate such algorithms. Personalisation using intra-cardiac potential mapping was investigated by [Relan 2011a, Wallman 2014, Konukoglu 2011], also including epicardial recordings. Calibration using non-invasive data was recently studied: [Dössel 2011] adjusted two parameters of an atrial EP model using BSPM data. [Zettinig 2014] used two features from the 12-lead ECG to recover 3 electrical diffusivity parameters using a polynomial regression. The method is novel and efficient, but it suffers from the fact that the earliest activation site was fixed but actually unknown, and only two features (QRS complex duration and electrical axis) may not be sufficient to describe the cardiac activation. Such approaches have explored the use of machine learn-

---

<sup>1</sup>ECVUE, CardioInsight Technologies Inc., Cleveland, Ohio

ing for EP personalisation, but as no patient-specific database exists, they can only rely on simulated patient-specific samples covering the parameter space. In terms of personalisation methodology, [Konukoglu 2011] is based on an inference method combining polynomial chaos and compressed sensing, [Zettinig 2014] employs polynomial regression into a statistical framework and [Wallman 2014] relies on a Bayesian inference model.

### 2.1.2 The Forward Problem of Electrocardiography

The two classical numerical approaches are based either on the Boundary Element Method (BEM) or the Finite Element Method (FEM). They both propagate the epicardial heart action potentials to the surface of the body by taking into account the distance, the null current across the body surface, and the different properties of the tissues in between. Forward models differ also by their incorporation of heterogeneous conductivity regions associated with various organs within the torso. By taking into account the physical properties of the different tissues, the computed ECG account for more complex current pathways. In [Keller 2010], Keller et al. demonstrates the importance of the torso inhomogeneity by ranking the influence of the different tissue conductivities on forward-calculated ECGs. Ramanathan et al. [Ramanathan 2001] showed, however, that at a first order approximation the torso inhomogeneities are not necessary for non-invasive reconstructions. Some techniques rely neither on BEM nor on FEM and assume a homogeneous and infinite torso domain using a dipole formulation [Chávez 2015]. While neglecting some the null current flow constraint at the body surface, it has been shown to be efficient on in-silico experiments.

### 2.1.3 The Inverse Problem of Electrocardiography

BSPM data has been widely used in the last decades to directly compute the cardiac action potentials by solving an ill-posed inverse problem: finding the transfer matrix linking the torso potentials to the cardiac potential sources [Dössel 2000, Pullan 2010]. If most of the methods are only estimating the potential on the surface of the heart (e.g. [Huiskamp 1988, Ghosh 2009]), transmural-based methods have been investigated in the last few years but are computationally more demanding [Messnarz 2004, Jiang 2009]. Rather than estimating directly the transmembrane potentials, the 3DCEI technique [Liu 2006, Han 2011, Han 2013, Han 2015] solves the inverse problem by estimating the equivalent current density. Aside from standard regularization techniques, some inverse problem studies have been investigated imposing constraints in temporal and spatial domains [Messnarz 2004, Yu 2015] or trying to take advantage of the space/time coupling of the electrical wave propagation [Oster 1992, Chávez 2015]. Some methods are also looking into integrating physiological and model-based priors in a Bayesian framework [Rahimi 2016, Wang 2011]. The work by Li and He [Li 2001] solves the inverse problem by means of heart-model parameters (onset activation location) and

was further extended [He 2002] and validated on rabbits [Zhang 2005] and swines [Liu 2008, Liu 2012]. A preliminary step is based on a priori knowledge using artificial neural network and an optimization algorithm refines the parameters. ECGI (Electrographic imaging) is already commercially available, as the CardioInsight Technologies software [Ramanathan 2003] which was also used in recent ECGI studies [Dubois 2015]. ECGI can help in understanding dyssynchrony and selecting CRT candidates : Varma et al. [Varma 2007] and Ghosh et al. [Ghosh 2011] worked on characterizing the EP substrate and electrical dyssynchrony on HF patients undergoing CRT while Dawoud et al. [Dawoud 2016] investigated regional electromechanical uncoupling in patients referred for CRT.

### 2.1.4 Proposed Approach

Our method is based on adjusting a forward model to measured BSPM in order to estimate patient-specific parameters and activation maps. Our personalisation involves identifying the parameters to predict new patient-specific pacing conditions. In order to avoid local minima we used a machine learning approach with the generation of a large patient-specific database of simulated BSPM. Some relevant shape descriptors were extracted from the simulated BSPM and used as patient-specific training set. We first learned the onset activation location using a Kernel Ridge Regression on activation maps, then use a second regression to calibrate the global ventricular conduction velocity. Because the onset activation is a local parameter, this method can be associated with a model personalisation. The contributions of this chapter are:

- A two-step algorithm that learns the parameters of the simulation by estimating the onset activation location and the global conduction velocity. The algorithm relies on machine learning approaches based on a few QRS shape-related features extracted from each BSPM sensor.
- A straightforward and efficient coupled forward model based on the Mitchell-Schaeffer model and on a current dipole formulation, allowing to simultaneously calculate transmural cardiac potentials and BSPMs. The Mitchell-Schaeffer model previously showed good predictive power in intra-cardiac studies [Chen 2016].
- An evaluation (onset localisation and errors on the BSPM signals) on 52 different cardiac beats from 6 patients with 2 different types of pathologies: dyssynchrony and premature ventricular contraction. All the results were compared with standard inverse problem methods commercially available or other state-of-the-art methods, outperforming in a large majority of beats.
- A prediction of biventricular pacing activation maps and BSPM from personalised EP model parameters on 14 settings from 5 patients. Predicted BSPM are compared with measured BSPM.
- A quantification on the impact of myocardial geometry quality and scar tissue.

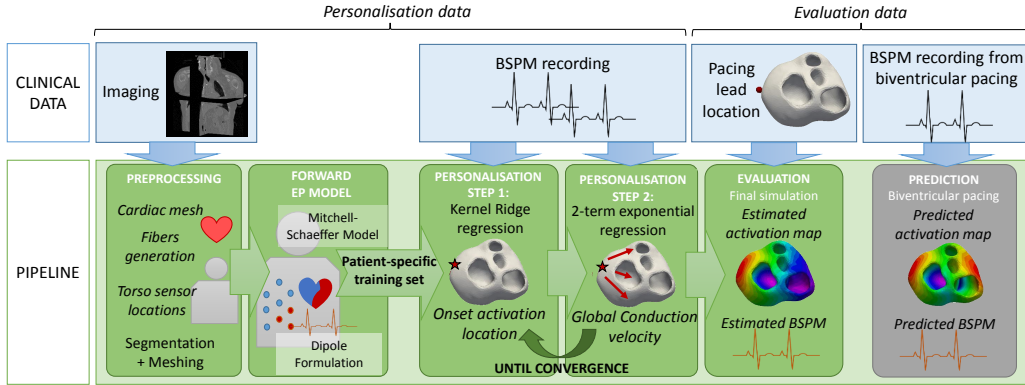


Figure 2.1: Personalisation framework of Chapter 2. Patient-specific geometrical data (section 2.2.1) are used to build the coupled forward model (section 2.2.2). Using Patient-specific training sets, the two-step personalisation (section 2.2.3) based on machine learning techniques estimates the earliest activation location and the global conduction velocity from univentricular pacings or ectopic foci. The true location of the pacing lead is used for evaluation. A prediction of biventricular pacings (section 2.3.3) is performed using estimated parameters from sinus rhythm personalisation.

### 2.1.5 Outline of the Chapter

In the following section 2.2 we will present our personalisation framework (Figure 2.1): clinical data, forward EP model and machine learning algorithm. Section 2.3 is dedicated to two evaluations on different datasets and to predictions of biventricular pacing. Finally, section 2.4 discusses different aspects of the method, related in particular to the robustness and to the influence of the myocardial geometry and scar tissue.

## 2.2 Materials and Methods

### 2.2.1 Clinical Data

In this study, two datasets with different devices were used. The pacing lead is either at the tip of a moving catheter on the LV cavity or from a pacemaker device. The BSPM potentials were acquired during the procedure at a sampling rate of 1kHz, with different number of torso sensors depending on the device. The anatomy as well as the location of the torso sensors and the pacing leads were extracted either with imaging (MRI or CT scanner) or through the EP mapping system using magnetic sensors. Fibre orientations were estimated with a rule-based method (elevation angle between  $-60^\circ$  to  $60^\circ$ ). More details on the data will be provided in sections 2.3.1.1 and 2.3.2.1.

## 2.2.2 Simulating BSPM data: EP Forward Model

### 2.2.2.1 Mitchell-Schaeffer Cardiac Model

We simulated the electrical activation of the heart using the monodomain version of the Mitchell-Schaeffer's EP model [Mitchell 2003] as presented in section 1.3.1.2. It has two variables, the transmembrane potential  $v$  and  $z$  a secondary variable controlling the repolarization phase. The diffusion term is defined by an anisotropic diffusion tensor  $D = d \cdot \text{diag}(1, r, r)$  where  $d$  is the tissue electrical diffusivity. The anisotropy ratio  $r$  enables conduction velocity in the fibre direction to be larger than in the transverse plane (we used  $r = (1/2.5)^2$ ).

The diffusivity  $d$  (in  $m^2s^{-1}$ ) can be expressed as a conductivity  $\sigma$  (in  $S/m$ ) by using  $\sigma = C_m\beta d$  with  $C_m$  the membrane capacitance and  $\beta$  the surface-to-volume ratio. From [Potse 2006], we took  $C_m = 10^{-2} F/m^2$  and  $\beta = 10^5 m^{-1}$ . The local conductivity  $\sigma$  can be written in terms of intracellular and extracellular conductivities:  $\sigma = \frac{\sigma^i\sigma^e}{\sigma^i+\sigma^e}$

The reduction of the monodomain model implies  $\sigma^i = \lambda\sigma^e$  for some scalar  $\lambda$  resulting in a linear relationship between  $\sigma$  and  $\sigma^i$ . Finally, the diffusion  $d$  is linked to the conduction velocity  $c$  in  $m/s$  by  $c = k\sqrt{d}$ , where the constant  $k$  was estimated numerically in our simulations as  $0.35 s^{-1/2}$ .

### 2.2.2.2 From Cardiac Simulations to BSPM, Current Dipole Formulation

We can compute simultaneously the cardiac electrical sources simulated in section 2.2.2.1 and the BSPM. As in [Chávez 2015], we modelled every myocardium volume element (tetrahedron) as a spatially fixed but time varying current dipole. We define the equivalent current density  $\mathbf{j}_{eq}$  as:

$$\mathbf{j}_{eq} = -\sigma^i\nabla v \quad (2.1)$$

$\mathbf{j}_{eq}$  is a current dipole moment per unit of volume and the local dipole moment  $\mathbf{p}$  in the volume  $V$  writes as  $\mathbf{p} = \int_V \mathbf{j}_{eq} dV$ .

The torso is composed of different organs that behave as different volume conductors. In a rough approximation, we consider an homogeneous, infinite volume of conductivity  $\sigma_T$ , and we took  $\sigma_T = 0.2S/m$ . According to the volume conductor theory [Malmivuo 1995], the electric potential at a distance  $R$  in a homogeneous volume conductor of conductivity  $\sigma_T$  is:

$$\Psi(R) = \frac{1}{4\pi\sigma_T} \int_V \mathbf{j}_{eq} \cdot \nabla\left(\frac{1}{R}\right) dV \quad (2.2)$$

We model the moving propagation front as a dipole field. The infinitesimal dipole moment of the volume  $dV_X$  located at position  $X$  is defined as  $\mathbf{p}_X = \mathbf{j}_{eq,X} dV_X = -\sigma_X^i \nabla v_X dV_X$ . As we use linear tetrahedra in the FEM discretization of the myocardium, the potential  $v$  is linear and  $\nabla v$  is constant over the tetrahedron. We get

the following formulation of the dipole moment of the charge in the volume  $V_H$  of tetrahedron  $H$  of the myocardial mesh:  $\mathbf{p}_H = -\sigma_H^i \nabla v_H V_H$

The gradient of the electric potential  $\nabla v_H$  for a tetrahedron  $H$  is estimated using the node positions  $X_H^k$  and the shape vectors  $\overrightarrow{D}_H^k$  of the tetrahedron  $H$  [Delingette 2004]:

$$\overrightarrow{D}_H^k = \frac{s}{V_H} ((X_H^{k\oplus 2} - X_H^{k\oplus 1}) \times (X_H^{k\oplus 3} - X_H^{k\oplus 1})) \quad (2.3)$$

where  $s = 1$  for  $k = 2, 4$ ,  $s = -1$  for  $k = 1, 3$ , and  $k \oplus l = (k - 1 + l) \bmod 3 + 1$ . The gradient of the electric potential in the tetrahedron  $H$  is then computed from the potentials  $v(X_H^k)$  at the nodes  $X_H^k$  as:

$$\nabla v_H = \sum_{k=1}^4 v(X_H^k) \overrightarrow{D}_H^k \quad (2.4)$$

From Equation 2.2, the contribution  $\Psi_H$  of the tetrahedron  $H$  to the potential field calculated at position  $X_T$  is:

$$\Psi_H(X_T) = \frac{1}{4\pi\sigma_T} \frac{\sigma_H^i V_H (\nabla v_H \cdot \overrightarrow{HT})}{\|\overrightarrow{HT}\|^3} \quad (2.5)$$

with  $\overrightarrow{HT}$  the vector from the center of the tetrahedron  $H$  to the torso electrode location  $T$ . Finally, we sum over the whole mesh to get the potential field at  $X_T$ .

The implementation was done using the SOFA platform<sup>2</sup>, with a direct coupling to the Mitchell-Schaeffer model. For a generic volumetric mesh of 65 000 vertices, every coupled simulation (cardiac model and dipole formulation) of 300 ms runs in less than 6 minutes, with a time step of 0.01 ms (using a dual-Xeon X5670 with 12 cores at 2.93GHz). With GPU version of the implementation [Talbot 2012], the simulation was performed in 2 minutes (using a dual-Xeon X5650 and a Tesla C2050 with 112 cores at 1.147 GHz).

### 2.2.2.3 Comparison of the Current Dipole Results with BEM

While being straightforward and efficient, this method includes some simplifications as the absence of a null current flow constraint at the body surface. To validate and estimate the errors of our forward model, we compared our results with a classical BEM forward formulation. We used the symmetric BEM from the OpenMEEG software<sup>3</sup> because it was shown to provide an excellent accuracy [Kybic 2005]. As input, the isolated dipole source were set at the center of each tetrahedra on the myocardium and calculated the vector sources of each tetrahedron at each time using Equation 2.1. We defined 3 domains: the myocardium, the torso and the air outside

<sup>2</sup>SOFA is an Open Source medical simulation software available at <http://www.sofa-framework.org>

<sup>3</sup>OpenMEEG is an Open Source software that solves problems related to EEG and MEG, available at <http://openmeeg.github.io>.

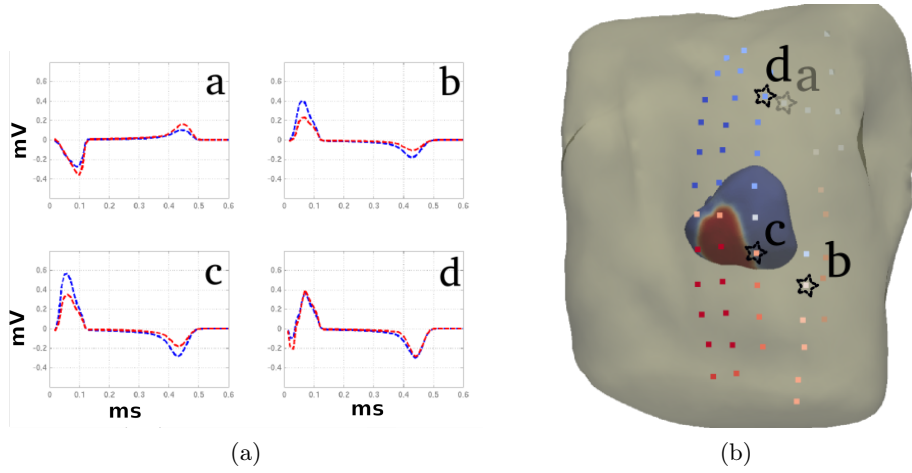


Figure 2.2: (a) Body surface potentials over one cardiac cycle (4 examples): OpenMEEG (blue), dipole formulation (red). (b) positions of the 4 sensors on the torso, the sensor **a** is on the back.

the torso (null conductivity). Their interfaces were defined using closed surface meshes. The linear operator  $L$  which associates dipolar sources to the resulting sensor measurements is calculated by solving  $L = S G^{-1} D$ , where  $D$  is the dipole matrix,  $S$  is the sensor matrix and  $G$  is the geometry matrix. With a torso surface mesh of 4K vertices, a heart surface mesh of 7K, 75K dipolar sources and 52 sensors, the  $L$  matrix is computed in 7 hours. As an example, the potentials at 4 random sensor locations simulated with OpenMEEG (blue) and our dipole formulation (red) are shown in Figure 2.2. In some surface potentials the OpenMEEG ECG has larger amplitude as on b and c, whereas on some other the amplitude is lower as on a and d. The difference is due to the absence of boundary conditions in our formulation. A key point to notice is that the signal shape and sign are similar, while reducing the computation time from 7 hours to a few minutes.

## 2.2.3 Personalising a Cardiac EP Model from BSPM

### 2.2.3.1 A Two-step Machine Learning-based Personalisation

The two machine learning algorithms are two different regressions, both using simulated patient-specific data as training sets. For the first step, a Kernel Ridge Regression is estimating the onset activation location. From 250 random onset activation locations, their respective activation maps are simulated together with their simulated BSPM. After a feature extraction on both the measured and the simulated BSPM, the Kernel Ridge Regression estimates the cardiac activation time corresponding to the measured BSPM on each node of the cardiac mesh from the cardiac activation times of the simulated BSPM with the closest features. The onset location is identified as the node with the smallest activation time. During the second step, 100 conduction velocity values and their simulated BSPMs are used as a train-

ing set for a two-term exponential regression. Once the unknowns of the regression function are estimated, the conduction velocity of the true signal is estimated (see Figure 2.1).

### 2.2.3.2 BSPM Feature Description

Important aspects of the torso electrical signal are the shape, the timing and the sign of the QRS complex. Because the reference electrode is often not localized, each signal (measured and simulated) was first subtracted by the mean BSPM signal (measured or simulated). Then each signal (measured or simulated) was normalized and smoothed with a local Gaussian filter. We then defined  $7 \times n_s$  descriptors ( $n_s$  being the number of sensors in the jacket) of the QRS window as (see Figure 2.3): (1) timing of the global extremum, (2) absolute potential of the global extremum, (3) sign the global extremum, (4) number of zero crossings, (5) number of local extrema, (6) relative algebraic area, (7) sign of the first extremum. This choice was inspired by previous works on ECG analysis, e.g. [Tereshchenko 2011].

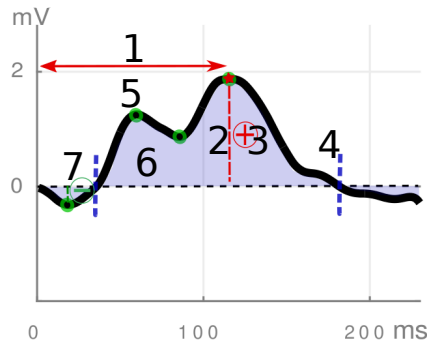


Figure 2.3: Example of BSPM for one sensor. The extracted features are the position of the global extremum (1: red arrow), the absolute potential of the global extremum (2: red bar), the sign of the global extremum (3: red sign), the number of zero crossings (4: blue lines), the number of local extrema (5: green dots), the algebraic area (6: blue), the sign of the first extremum (7: green sign).

### 2.2.3.3 First Step, Locate the Activation Onset with Kernel Ridge Regression

The shape of the measured torso signals strongly depends on the position of the onset activation. The first step of the non-invasive cardiac model personalisation is an automatic estimation of the onset activation site on the cardiac mesh. From a list of 250 random nodes on the surface of the cardiac mesh (epicardium and endocardium), we simulated a set of activation maps and corresponding BSPM. We fixed the global ventricular conduction velocity to a nominal value of  $0.5 \text{ m.s}^{-1}$  and we only used the 6 features that are invariant to a small change of the global conduction velocity (i.e. we excluded the timing of the global extremum). The training feature database was

normalized along each feature. We used a Kernel Ridge Regression between features extracted from the BSPM to predict the activation time on each node of the cardiac mesh. A Ridge Regression is a regularized least square method which is suited for a reasonable number of training examples. The kernel trick is useful here because the number of features (roughly 1500) is larger than the number of samples (250). We simulated a database composed of 250 couples  $(x_i, y_i)$  of feature vectors  $x_i$  and corresponding depolarization time vectors  $y_i$ . The predicted target  $y$  for a new test point  $x$  was estimated using:

$$y = \mathbf{y}(K + \frac{1}{\gamma}\mathbf{I}_n)^{-1}\kappa(x)$$

where  $\mathbf{y}$  is the matrix of the sampled targets  $y_i$ ,  $K(x_i, x_j) = \exp(-(x_i - x_j)^2/\sigma^2)$  is a Gaussian kernel of bandwidth  $\sigma$ , and the  $i$ -th coordinate of the vector  $\kappa(x)$  is defined as  $(\kappa(x))_i = K(x_i, x)$ .  $\gamma$  is the coefficient balancing the smoothness and the adherence to the data. The tuning of  $\sigma$  and  $\gamma$  was performed by a ten fold cross-validation. The same values were used for other patients. For each couple of parameters  $(\sigma, \gamma)$  the mean distance to the synthetic onset location is plotted in Figure 2.4a. It represents the error, since a perfect initial position estimate would result in a null distance. The estimated prediction error is  $5.7mm$  for the couple  $(\sigma = 10^{3.5}, \gamma = 10)$ . We notice that the value of  $\sigma$  is of the same order of magnitude as the size of the feature vector  $x_i$ . This is coherent, because each component of  $x_i$  belongs to a distribution with unitary standard deviation, so the distance between  $x_i$  and  $x_j$  is also of the order of their size. Figure 2.4b shows the distance error to the true pacing location for a clinical case when varying dataset size (result unchanged after 200 samples).

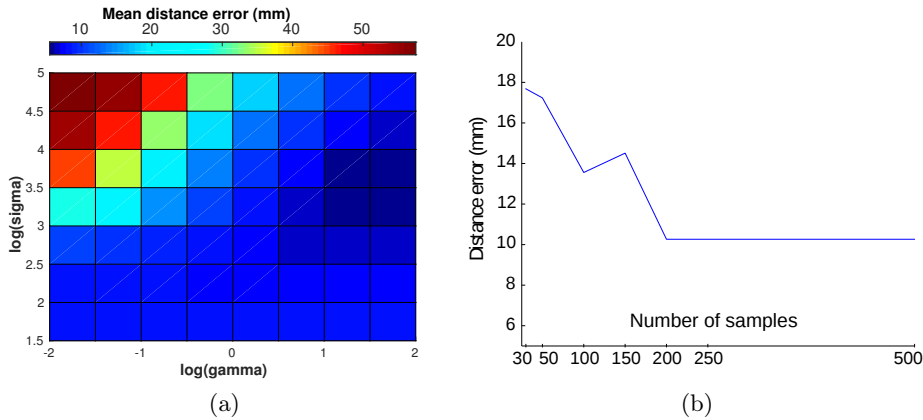


Figure 2.4: First Step. (a) Cross-validation: error in terms of mean distance to the synthetic true initial activation when varying the two parameters of the Kernel Ridge Regressor. (b) Distance error to the true onset for one clinical case with respect to the size of the database (retained size is 250 samples).

### 2.2.3.4 Second Step, Estimate the Ventricular Cardiac Conduction Velocity with Two-term Exponential Regression

The previous estimation of the onset location allowed us to further calibrate the EP model. We modelled the ventricles as an homogeneous tissue with a uniform conduction velocity (CV) that we want to estimate. We randomly sample 100 CV in the range  $[0.2, 1.5]m.s^{-1}$ . We generated the corresponding personalised BSPM database with fixed onset location. We extracted from the simulated BSPM one type of feature directly related to the CV: the position of the global extremum. The size of one feature vector is thus  $1 \times n_s$ , and the database was composed of 100 couples  $(x_i, y_i)$  of feature vectors  $x_i$  and corresponding CV parameters  $y_i$ . The predicted target  $y$  for a new test point  $x$  was estimated by a regression between the first mode of the PCA of the training feature vectors  $X_{1,i}$  and the conduction velocities  $y_i$ . The estimated function  $f(X_1) = y$  was fitted using a two-term exponential regression:

$$f(x) = ae^{bx} + ce^{dx} \quad (2.6)$$

In some cases, a too small conductivity can make the extremum of the signal exceed the QRS time frame; so the corresponding samples were automatically excluded. Finally, the measured BSPM can be projected into the PCA space and the CV is estimated from the regression (Figure 2.5).

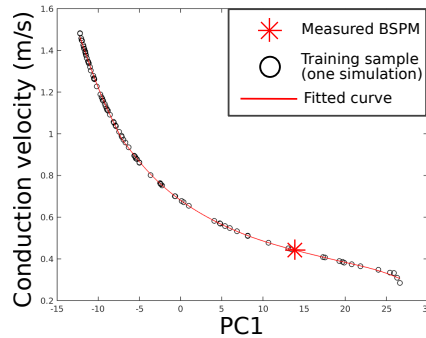


Figure 2.5: Second Step. Example for one patient and one pacing. 2-term exponential regression using the first principal component with automatic exclusion of outliers (small conductivities). The red star is the measured BSPM projection.

### 2.2.3.5 Iterating and Final Simulation Using Estimated Parameters

Step 1 and 2 are then iterated until convergence ( $\Delta c < 0.05m/s$ ). The final step consists in re-running the EP model during one cardiac cycle using the estimated onset location and the estimated global CV. The final result consists in a transmural activation map, where the depolarisation times are computed at each node of the mesh. In addition we simulate the corresponding BSPM. An estimation of the result confidence is given by the averaged correlation coefficient (CC) between the simulated and measured BSPM.

## 2.3 Personalisation Experiments and Results

### 2.3.1 Evaluation on PVC Benchmark Clinical Dataset

#### 2.3.1.1 BSPM and Intracardiac Acquisitions

We tested our method on a benchmark study of the ECGI community which provides clinical data from 63 BSPM electrodes on one non-ischemic patient recorded during an Premature Ventricular Contraction (PVC) ablation procedure. Ventricularly paced beats from a catheter were also recorded. The dataset<sup>4</sup> includes the geometry of the myocardium, the location of the 63 torso electrodes and the 7 pacing sites, as well as an estimation of the PVC site, see Figure 2.6. For the PVC ground truth, both the earliest measured local activation time measured by intracardiac CARTO system and the latest successful ablation site were recorded: they do not match but they both give an indication about the real PVC location. The BSPMs consist in several QRS time windows at a sampling rate of 1kHz. The QRS without pacing (marked as 'PVC') was recorded 10 times (10 runs), while for the 7 pacing sites the number of runs varies from 1 to 14. A volumetric myocardial mesh of roughly 10K elements was created from the provided surface mesh using the CGAL<sup>5</sup> meshing software, and fibre directions were estimated (see Section 2.2.1).

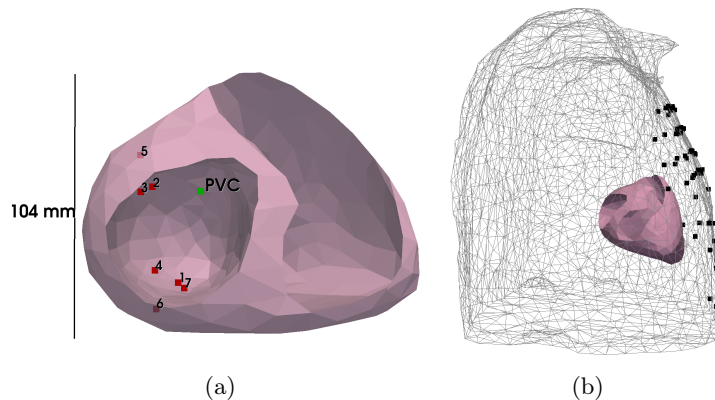


Figure 2.6: PVC data geometry. (a) myocardial mesh with measured pacing locations (red) and PVC location as the earliest activation time measured (green). (b) 64 BSPM electrodes (black), myocardial mesh (pink).

#### 2.3.1.2 Results for PVC and Pacing Sites Localisation

Our personalisation pipeline was launched for every run, and we compared the localization errors with those of the inverse method of [Schulze 2015]. Figure 2.7a

<sup>4</sup>This dataset was provided by the Institute of Biomedical Engineering, Karlsruhe Institute of Technology (KIT), Germany and the First Department of Medicine (Cardiology), University Medical Centre Mannheim, Germany.

<sup>5</sup>CGAL is a Computational Geometry Algorithms Library, available at [www.cgal.org](http://www.cgal.org)

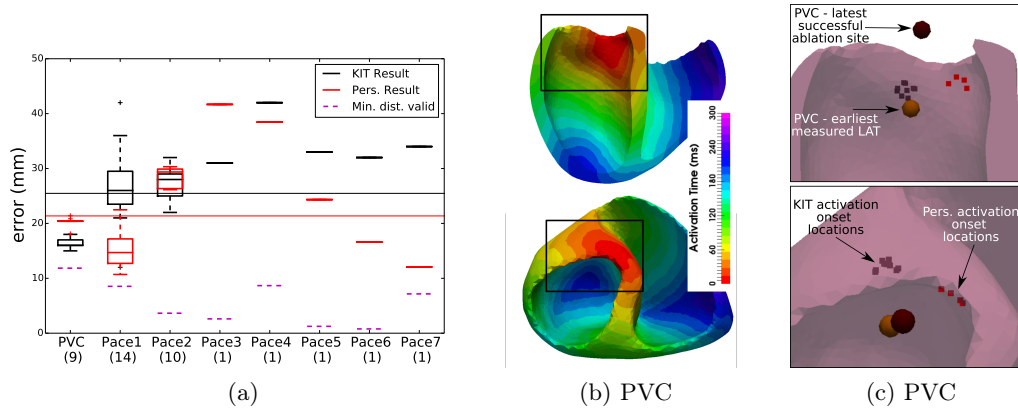


Figure 2.7: PVC results. (a) Error distances (mm) of estimated onset location to the measured location by the CARTO system for the PVC (9 runs) and to the catheter pacings for the 7 pacing sites of Figure 2.6 (29 runs in total). Comparison between our personalisation and the KIT inverse method. 'Minimal distance valid': distance of the measured excitation origin to the closest point in the mesh. Mean values are represented by the lines. (b) Personalised PVC transmural activation map. (c) Long and short axis zooms showing the estimated 9 PVC activation onset locations from KIT (black) and from our personalisation (red). Ground truth is taken as the earliest measured local activation time (brown). The latest successful ablation site (dark brown) was found in the aorta.

presents the error distances for the PVC (mean distance error or  $MDE = 20.3mm$ ) and for 7 catheter pacing locations ( $MDE = 21.69mm$  among all pacings). The error distances have to be compared to the distance of the measured excitation onset point to the closest point of the mesh ( $11.8mm$  for the PVC, pink dotted line), showing that the registration between the intra catheter localisation and the pre-operative imaging is not very accurate. From Figure 2.7a, our personalisation method provides results comparable to other state-of-the art inverse problem methods like [Schulze 2015], with better results for a majority of pacing sites locations. Global CV for all PVC runs was found in the range  $[0.33, 0.38]m/s$ . Looking at Figures 2.7b and 2.7c, the estimated PVC location is found to be close to the location of the earliest activation time measured and the latest successful ablation site lying in the aorta. The former was measured by catheter, while the latter is the location where the ablation procedure succeeded.

## 2.3.2 Evaluation on Five Implanted CRT Patients

### 2.3.2.1 BSPM Acquisitions with CardioInsight Jackets

The second dataset was acquired at St Thomas' Hospital, London. The CardioInsight jacket is able to acquire simultaneously 256 signals on the torso surface. The dataset consists of 5 patients, all being implanted CRT patients and non ischemic.

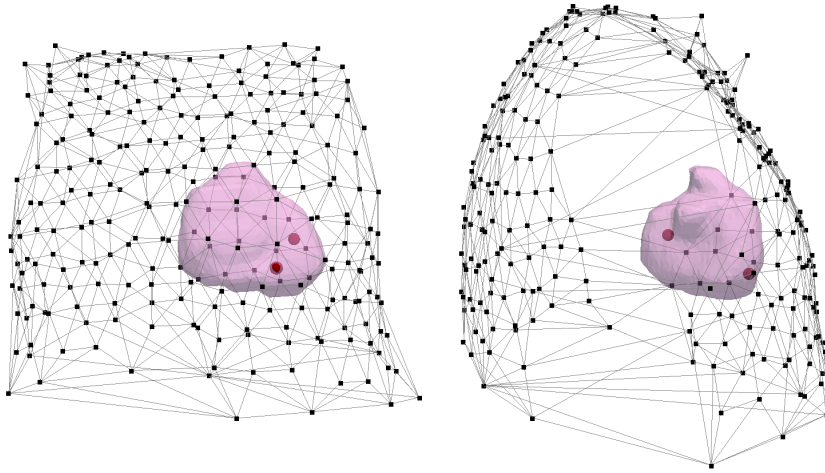


Figure 2.8: CRT patients geometry. CardioInsight geometries from hand segmentation of CT image: Torso sensors (black dots), left and right pacing sites (red), epicardial surface (pink).

Table 2.1: CRT patients. Baseline information of the 5 patients treated.

<b>Id</b>	<b>Age</b>	<b>Gender</b>	<b>Sinus rhythm</b>	<b>MRI</b>	<b>Presence of scar</b>
1	82	M	X		
2	49	F	X		
3	87	M			
4	69	F			
5	49	M	X	X	X

In the optimisation procedure, the cardiologists performs several recordings corresponding to different pacing combinations and delays between the right ventricle (RV pacing, endocardial) and the left ventricle (LV pacing, epicardial) pacing leads. In total, 114 different settings were recorded. For all patients, an LV pacing and an RV pacing were performed, together with several biventricular pacings where the two stimulations are either simultaneous or separated by a delay. A sinus rhythm sequence is also recorded on patients that do not have complete heart blocks, see Table 2.1. The QRS time window was recorded at a sampling rate of 1kHz. From the information given on the state of every sensor (*good*, *disconnected*, *missing*, *bad*), the non reliable sensors of each recording was removed. The number of sensors used in our personalisation varied between 175 and 220.

The relative position of electrodes and pacing sites with respect to an epicardial geometry were hand-extracted from a CT scanner performed the day of the intervention (Figure 2.8). Important artifacts on the CT scanner coming from the

pacemaker prevents creating a better segmentation. The CardioInsight Technologies software is solving the inverse problem on this epicardial surface. The method estimates the epicardial potentials based on the standard formulation using a Tikhonov regularization and the generalized minimal residual algorithm [Ramanathan 2003]. Clinicians can use the activation maps from the CardioInsight software for diagnosis or therapy planning. In this work, we used these activation maps to evaluate our personalisation algorithm.

For patient 5 the precise geometry of the heart was extracted using Magnetic Resonance Imaging (MRI), allowing us to segment properly the myocardium. In addition, delayed contrast enhancement MRI (DCE-MRI) was also acquired and a scar region was segmented (patient 5 has a non-ischemic cardiomyopathy, NICM). The other patients with recorded BSPM did not undergo MRI as they were already implanted (Table 2.1). We used this patient to evaluate the effects of the precise myocardium geometry and the presence of scar tissue.

### 2.3.2.2 Pre-processing

For Patient 5, the myocardial mesh was generated using the VP2HF<sup>6</sup> platform and the VP2HF meshing pipeline [Groth 2012] creating a tetrahedral mesh with roughly 150K elements. The scar was semi-automatically segmented by a clinician and registered to the myocardial mesh. We imposed the scar tissue to have no reaction term in the Mitchell-Schaeffer model by setting much higher values of  $\tau_{in}$  and  $\tau_{out}$  (cf. Eq. 1.1) and a small conduction velocity of  $0.2m/s$ . We manually rigidly registered this volumetric mesh to the epicardial surface extracted from the CT scanner. For other patients, as no precise geometry was available a generic volumetric myocardial mesh of roughly 65K tetrahedra was manually registered to the CT image. Even if the shape of the myocardium is generic, its orientation, its position and its size is patient-specific.

### 2.3.2.3 Error on Onset Activation Location

Figure 2.9 shows for the 5 patients the Euclidean distance between the onset activation location and the true pacing lead. For all patients, 3 iterations were necessary and the mean improvement in terms of localization error was 2mm. The CardioInsight onset location is constrained to lie on the CardioInsight epicardial mesh whereas our method constrain it to lie on the volumetric mesh (but often generic), so both models include geometry uncertainties. The *MDE* for both LV and RV pacings were found at  $24.6(std = 11.9)mm$  for our personalisation results, and  $39.3(std = 15.8)mm$  for the CardioInsight inverse solution. Patient 2 has very poor data quality (obese person with 20% of torso sensors disconnected and located in the sensitive zone) explaining the poor result in terms of localization by the personalisation (43mm for RV/LV) as well as by CardioInsight (RV:62mm, LV:52mm).

<sup>6</sup>VP2HF is a European Seventh Framework Program, <http://www.vp2hf.eu>

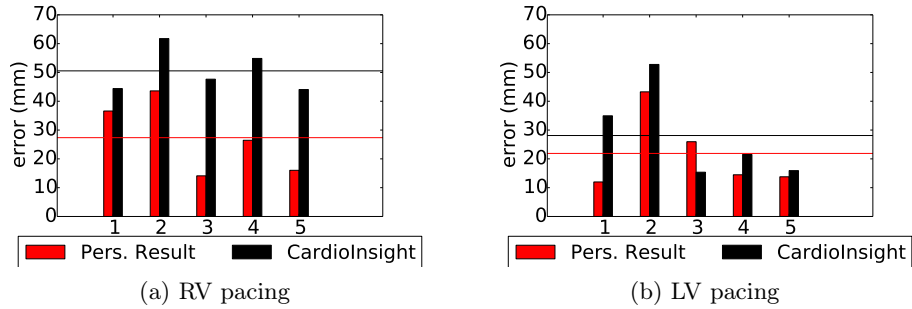


Figure 2.9: CRT patients. Error distances of estimated onset location to the true pacing lead position for every patient. Comparison of the proposed personalisation (red) to the CardioInsight inverse solution (black). The means (*med*) are represented by the lines.

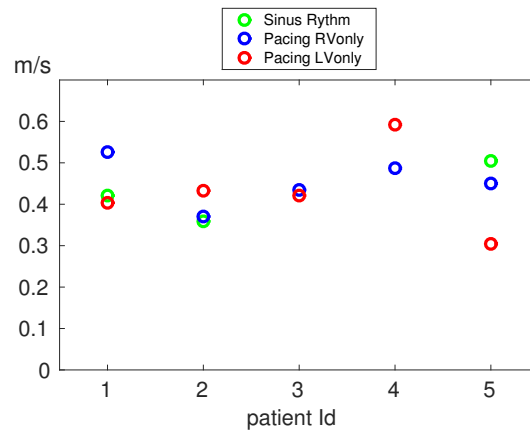


Figure 2.10: CRT patients. Estimated conduction velocity for every patient, using the LV pacing (red), the RV pacing (blue) and the sinus rhythm (green) when available.

### 2.3.2.4 Results on Conduction Velocity

The estimated CV could not be quantitatively evaluated because the ground truth is not available but we can look at the coherence between several acquisitions with different pacing conditions for the same patient. Figure 2.10 shows the CV values for the sinus rhythm, the LV pacing and the RV pacing. We can see that based on a broad range of possible values (uniformly in  $[0.2, 1.5]$ m/s), all CVs lie within a clinically acceptable range ( $[0.29, 0.62]$ m/s) [Durrer 1970]. Moreover, the global CV found with different pacing locations on the same patient are usually in good agreement.

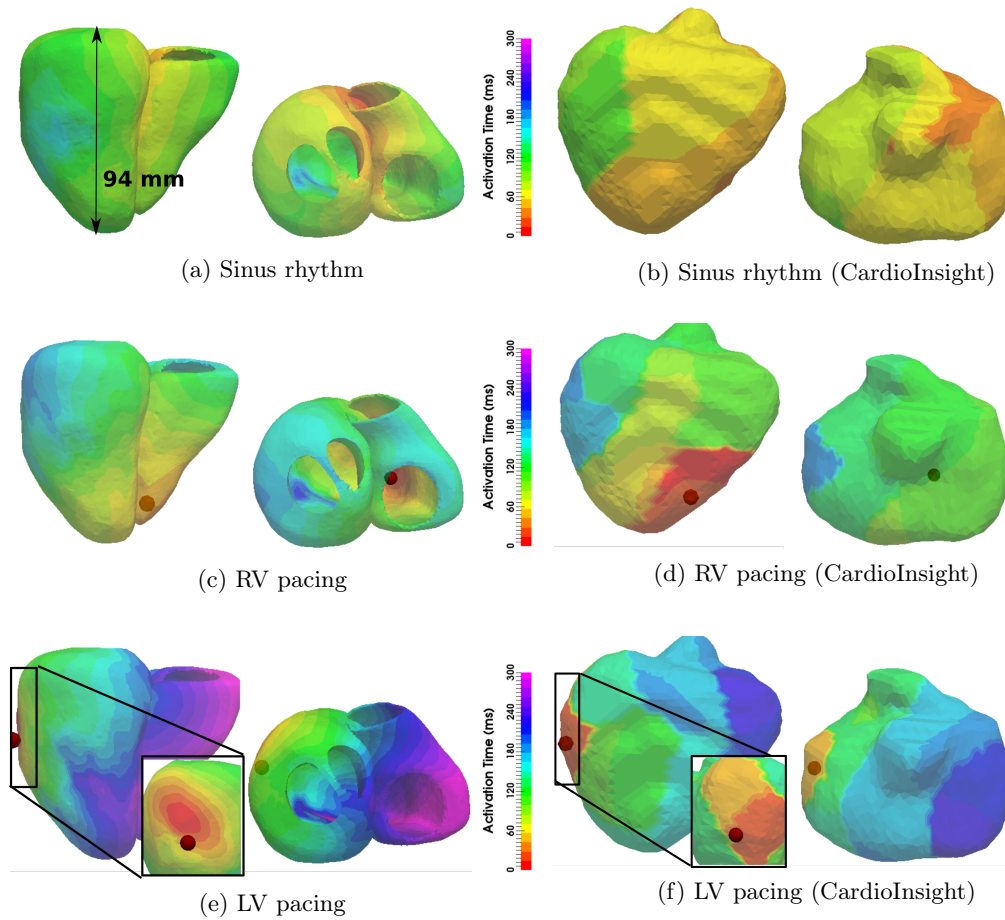


Figure 2.11: CRT Patient 5 activation maps, the red dot corresponds to the true pacing lead position. (a)(c)(e) Our personalisation result (transmurular), (b)(d)(f) CardioInsight solutions (epicardial). (a)(b) Sinus rhythm, (c)(d) RV pacing and (e)(f) LV pacing.

### 2.3.2.5 Comparison of the Estimated Activation Maps

Figures 2.11a, 2.11c, 2.11e show for Patient 5 the estimated transmural activation maps obtained after our personalisation for the sinus rhythm, the RV pacing and the LV pacing. The red dot indicates the true pacing lead position as segmented from the CT scanner. The early activation zones were found near the true pacing lead. We are also showing the CardioInsight epicardial solution (Figures 2.11b, 2.11d, 2.11f). If the comparison shows a good agreement, on this case our personalisation gives a more precise solution. For example, we can see that the sinus rhythm onset was found on the septum, which is not visible in the CardioInsight solution.

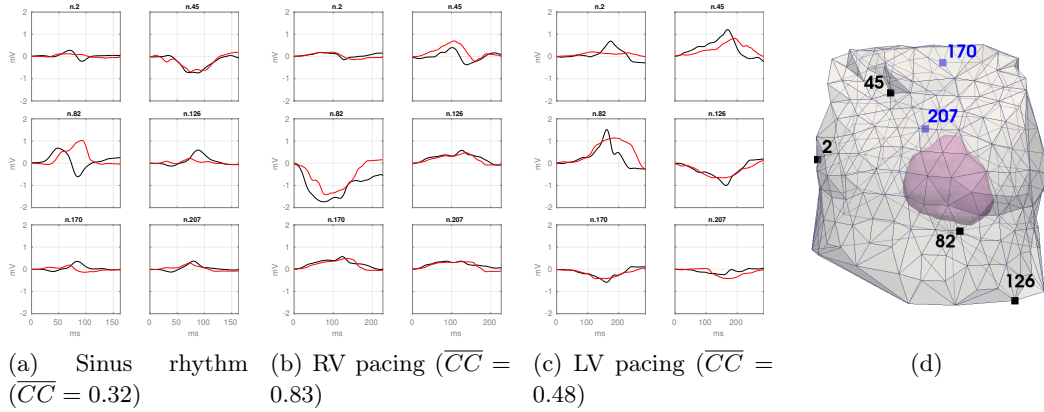


Figure 2.12: CRT Patient 5. Example of 6 BSPM sensors of the QRS measured (black) and personalised (red) in mV per ms. (a) Sinus rhythm (b) RV pacing only (c) LV pacing only. The averaged correlation coefficient are indicated below. (d) Locations of the 6 chosen BSPM sensors, the blue ones are on the back.

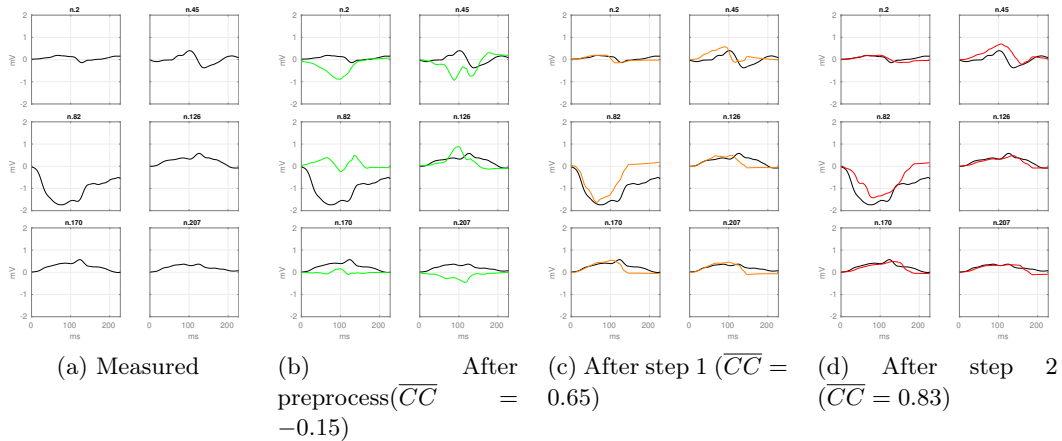


Figure 2.13: CRT Patient 5. Example of 6 BSPM sensors for the RV pacing in mV per ms. (black) QRS measured. (green) Pre-processing: simulated QRS using patient-specific geometry with random onset location. (orange) Step 1: simulated QRS after activation onset location estimation. (red) Step 2: simulated QRS after CV estimation. The averaged correlation coefficient are indicated below.

### 2.3.2.6 Results in terms of BSPM signals

The simulated and the measured BSPMs of patient 5 are represented in Figure 2.12 for 6 sensors uniformly chosen. The simulated BSPM has been scaled by its total norm and multiplied by the measured BSPM total norm. We calculated for each recording the averaged CC between measured and estimated BSPM. We can see a good agreement for the RV pacing and the LV pacing, while the signals of the sinus rhythm are more difficult to reproduce for this patient ( $\overline{CC} = 0.32$ ). It may be due to the fact that this sinus rhythm sequence is complex (presence of scar, possibly multiple onsets). For the two other sinus rhythm personalisations (patients 1 and 2) we found a better agreement with a  $\overline{CC}$  of 0.58 and 0.62. Figure 2.13 depicts the evolution of the estimated signal during the different steps of our personalisation for the RV pacing. The averaged CC is improved after each step (from -0.15 to 0.83).

### 2.3.3 Prediction of Stimulation Results from Personalised Model

While our approach does provide an activation map of the myocardium, the main aim of this personalisation is to benefit from the predictive power of the underlying forward model. We therefore tested in this section how well the personalised models could predict different pacing conditions. To this end, we used the CV results of our personalisation from the sinus rhythm (estimated in section 2.3.2.4) to simulate biventricular pacing (when the sinus rhythm was not available, we took the mean of the LV pacing and RV pacing). In the clinical procedure several types of biventricular pacings were tested by changing the timing between the two stimuli. The 3 classical combinations are: simultaneous pacings; LV stimuli ahead by 40 ms (LV40); RV stimuli ahead by 40 ms (RV40). Results are shown on Figure 2.14 for the RV40 of Patient 5 and for the LV40 of Patient 4, indicating a reasonably correct prediction in terms of BSPM shape, timings and averaged CC.

## 2.4 Discussion

### 2.4.1 Quantifying the Impact of a Precise Myocardial Geometry

Only the data from Patient 5 of the CRT database included MRI and thus allowing a precise myocardial segmentation. For other patients, a generic heart mesh was rigidly registered and scaled to the myocardial shape from a CT scanner with important artifacts. In this section we want to quantify the impact of a precise myocardial geometry to our personalisation results in terms of onset location and errors on BSPM. The results of patient 5 using the MRI segmentation were compared to the results using the generic heart manually rigidly registered and scaled to the same location. Since Patient 5 has a scar segmentation available (see Section 2.3.2.2), the scar region was also mapped to the generic heart mesh. From Figure 2.16, the onset location was found to be less accurate with the generic mesh for the LV pacing (error is 43.4mm for the generic heart, 13.7mm for the MRI segmentation) as well as for the RV pacing (24.3mm for the generic heart, 16.0mm for the

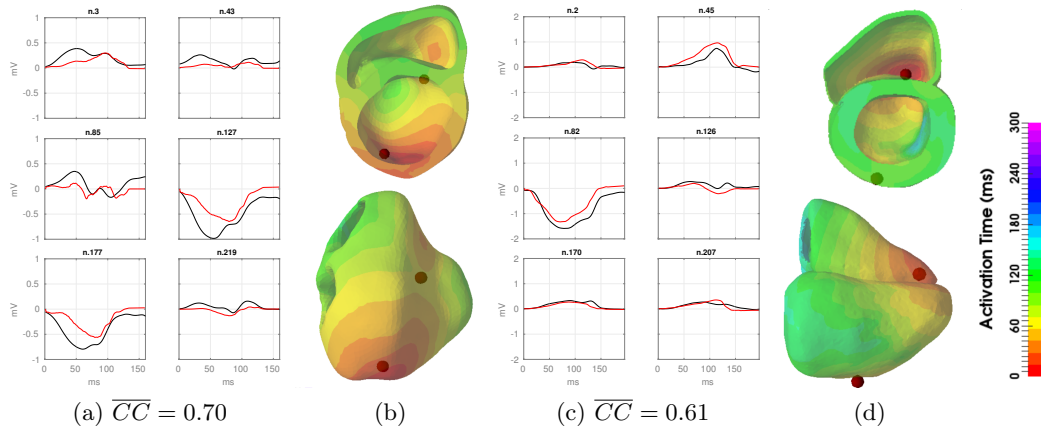


Figure 2.14: CRT Patients 4 and 5: predictions. (a)(b) Patient 4: biventricular pacing with LV lead ahead by 40ms, using the parameters estimated by our personalisation of the LV only and RV only. (a) example of 6 BSPM sensors of the QRS measured (black) and estimated (red). (b) activation map (generic mesh). (c)(d) Patient 5: biventricular pacing with RV lead ahead by 40ms, using the parameters estimated by our personalisation of the sinus rhythm. (c) example of 6 BSPM sensors of the QRS measured (black) and estimated (red). (d) activation map. The red dots corresponds to the true pacing lead positions.

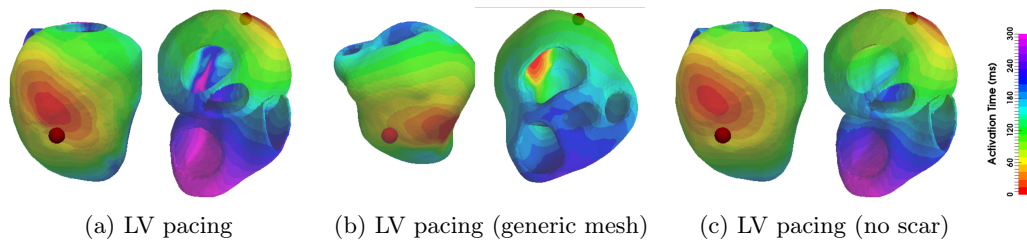


Figure 2.15: CRT Patient 5 estimated activation maps for LV pacing, the red dot corresponds to the true pacing lead position. (a) Result with a personalized geometry and scar (same as Figure 2.11e), (b) result with a generic geometry and scar, (c) result with a personalized geometry but no scar.

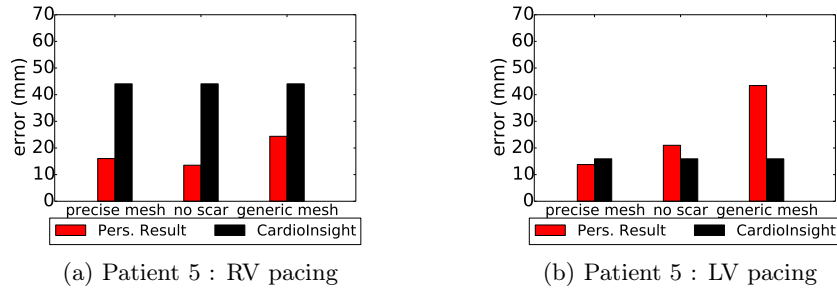


Figure 2.16: CRT patient 5. Onset location distance error. Result with a personalised geometry and scar, result with a personalised geometry but no scar and result with a generic geometry and scar.

MRI segmentation). The activation map using the generic mesh for the LV pacing can be seen in Figure 2.15b. We can notice that the estimated onset locations using a generic heart are still in an acceptable error range. We can conclude that a patient-specific geometry leads to a more accurate personalisation while the use of a generic mesh is still a fair approximation on this case.

### 2.4.2 Modelling Scar Tissue: Its Impact on our Personalisation

The 6 patients from both datasets were identified as non-ischemic. However, patient 5 has a NICM with an annotated scar from DCE-MRI. In the presence of scar tissues we suppress the reaction term in the Mitchell-Schaeffer model and reduce the conductivity of the tissues to  $0.2m/s$ . In order to measure the impact of a scar on the personalisation process, we compared in Figure 2.16 the precision obtained with and without the scar information. We can see that including the scar information yields better results for the LV pacing, where the pacing lead is closer to the scar region (see Figure 2.15c for the estimated activation map). By incorporating some structural information, we were able to improve the personalisation results. However, as the scar information is not always available we believe that it could be learned directly through the personalisation process, by detecting regions where the conductivity has to be locally reduced.

### 2.4.3 Future Works

In this chapter, we have been estimating the parameters of singular pacing sites and predicting the response to multiple pacings. The natural extension of this study is the estimation of the location of more than one activation site (Chapter 3). Another goal is to help the clinicians in predicting the best combination and the best lead locations among the possible and reachable zones before the implantation. As the work by Swenson et al. [Swenson 2011] reveals the importance of the cardiac position in the ECG forward problem, we believe that a more precise registration of the myocardial mesh to the CT scanner would have a positive impact. Finally,

in this chapter we did not include a Purkinje system model as most of the patients have bundle branch blocks, but we believe it to be also interesting (see Chapter 5). To account for more drastic variations of onset and conductivities, it is needed to use advanced non-linear dimensionality reduction techniques (see Chapter 3 and Chapter 4). Even if the current difficulty of the personalisation is to understand and model to complex pathologies, we do think that it could help the analysis of ECGI because the problem is more physiologically constrained.

## 2.5 Conclusion

From non-invasive measures including BSPM signals, we were able to personalise the location of the onset activation location and the global conduction velocity of the myocardium with a two-step algorithm. We built a large database of simulated BSPM in order to train a machine learning algorithm based on a few QRS shape-related features from each BSPM sensor. The simulated BSPM relies on a transmural forward model based on the Mitchell-Schaeffer model and a current dipole formulation. We validated our approach on a PVC localisation ( $MDE = 20.3mm$ ), on 29 runs from 7 pacing sites by catheter ( $MDE = 21.6mm$ ) and on 10 different pacing sequences from 5 CRT patients ( $MDE = 24.6mm$ ). A comparison with two standard inverse methods revealed that our personalisation provides comparable results. We also showed that we were able to predict the response to biventricular pacings based on our personalised models with concordance in the BSPM signals. Finally, we showed on limited cases that personalised scar and myocardial geometry improved the results. This is an encouraging first step towards a pre-operative prediction of different pacing conditions in order to assist clinicians for CRT decision and procedure.

The adaptation of this work to 12-lead ECG data was tested and reported in Section 5.3.

# Sparse Bayesian Non-linear Regression for Multiple Onsets Estimation in Non-invasive Cardiac Electrophysiology

---

## Contents

---

<b>3.1</b>	<b>Introduction</b> . . . . .	<b>48</b>
<b>3.2</b>	<b>Materials and Methods</b> . . . . .	<b>49</b>
3.2.1	Clinical Data . . . . .	49
3.2.2	Non-invasive Personalisation of a Cardiac EP Model . . . . .	49
3.2.3	Dimensionality Reduction of the Myocardial Shape . . . . .	49
3.2.4	Parameter Estimation using Relevance Vector Regression . . . . .	51
<b>3.3</b>	<b>Application to the Personalisation of a Simultaneous Biventricular Pacing</b> . . . . .	<b>51</b>
3.3.1	Simultaneous Biventricular Pacing Personalisation . . . . .	51
3.3.2	Results . . . . .	53
3.3.3	Evaluation on 3 Other Patients . . . . .	55
<b>3.4</b>	<b>Discussion</b> . . . . .	<b>55</b>
<b>3.5</b>	<b>Conclusion</b> . . . . .	<b>56</b>

---

This chapter is based on the following paper:

**Sparse Bayesian Non-linear Regression for Multiple Onsets Estimation in Non-invasive Cardiac Electrophysiology**, *Sophie Giffard-Roisin, Hervé Delingette, Thomas Jackson, Lauren Fovargue, Jack Lee, Aldo Rinaldi, Nicholas Ayache, Reza Razavi, and Maxime Sermesant*. In Functional imaging and modelling of the heart (FIMH) 2017 Proceedings, Toronto, Canada, June 2017.

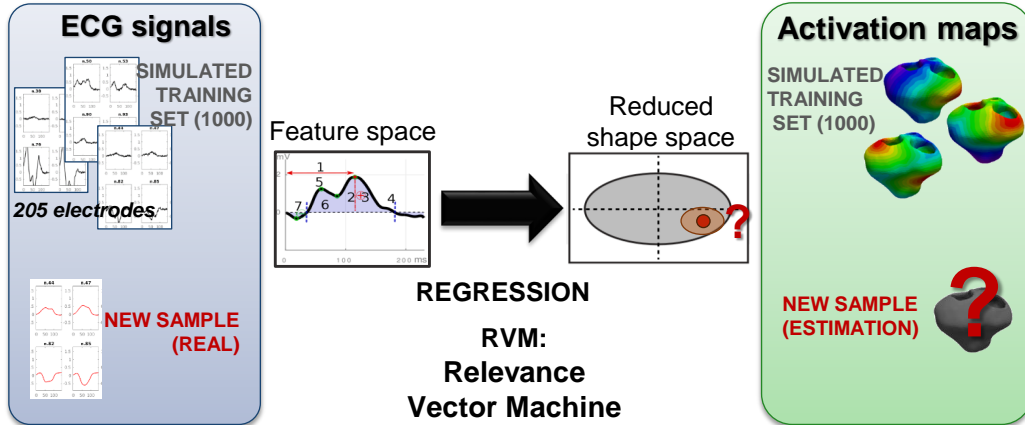


Figure 3.1: Chapter 4 pipeline: The RVM (relevance vector machine) regression is performed between BSPM features and a reduced shape space where the patient-specific training activation maps were projected. For a new sample (BSPM data) we estimated its activation map and the regression error. In this paper, the onset locations were further extracted from this estimated activation map.

### 3.1 Introduction

We personalised in Chapter 2 the cardiac EP model from body surface potential mappings (BSPM). The onset activation location and the global conduction velocity were estimated in different pacing locations from several patients. However, personalisation may often be needed in more complex situations, such as multiple activation onsets, heterogeneous myocardial tissue (scar) or a particular pathology. Estimation of heterogeneous myocardial conduction using a Bayesian framework has been explored by [Dhamala 2017a], but the other parameters such as the onset are supposed to be known, and the uncertainty on the result is not estimated. The problem of uncertainty in the field of cardiac EP model parameter estimations is very recently raising interests, for example using Gaussian Process-Based Markov Chain Monte Carlo [Dhamala 2017b].

The contributions of this chapter are the extension of a cardiac EP personalisation in order to handle non-linear situations (from single to multiple onsets) and to acquire information relative to the confidence on the results. The methodology, based on a relevance vector regression and on a myocardial shape dimension reduction, is tested and compared with the method from Chapter 2 ([Giffard-Roisin 2017b]) on four real biventricular pacing datasets. The methodology is summarized in Figure 3.1.

## 3.2 Materials and Methods

### 3.2.1 Clinical Data

In this study, we considered a patient dataset composed of BSPM signals, ventricular myocardial geometry (since only the QRS complex is studied, the atria were not included in the model), torso leads and pacing leads locations. The BSPM potentials (from a CardioInsight jacket) were acquired during the procedure at a sampling rate of 1kHz, with a number of torso sensors of 205. The protocol of this study was approved by the local research ethics committee. The approximated myocardial surface as well as the location of the torso sensors and the pacing leads were extracted from 3D imaging (CT scanner). On a rigidly registered generic and volumetric mesh, cardiac fiber orientations were estimated with a rule-based method (elevation angle between  $-70^\circ$  to  $70^\circ$ ).

### 3.2.2 Non-invasive Personalisation of a Cardiac EP Model

We used a fast forward EP model derived from the anisotropic Mitchell-Schaeffer cardiac model and a current dipole formulation for computing simultaneously the cardiac electrical sources and body surface potentials (see Chapter 2). From the generation of a large database of simulated transmural myocardial potentials and torso signals, we learned patient-specific parameters of the EP cardiac model. In order to retain the important aspects of the QRS complex from the BSPM signals, specific descriptors on the normalized BSPM signals were extracted (such as timings, area under the curve, sign of extremum). Specifically, the location of the onset activation was estimated by firstly regressing the activation times of the transmural myocardial mesh, before localizing the minimal time. Every simulated set of BSPM signals  $v_i$  was perturbed by a Gaussian random noise of mean 0 and  $std = 2e - 3 \times norm(v_i)$ . This was done for robustness and in order to give more confidence to electrodes closer to the heart: where the potentials are of higher amplitude, the signal-to-noise ratio would be larger.

### 3.2.3 Dimensionality Reduction of the Myocardial Shape

The myocardial tetrahedral mesh can have a large number of elements or vertices. At the same time, the signal to be reconstructed, the activation map, is strongly correlated spatially due to the propagation of the electric potential throughout the myocardium. Therefore, it is meaningful to reduce the dimension of the regression variable, the activation times. A simple way would be to use a coarser mesh but this would be at the expense of reducing the accuracy of the onset locations. Instead, we propose to use a hierarchical decomposition of the mesh, naturally provided by the eigenmodes of a structural matrix. To this end we chose the eigen-decomposition of the stiffness matrix associated with the Laplacian operator. This decomposition has been widely used in various spectral shape analysis [Reuter 2005, Umeyama 1988] and is closely related to the modes of vibration of the myocardium. The extracted

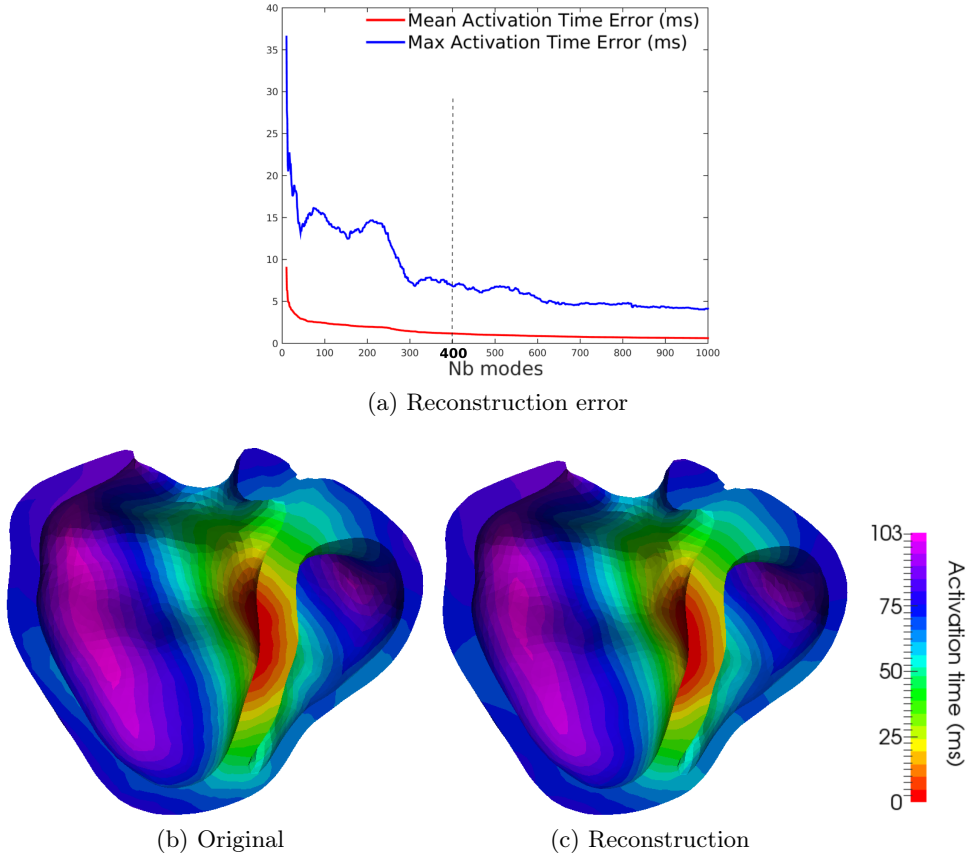


Figure 3.2: Example of reconstruction of an activation map (on 14430 vertices) from the eigenvectors of the stiffness matrix: (a) Reconstruction error wrt. the number of modes (b) original activation map (c) reconstructed activation map from 400 modes.

eigenvectors are naturally sorted by ascending order to spatial frequency. By selecting the first few eigenmodes, we only keep the large spatial variations. If we call  $\mathbf{t}$  the vector of  $N$  activation times at each vertex of the myocardial mesh, we get the following reduction and reconstruction formulas:

$$\mathbf{t}_{red} = \mathbf{V}_M \mathbf{t} ; \mathbf{t}_{rec} = \mathbf{V}_M^T \mathbf{t}_{red}$$

with  $\mathbf{t}_{red}$  the coordinates of  $\mathbf{t}$  in the reduced space,  $\mathbf{V}_M$  the  $N \times M$  matrix of the first  $M$  eigenvectors of the stiffness matrix, and  $\mathbf{t}_{rec}$  the reconstructed activation times. The matrix  $V_M$  is independent of  $\mathbf{t}$  and is thus computed only once. An example of reconstructed activation map (on 14K vertices) using 400 modes is shown in Figure 3.2c. From Figure 3.2a, we can see that the mean reconstruction error is less than 2 ms (max: 7 ms) for 400 modes. Finally, in Figure 3.3 are represented the first three modes of the cardiac shape together with the mode n. 100. We can see that the first modes capture global variations while mode n. 100 captures more local variations.

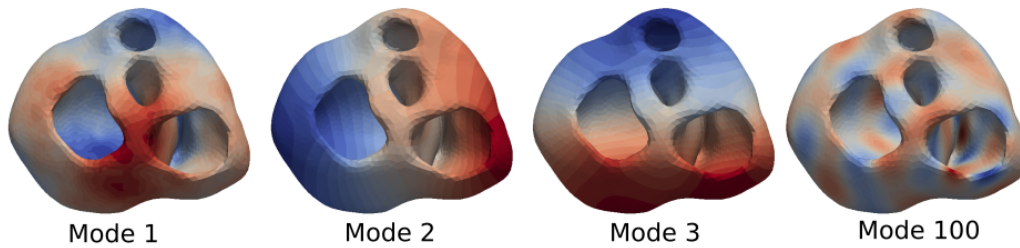


Figure 3.3: Shape modes 1, 2, 3 and 100. We can see that the first modes capture global variations while mode n. 100 captures more local variations.

### 3.2.4 Parameter Estimation using Relevance Vector Regression

In order to regress the myocardial activation times from the BSPM features, we use the Relevance Vector Machine (RVM) regression method [Tipping 2003]. This approach performs sparse kernel regression based on a sparsity inducing prior on the weight parameters within a Bayesian framework. Unlike the commonly used Elastic-Net or Lasso approaches (based on L1 Norm a.k.a Laplace prior), the RVM method does not require to set any regularization parameters through cross-validation. Instead, it automatically estimates the noise level in the input data and performs a trade-off between the number of basis (complexity of the representation) and the ability to represent the signal. Furthermore, unlike SVM regression or Elastic-Net, it provides a posterior probability of each estimated quantity which is reasonably meaningful if that quantity is similar to the training set. In our setting, we used Gaussian kernels for the non-linear regression whose variance of the kernel parameters need to be defined. The RVM regression only selects the input BSPM feature set that can best explain the activation map in the training set, thus limiting the risk of overfitting. For more details on the relevance vector regression, please refer to Section 1.3.5.6. RVM is a multivariate but single-valued approach and therefore the regression was directly performed on the reduced space of section 3.2.3: only 400 regressions are needed to perform an estimation of the 14K activation times. We used a Gaussian radial basis function with a kernel bandwidth of  $1e4$  (from cross-validation). On an EliteBook Intel Core i7, a regression of 1000 training samples and 1235 features runs in 40 sec.

## 3.3 Application to the Personalisation of a Simultaneous Biventricular Pacing

### 3.3.1 Simultaneous Biventricular Pacing Personalisation

We consider here a non-ischemic implanted CRT patient that underwent a pacing lead optimization procedure with a BSPM device. In particular, the 205 working torso electrodes recorded a biventricular simultaneous pacing. The anatomy as well as the location of the torso sensors and the pacing leads were extracted from

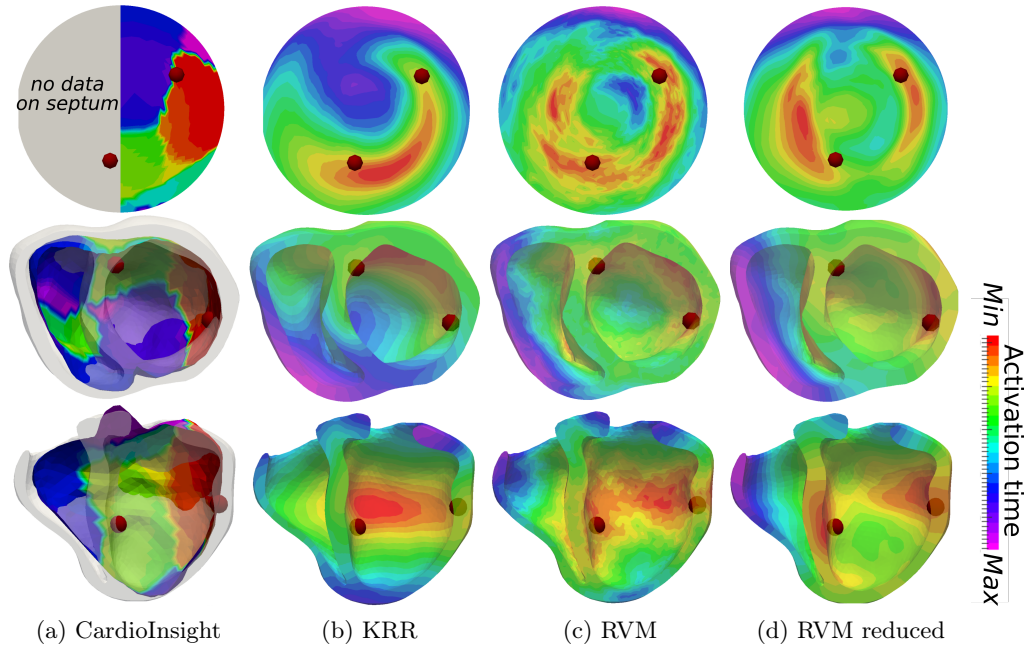


Figure 3.4: Results for locating both onsets: ground truth lead locations are the red dots. (a) CardioInsight inverse solution (b) kernel ridge regression activation map result (c) relevance vector regression separately for the 14K vertices (d) relevance vector regression on 400 modes of the reduced space. The color maps are showing short activation times (red) to large ones (purple). On top: flattened representation of the left endocardium in the conventional orientation (i.e. anterior on top).

CT images. Because of important artifacts coming from the pacemaker, only a coarse epicardial geometry of the myocardium is visible. That is why a generic volumetric myocardial mesh of roughly 65K tetrahedra was manually registered and scaled to the epicardial geometry. The CardioInsight Technologies software also solves the inverse problem on this epicardial surface (based on the standard formulation using a Tikhonov regularization and the generalized minimal residual algorithm), see Figure 3.4a. In this work, we used this activation map as part of the evaluation of our method. From this simultaneous pacing, we want to retrieve the two onset locations. Locating both activation onset locations by means of an EP model parameter estimation has first been studied by He et al. [He 2002], but only on synthetic data. For this particular goal, our simulated training set was composed of 1000 simulations with fixed conduction velocity ( $0.5m/s$ ) and with two onset locations randomly selected on the surface of the myocardial mesh (endocardium and epicardium).

### 3.3.2 Results

We compare here the results of the activation map regression of (i) the Kernel Ridge Regression from Chapter 2, (ii) the RVM regression independently on each point of the cardiac mesh and (iii) the RVM regression using the reduced shape space (Figure 3.4). The two ground truth onset locations (pacing sites) are the red dots. On top is the flattened representation of the left ventricular endocardium, where the apex is at the center [Soto-Iglesias 2016]. The activation map provided by the CardioInsight system on the coarse surface mesh is shown in Figure 3.4a. Although this map is not precise and cannot be used as a ground truth, it gives an idea of the wave shape. We can see that the kernel ridge regression acts as a blurry mixture of both initializations, not able to separate them. The RVM regression performed on each vertex captures the two onset zones, but the resulting activation maps are noisy and the two minimal values are not easy to capture. The error distances to the true pacing leads are 31.7 mm (left lead) and 41.2 mm (right lead). On the other hand, the RVM performed on the reduced space captures two onset locations with an error distance of less than 23mm for both leads, while having a smooth solution. The mean number of relevance vectors retained was 213 (out of 1000 samples).

The RVM provides the result as a Gaussian probability distribution, where the retained solution of each regression was the mean. By looking at the estimated variance across each mode, we can estimate the confidence on our result. On Figure 3.5 are plotted the projections on the first spectral modes of the simulated activation maps (training set) as well as the estimated solution. We have also represented the confidence interval (+/- standard deviation, std). First, we can see that the retained sample lies inside the training set point cloud, which is important for RVM to perform well. We have projected the point-wise estimated std onto the myocardial mesh (Figure 3.6a) where we can see that all the vertices from the left ventricle have an estimated std below 17ms (and below 14 ms for the septum). Although higher values (max: 28.9 ms) are found in the right ventricle, we can notice that the estimated activation times from this region were greater than 100 ms.

However, the confidence on the activation times is not sufficient to quantify the onset location error. This is why we additionally randomly sampled 10K coordinates from the estimated Gaussian distribution in the reduced space (see red ellipsoid from Figure 3.5). We then reconstructed the activation maps for each one of them and retrieved their minima as estimations of left and the right onsets (see Figure 3.6b for the right onset). For the most probable location, the distance error to the ground truth location was 12.3mm for the left lead and 24.5mm for the right lead. The standard deviation of the error was 18mm for the left onset and 11.4mm for the right onset. We can notice that the left onset was located more accurately, however with less confidence.

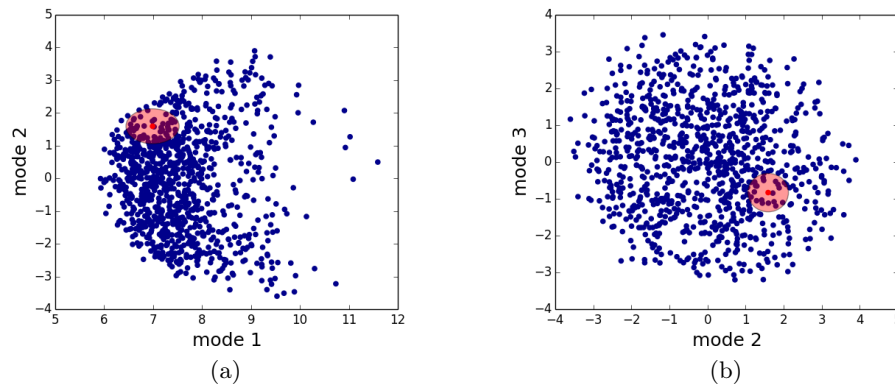


Figure 3.5: Confidence interval in the reduced space (+/- std): (a) projection on modes 1 and 2 (b) projection on modes 2 and 3. blue dots: projection of the 1000 simulated activation maps used for training. Red dot: estimated activation map.

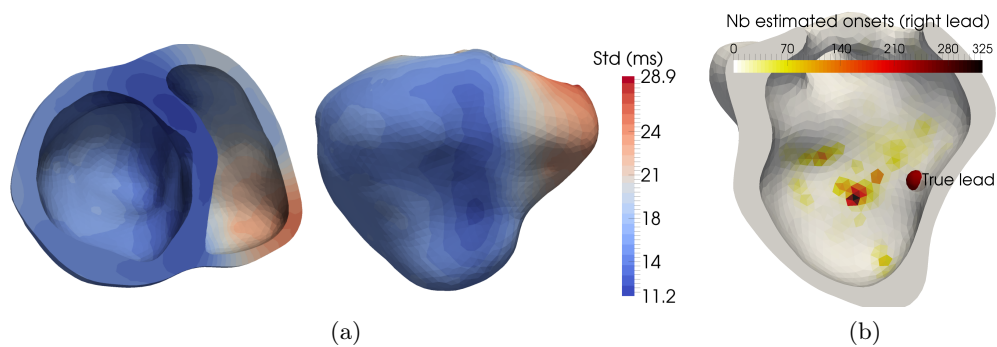


Figure 3.6: (a) Standard deviation (std) of the estimated activation time, in milliseconds. All the points in the left ventricle have an estimated std below 17 ms. (b) Locations of the right onset when randomly sampling the estimated Gaussian distribution of the reduced space (10K samples).

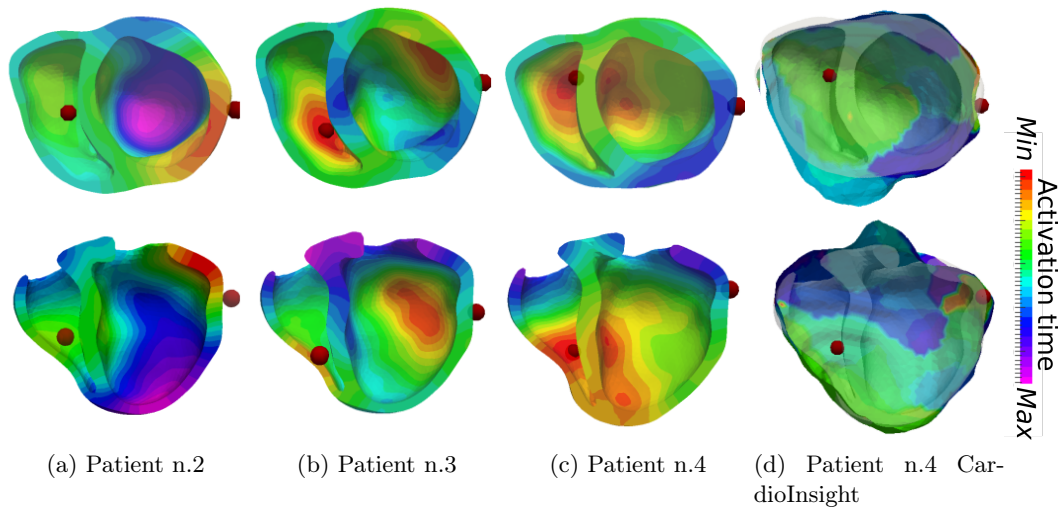


Figure 3.7: (a)(b)(c) Results for locating both onsets on 3 other patients: ground truth lead locations are the red dots. (d) CardioInsight inverse solution for patient n.4 where late activated zones are visible near the LV pacing lead (probably scar). The color maps are showing short activation times (red) to large ones (purple).

### 3.3.3 Evaluation on 3 Other Patients

We have evaluated our onset estimations on 3 other patients with the same clinical and same processing protocols. The generic cardiac geometry was also used for these patients. We can see in Figure 3.7 the mean estimation of the RVM for the 3 patients. All activation onsets seem to be captured, with a clear exception for the patient n.4, where only one onset was captured (the RV onset, on the left). By looking at the CardioInsight inverse solution for patient n.4 in Figure 3.7d, we can notice that the LV pacing site seem to be surrounded by very late activated zones, probably damaged or scar tissue.

## 3.4 Discussion

The presented method holds several limitations. One current limitation of the RVM regression is the fact that it only performs multivariate regression of a single output scalar value but not of a vector value (unlike KRR for instance) although multivalued versions have been recently proposed [Le Folgoc 2017]. Concerning the reconstruction from the reduced space, we also tested it with sharp edges in the activation map, like scar tissue blocking the activation wave. Despite higher errors of activation times in the scar, the boundaries of the scar were well captured so we can extend our method to ischemic patients. As seen in Figure 3.7c and Figure 3.7d, this extension is necessary for scarred patients.

The estimations of the covariance matrix of the activation map are provided as a by-product of the RVM regression, giving an estimation of the regression error.

However, other sources of error may be taken into account in order to have a full apprehension on the confidence of the result. We think it is the reason why the cloud of possible onsets of Figure 3.6b did not exactly include the true lead. If the torso sensors were well localized by the CT scan, we had to use a generic mesh because no precise myocardial shape was available. We would like to test our method on patient-specific myocardial meshes which will also help in modelling the error source when using generic meshes. Regarding the errors coming from the BSPM data, they were considerably reduced by the fact that the disconnected or bad leads were automatically excluded, and that we added some Gaussian noise to our simulated BSPM for robustness. Finally, we should also evaluate the EP modelling errors, for instance by analyzing the discrepancy between the true and simulated BSPM signals.

This new method has been tested on only 4 patients so more experiments are needed for its validation. As a future work, we want to exploit the generic properties of this approach to robustly estimate additional cardiac parameters, like the (local) conduction velocity for instance (see Chapter 4).

### **3.5 Conclusion**

In this chapter, we presented a new methodology for multiple onset estimation from BSPM and applied it to 4 clinical datasets. This was integrated in a novel framework for the personalisation of cardiac EP parameters from BSPM data. This method relies on the generation of a simulated patient-specific database on which a relevance vector regression estimates the activation map from a new set of BSPM signals. As input, specific shape-related features were extracted from the BSPM. As output, the activation map was projected onto a reduced space defined from myocardial shape oscillations. This pipeline enables the estimation of parameters in more complex situations, as the example presented here with the location of two onsets from a real biventricular pacing BSPM sequence. This method could be useful for a generalization of cardiac EP personalisation, one of the advantages being the confidence on the regression provided by the RVM.

# Learning Relevant ECGI Simulations on a Reference Anatomy for Personalised Predictions of CRT

---

## Contents

<b>4.1</b>	<b>Introduction</b>	<b>58</b>
4.1.1	EP Model-based Inverse Problem of Electrocardiography	58
4.1.2	Reference Anatomy in ECGI	59
4.1.3	Contributions	59
4.1.4	Outline of the Chapter	60
<b>4.2</b>	<b>Materials and Methods</b>	<b>60</b>
4.2.1	Clinical Data	60
4.2.2	BSPM Reference Anatomy	62
4.2.3	Offline Simulated Common Database	63
4.2.4	Relevance Vector Regression for SR Sequence Personalisation	65
<b>4.3</b>	<b>Personalisation Results and Pacing Predictions</b>	<b>69</b>
4.3.1	Projections on the Reduced Shape Space	69
4.3.2	Estimated Sinus Rhythm Activation Maps	69
4.3.3	Pacing Predictions Results	71
<b>4.4</b>	<b>Discussion</b>	<b>74</b>
4.4.1	Reference Anatomy	74
4.4.2	Estimating conduction velocity from activation times	75
4.4.3	Estimating the uncertainty	75
4.4.4	AV node Activation	76
<b>4.5</b>	<b>Conclusion</b>	<b>76</b>

---

This chapter is based on the following paper:

**Learning Relevant ECGI Simulations on a Reference Anatomy for Personalised Predictions of Cardiac Resynchronisation Therapy**, *Sophie Giffard-Roisin, Hervé Delingette, Thomas Jackson, Jessica Webb, Lauren Fovargue, Jack Lee, Christopher A. Rinaldi, Reza Razavi, Nicholas Ayache and Maxime Sermesant*. To be published.

## 4.1 Introduction

As we have seen in Chapter 1, estimating accurately electrophysiological (EP) patient-specific model parameters is crucial for treatments such as cardiac resynchronization therapy, and it often involves invasive measurements [Sermesant 2012]. In order to replace these invasive measurements -at risk for the patient-, some studies proposed to personalise the cardiac EP model from body surface potential mappings (BSPM) [Li 2001, Giffard-Roisin 2017b, Dhamala 2017a]. In one of them [Giffard-Roisin 2017b], the onset activation location and the global conduction velocity were estimated in different pacing locations for several patients using a patient-specific simulated training set. However, personalisation may often be needed in more complex situations, such as multiple activation onsets or heterogeneous myocardial tissue (scar). Besides, such patient-specific methods are time consuming because a large number of model simulations are needed: the total computational time of one model personalisation of Chapter 2 was more than 5 hours on our cluster using parallel computing.

The aim of this article is to develop a reference anatomy model allowing us to perform a common and offline learning. While reducing considerably the computational time of online inference, it also allows to multiply the pathological configurations in the simulated training set as it is built only once. We have thus extended the cardiac EP model personalisation to infarct situations and applied it to a 20 patient database where the BSPM were recorded using the CardioInsight<sup>1</sup> jacket now commercially available. The personalised model was then used to predict the electrical response to CRT.

### 4.1.1 EP Model-based Inverse Problem of Electrocardiography

BSPM data has been widely used in the last decades to directly compute the cardiac action potentials by solving an ill-posed inverse problem: finding the transfer matrix linking the torso potentials to the cardiac potential sources [Pullan 2010]. Some electrocardiographic imaging (ECGI) methods are integrating physiological and model-based priors in a Bayesian framework [Rahimi 2016, Wang 2011]. The work by Li and He [Li 2001] solves the inverse problem by means of heart-model parameters (onset activation location) and was validated with in vivo studies [Liu 2008]. With a known onset activation location, the estimation of heterogeneous myocardial conduction using a Bayesian framework has been recently studied by Dhamala et al. [Dhamala 2017a]. The use of non-invasive personalised cardiac parameters for the prediction of new situations (such as pacing procedures) has been tackled on a few cases only and with a global conductivity parameter in Chapter 2.

---

<sup>1</sup>ECVUE, CardioInsight Technologies Inc., Cleveland, Ohio

### 4.1.2 Reference Anatomy in ECGI

These personalisations of EP cardiac model parameters from BSPM data rely on time-consuming patient-specific computations. Because of the natural similarity of the anatomical structures between patients, a reference anatomy can be used.

One study showed the importance of the interindividual variability (averaged standard deviation) of electrocardiograms (ECG) on 25 healthy subjects [Hoekema 1999]. A large part of this variability is due to the heart position and orientation relative to electrodes. In terms of geometry, the larger variations are found for the heart long axis angle. Swenson et al. [Swenson 2011] also revealed the importance of cardiac angulation in the ECG forward problem. Another study showed that ECG imaging is sensitive to global anatomical parameters such as the heart orientation and location with regard to the lead positions [Huiskamp 1989]. The use of a reference anatomy model, able to represent every patient, is thus a difficult task. Hoekema et al. [Hoekema 1999] showed that by only moving the electrodes in a frontal plane to a common reference, the interindividual variability is not reduced because the heart orientation is not preserved. Another study created a patient-specific adapted torso model by stretching and squeezing a standard torso model according to the measures [Lenkova 2012]. They concluded that it was crucial to adapt both the outer shape of the torso model and the position of electrodes according to reality. Yet, it has been also shown that some adapted ventricle-torso standard model were able to get good ECGI results while excluding local geometrical details [Wang 2010, Rahimi 2015]. To the best of our knowledge, the goals of these geometrical models were only to simplify the anatomical modelling process. However, a study has recently tackled the interindividual variability by separating the factors of variation throughout a deep network using a denoising autoencoder on a large ECG dataset [Chen 2017b] for learning the ventricular tachycardia origin. Inter-subject variations coming from cardiac EP differences and geometry differences are however not separable, so a personalised EP model could not be estimated with this approach.

### 4.1.3 Contributions

The different contributions of this chapter are:

- A novel reference anatomy approach able to easily represent every patient with preserved heart orientation and position with respect to the lead positions. It reduces considerably the computational cost of the personalisation.
- A simulated common database composed of 5 000 heart-torso EP simulations having random parameter values in terms of onsets, global conduction value and scar localisation.
- An EP model-based ECGI technique able to personalise an EP cardiac model from a sinus rhythm BSPM sequence. It is based on a dimensionality reduction of the myocardial shape and a sparse relevance vector regression.

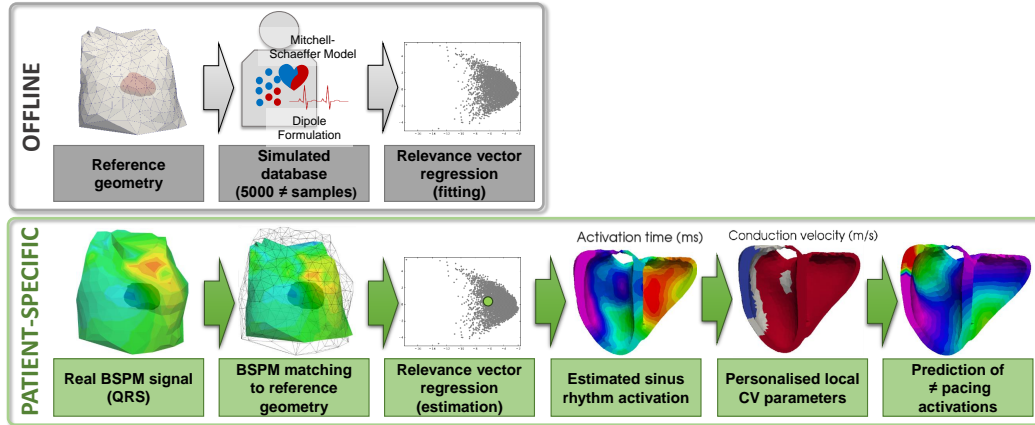


Figure 4.1: Fast model-based prediction pipeline: the database composed of 5000 EP simulations and the activation map regression fitting are common for the 20 patients

- An evaluation on an important database of clinical data composed of 20 patients with a CRT device, and with a comparison to a commercially available ECGI method.
- The simulated predictions of 100 different pacing QRS compared with the measured BSPM and the commercially available ECGI mapping.

#### 4.1.4 Outline of the Chapter

In the following section 2.2 we will present our prediction framework (Figure 4.1): the clinical data, our reference anatomy model, the simulated EP database and the personalisation of the sinus rhythm sequence. Section 4.3 is dedicated to the results and the pacing predictions. Finally, section 4.4 discusses the different aspects of the method.

## 4.2 Materials and Methods

### 4.2.1 Clinical Data

Our 20 patients dataset is composed of BSPM signals, ventricular myocardial geometry, torso leads and pacing leads locations. All patients have dyssynchrony (either left or right bundle branch block) and were implanted with a biventricular pacemaker (see Table 2.1). The BSPM potentials (from a CardioInsight jacket) were acquired at a sampling rate of 1kHz during one QRS complex by 200 to 250 torso sensors. The protocol of this study was approved by the local research ethics committee. The approximated myocardial surface, the location of the torso sensors and the pacing leads were extracted from the 3D CT scanner image. In the stimulation

Table 4.1: CRT patients. Baseline information of the 20 patients treated. *NA* = information not available; *SR* = sinus rhythm sequence available; *LBBB/RBBB* = Left/Right bundle branch block; *ICM/NICM/HCM* = ischemic/non-ischemic/hypertrophic cardiomyopathy; \*: patient #2 was acquired 2 times with a 6-months follow-up.

Id	Age	Gen.	Block type	Aetiology	SR
1	67	M	LBBB	ICM	X
2	72	M	LBBB	HCM	
2 6M*	72	M	LBBB	HCM	X
3	82	M	LBBB	NA	X
4	49	F	LBBB	NICM	X
5	79	M	RBBB	ICM	X
6	87	M	LBBB	NICM	
7	62	M	LBBB	ICM	X
8	87	M	LBBB	ICM	X
9	77	M	LBBB	NA	X
10	69	F	LBBB	NICM	
11	49	M	LBBB	NICM	X
12	62	F	LBBB	NA	X
13	59	M	LBBB	ICM	X
14	82	F	LBBB	NA	
15	76	M	RBBB	NICM	X
16	55	M	LBBB	NA	X
18	49	M	LBBB	NA	X
19	78	M	LBBB	NA	X
20	73	M	LBBB	NA X	
22	71	M	LBBB	NA	X

optimisation procedure, cardiologists performed several recordings corresponding to different pacing combinations and delays between a right ventricular (RV) endocardial and a left ventricular (LV) epicardial pacing leads. For almost all patients, a *LV pacing* alone and a *RV pacing* alone were performed, together with the 3 following biventricular pacings: *simultaneous*, *LV 40ms* (LV lead ahead by 40ms) and *RV 40ms* (RV lead ahead by 40ms). An atrial pacing was active 200ms to 100ms before the ventricular pacings. A *sinus rhythm* sequence was also recorded on patients that do not have complete heart blocks. In total, 120 different settings were studied.

## 4.2.2 BSPM Reference Anatomy

### 4.2.2.1 Transformation to the Reference Anatomy

In this work, every patient  $p$  has a geometry data composed of the 3D biventricular cardiac geometry noted  $c_p$  and  $s_p = \{s_p^j\}_{j=1:N}$  the locations of the  $N$  torso sensors. We define a cardiac and BSPM reference anatomy template  $\{c_T; s_T\}$  with  $s_T = \{s_T^i\}_{i=1:M}$  onto which every patient data will be transformed.

The current dipole approach formulated in the volume conductor theory [Malmivuo 1995] has proven its efficiency in BSPM calculation [Giffard-Roisin 2017b]. The electric potential  $\Psi^v(s_p^j)$  generated by the volume element  $v$  and measured at the torso electrode  $s_p^j$  is based on the scalar product  $(j_{eq}^v, vs_p^j)$  between the equivalent current density  $j_{eq}^v$  of every cardiac volume element  $v$  and the vector directed from  $v$  to the torso electrode  $s_p^j$ . Consequently, the shape of the  $j$ th BSPM signal  $\Psi^v(s_p^j)$  is closely linked to the direction of  $vs_p^j$ . This result is echoing the conclusions of the ECGI sensitivity studies (see section 4.1.2) showing how the ECG signal is sensitive to the heart orientation and location with respect to the lead positions [Huiskamp 1989].

First, we propose to rigidly register the cardiac geometry  $c_p$  to the template  $c_T$  (it is done interactively, as  $c_p$  is only a coarse epicardial surface and  $c_T$  a complete biventricular tetrahedral mesh). We define  $H$  as the center of mass of the template cardiac geometry, and  $HS_T^i$  as the half-line from  $H$  towards the template torso sensor  $s_T^i$ . We propose the following matching between the template electrodes and the electrodes of a new patient  $p$ :

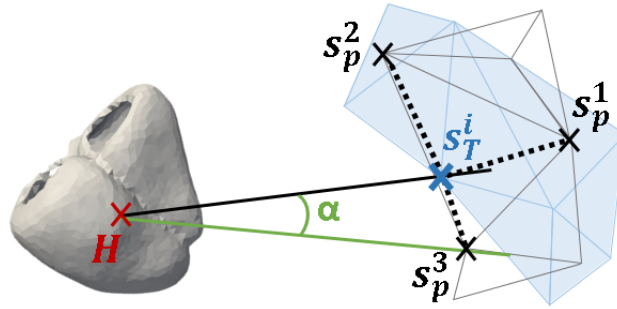
$$\forall i \leq M, \Psi(s_T^i) = \Psi(s_p^j)$$

$$\text{with } j = \arg \min_k \left( \text{dist} \left( s_p^k, HS_T^i \right) \right)$$

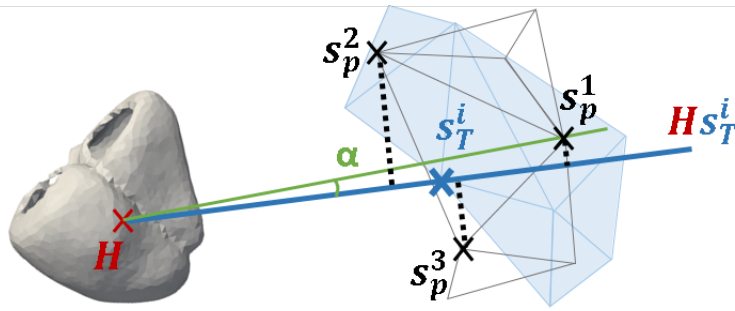
This matching between electrodes is not bijective. However, the advantages of this approach are that measured BSPM signals are not modified and the direction of  $vs_p^j$  is best approximated (see Figure 4.2). This projection, allowing the use of a reference simulated database, can also be seen as a transfer learning method between the reference domain and the patient-specific domain.

### 4.2.2.2 Choice of the template

The choice of the template reference anatomy  $\{c_T; s_T\}$  is important as  $c_T$  has to represent the general shape of the myocardium, and the torso sensors  $s_T$  should be located in relevant positions so that every patient would not be too far from it. In this study, we used a healthy cardiac mesh of 4K vertices and the 251 torso sensors  $s_T$  from one of our patients having median torso width and rotation (patient #22). One could estimate a mean shape, but for simplicity and consistency reasons we used real geometries. In Figure 4.3 is shown an example of the matching between an original BSPM signal and its translation to the torso geometry.



(a) Schematic simple minimal distance matching



(b) Proposed matching of minimal distance to the half straight line

Figure 4.2: Reference anatomy: matching between one template torso electrode  $s_T^i$  and the patient electrodes  $s_P$ . (a) By using a minimal distance between electrodes, the matched electrode would be  $s_P^3$ . (b) With the proposed method, the minimal distance to the half-line  $H s_T^i$  indicates a matching to the electrode  $s_P^1$ . The resulting angle  $\alpha$  corresponding to the difference in heart orientation is thus minimized.

### 4.2.3 Offline Simulated Common Database

#### 4.2.3.1 Simulated Database

As we do not have ground-truth intra-cardiac measurements on the 20 patients, it is difficult to learn inter-patient information in order to personalise the EP cardiac model. In order to generate a common large database with detailed cardiac data, we used EP simulations on the reference anatomy to generate 5 000 virtual cases with different parameter values. One simulation runs in approximately 2 minutes on our cluster (CPU core Xeon 2.6GHz). This offline database was used as the training set for all the personalisations of the cardiac EP model, reducing its online computational cost.

#### 4.2.3.2 Forward Electrophysiological Model

On the reference myocardial mesh, the cardiac fiber orientations were estimated with a rule-based method (elevation angle between  $-70^\circ$  to  $70^\circ$ ). We simulated

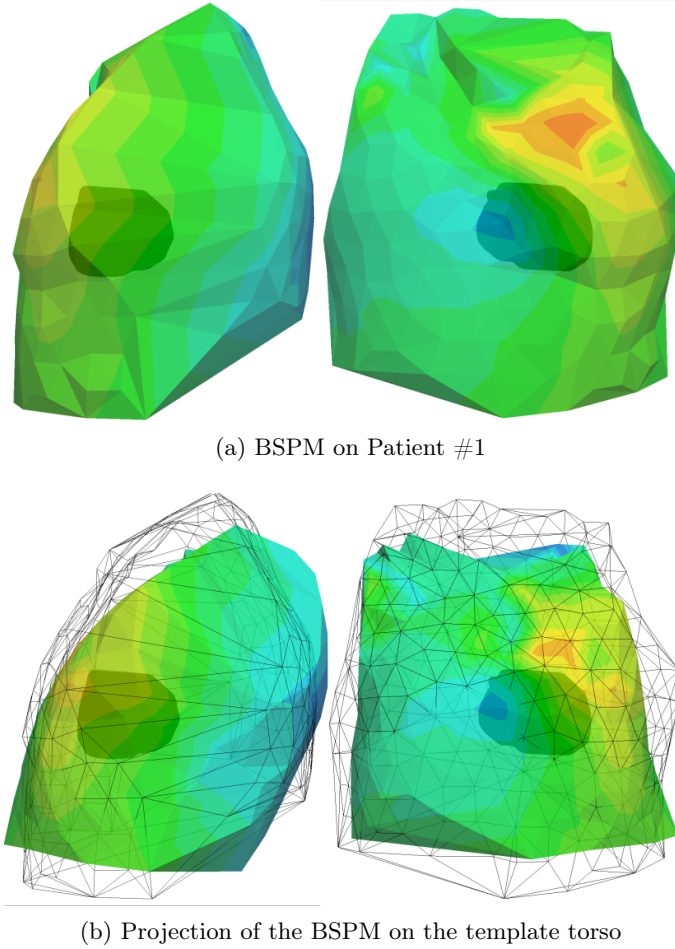


Figure 4.3: Example of real BSPM signal matching between the torso of patient #1 and the template, the color represents the voltage at one time point from blue (minimal) to red (maximal). (a) original BSPM signal on the torso of patient #1. (b) projected signal using the proposed matching method on the template, in wireframe are the original torso contours.

the anisotropic electrical activation of the heart using the monodomain version of the Mitchell-Schaeffer EP model [Mitchell 2003]. Our forward method is based on a simplified framework composed of sources and sensors in an infinite and homogeneous domain. We modelled every myocardium volume element (tetrahedron) as a spatially fixed but time varying current dipole. We computed simultaneously the cardiac electrical sources and body surface potentials (see Chapter 2).

#### 4.2.3.3 Variety of Simulations and Parameter Ranges

In order to simulate a large variability of activation maps and their related BSPM signals, 3 groups of cardiac EP parameters were randomly modified. First, the activation onset location was randomly selected among all the surface vertices of

the cardiac mesh. In order to simulate some more complex and realistic situations, an additional second onset location was selected for every simulation (see Chapter 3). Secondly, the global myocardial conduction velocity  $c$  was randomly picked in a clinically acceptable range  $[0.3, 0.7]m/s$ . Third, in order to capture the conductivity heterogeneity we modelled scar tissue as having no reaction term in the Mitchell-Schaeffer model and a diffusivity reduction of 80%. A varying scar location on the LV with a random and realistic shape [Duchateau 2016] was added in 50% of the simulations.

#### 4.2.4 Relevance Vector Regression for SR Sequence Personalisation

##### 4.2.4.1 Sinus Rhythm Activation Map Estimation

Using the reference simulated database, we wanted to personalise each patient’s EP behaviour from the cardiac at-rest recordings, i.e. the *sinus rhythm* sequence. For the patients where the *sinus rhythm* was not available because of complete heart blocks (see Table 4.1), we used the *RV pacing* sequence. The different parameters (activation onset locations, conductivity, presence of scar tissue) are linked together and their contributions in the resulting BSPM signals are hardly separable. We therefore estimated them at the same time, by regressing the cardiac activation map (the myocardial depolarisation times) from the BSPM signals. We first described the BSPM signals as a feature vector and we used a dimensionality reduction of the representation of the spatial domain given by the myocardial shape. A relevance vector regression was performed between the BSPM features and the reduced activation maps. The first part of the regression (the fitting, taking 6 hours to compute on average on our cluster) is common to every patient and was performed offline, while only the second step is patient-specific (the inference, taking 2 minutes to compute on average).

##### 4.2.4.2 BSPM Feature Description

For every patient, the torso sensors were matched with the transformation described in Section 4.2.2.1 to the 251 leads of the template torso. Because the reference electrode was not localized, the mean BSPM signal was first subtracted to each signal. Then each signal was normalized and smoothed with a local Gaussian filter. We defined specific features from the QRS sequence of every torso leads. Specifically, 7 features were extracted from each of the 251 QRS signals (figure 2.3). One BSPM sequence was then represented as the feature vector  $\mathbf{x}_i$  of size  $L=7 \times 251$ .

##### 4.2.4.3 Dimensionality Reduction of the Myocardial Shape

As seen in Chapter 3, the myocardial tetrahedral mesh can have a large number of elements or vertices. At the same time, the signal to be reconstructed, the activation map, is strongly correlated spatially due to the propagation of the electric potential

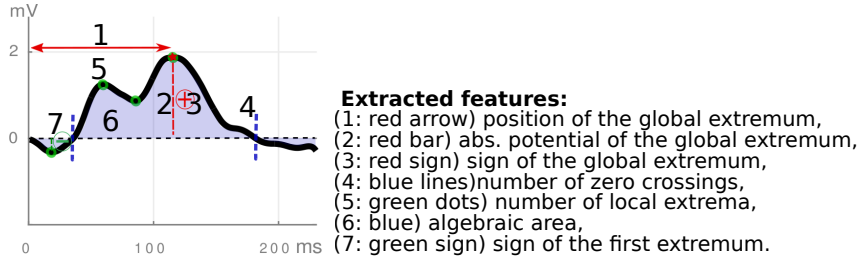


Figure 4.4: Example of BSPM for one torso sensor with the extracted features.

throughout the myocardium. Therefore, it is meaningful to reduce the dimension of the regression variable, the activation times. A simple way would be to use a coarser mesh but this would be at the expense of reducing the accuracy of the onset locations. Instead, we proposed to use a hierarchical decomposition of the mesh, naturally provided by the eigenmodes of a structural matrix. To this end we chose the eigen-decomposition of the stiffness matrix associated with the Laplacian operator of the tetrahedral shape.

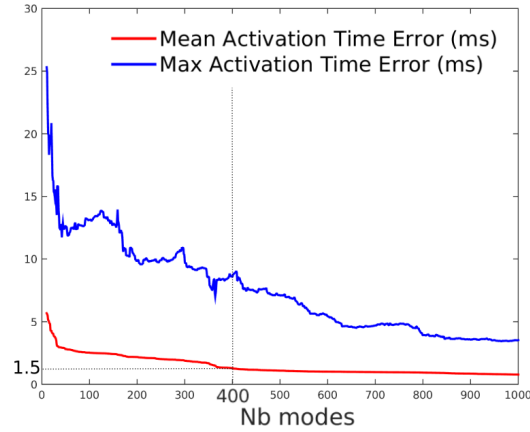
This decomposition has been widely used in various spectral shape analysis [Reuter 2005, Umeyama 1988] and is closely related to the modes of vibration of the myocardium. The extracted eigenvectors are naturally sorted by ascending order of spatial frequency. By selecting the first eigenmodes, we only kept the modes with the lowest frequencies corresponding to the largest spatial variations. If we call  $\mathbf{t}$  the vector of  $N$  activation times at each vertex of the myocardial mesh, we get the following reduction and reconstruction formulas:

$$\mathbf{t}_{red} = \mathbf{V}_M \mathbf{t} ; \mathbf{t}_{rec} = \mathbf{V}_M^T \mathbf{t}_{red}$$

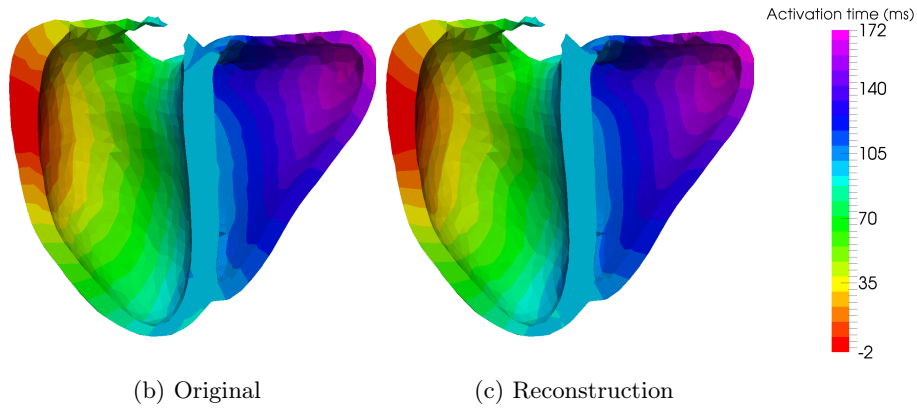
with  $\mathbf{t}_{red}$  the coordinates of  $\mathbf{t}$  in the reduced space,  $\mathbf{V}_M$  the  $N \times M$  matrix of the first  $M$  eigenvectors of the stiffness matrix, and  $\mathbf{t}_{rec}$  the reconstructed activation times. The matrix  $\mathbf{V}_M$  is independent of  $\mathbf{t}$  and is thus computed only once. An example of reconstructed activation map (on 4K vertices) using  $M = 400$  modes is shown in Figure 3.2c. From Figure 3.2a, we can see that the mean reconstruction error was less than 1.5 ms (max: 8 ms) for 400 modes.

#### 4.2.4.4 Relevance Vector Regression

In order to regress the myocardial activation times from the BSPM features, we used the relevance vector regression (RVR) method [Tipping 2003]. As seen in Chapter 3, this approach performs sparse kernel regression based on a sparsity inducing prior on the weight parameters within a Bayesian framework. Unlike the commonly used Elastic-Net or Lasso approaches (based on L1 Norm a.k.a Laplacian prior), the RVR method does not require to set any regularization parameters through cross-validation. Instead, it automatically estimates the noise level in the input data and performs a trade-off between the number of basis (complexity of the representation) and the ability to represent the signal. Furthermore, unlike SVM regression or



(a) Reconstruction error



(b) Original

(c) Reconstruction

Figure 4.5: Example of reconstruction of an activation map (on 4312 vertices) from the eigenvectors of the stiffness matrix: (a) Reconstruction error wrt. the number of modes (b) original activation map (c) reconstructed activation map from 400 modes.

Elastic-Net, it provides a posterior probability of each estimated quantity which is reasonably meaningful if that quantity is similar to the training set.

The RVR estimates the weights  $\mathbf{w}$  so that we can predict  $\mathbf{y} \in R^M$  (here an activation map in the reduced space) from an input  $\mathbf{x} \in R^L$  (here a BSPM feature vector) with a non-linear relationship between  $\mathbf{x}$  and  $\mathbf{y}$  as  $\mathbf{y} = \mathbf{w}^T \Phi(\mathbf{x})$  where  $\Phi$  is the non-linear mapping. We consider our dataset of input-target pairs  $\{\mathbf{x}_i, \mathbf{t}_i\}_{i=1}^K$  where we assume that each target  $\mathbf{t}_i$  represents the true model  $\mathbf{y}_i$  with an addition of a Gaussian noise  $\varepsilon_i = \mathcal{N}(0, \sigma^2)$ :

$$\mathbf{t}_i = \mathbf{w}^T \Phi(\mathbf{x}_i) + \varepsilon_i \quad (4.1)$$

The complexity of the learned relationship between  $\mathbf{x}$  and  $y$  is constrained by limiting the growth of the weights  $\mathbf{w}$ . This is done by imposing a zero-mean Gaussian prior

on  $w_i$ :

$$P(w_i) = \mathcal{N}(0, \alpha_i^{-1}) \quad (4.2)$$

where the  $\alpha_i$  are hyperparameters modifying the strength of each weight's prior.  $\alpha = \{\alpha_i\}_{i=1}^K$  and  $\sigma$  are estimated from a marginal likelihood maximisation [Bishop 2000] via an efficient sequential addition and deletion of candidate basis functions (or relevant vectors). Because the optimal values of many  $\alpha_i$  are infinite, the RVR only selects the BSPM input set that can best explain the activation map in the training set, thus limiting the risk of overfitting.

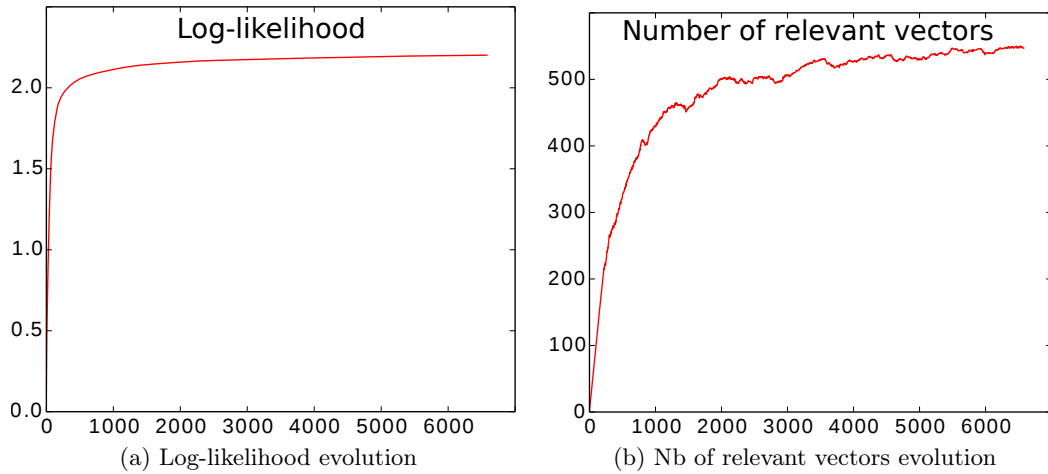


Figure 4.6: Evolution of the relevance vector regression fitting on the first mode.

RVR is a multivariate but single-valued approach and therefore the regression was directly performed on the reduced space of section 4.2.4.3: only 400 regressions are needed to perform an estimation of more than 4K activation times. In our setting, a training input-target pair corresponds to a BSPM feature vector  $\mathbf{x}_i$  and its related activation map projected on one mode of the reduced space  $t_{red,i}^m$ . We used Gaussian kernels for the non-linear mapping  $\Phi$  with a kernel bandwidth of  $1e4$ . The algorithm<sup>2</sup> evolution on the first shape mode (Figure 4.6) shows a rapid convergence even if small changes in the number of relevant vectors are still visible after 3000 iterations. The mean number of retained relevant vectors during the fitting phase was 178 (over 5000 training vectors). As a separate additional step, we regressed from every true BSPM feature vector  $\mathbf{x}$  its activation map estimation  $\mathbf{t}$ .

#### 4.2.4.5 Local Conduction Velocity Parameter Estimation

The estimated cardiac activation maps obtained from the *sinus rhythm* sequence were used to retrieve patient-specific conduction velocity (CV) parameters. Because the regression was performed on simulated activation maps, the resulting solution

<sup>2</sup>we used a python implementation available at <https://github.com/AmazaspShumik/sklearn-bayes>

is smooth and physiologically relevant. If we consider that a normal heart QRS is less than 120ms, we make the following hypothesis : regions that are late activated correspond to regions of slow conduction. Specifically, we threshold the estimated activation times  $t_a$  and defined 3 zones: healthy tissue ( $t_a < 120ms$ ,  $CV = 0.5m/s$ ), damaged tissue ( $120 < t_a < 170ms$ ,  $CV = 0.3m/s$ ), and scar tissue ( $170 < t_a$ , no reaction term and diffusion reduced by 80%). We used a single value for the healthy tissue based on Chapter 2 where the personalised global CV were all found close to  $0.5m/s$ .

#### 4.2.4.6 Pacing Prediction and AV node Activation

For every patient, the true ventricular pacing locations were segmented from the CT scanner image, however the image artefacts due to the device only allow an approximate lead location. The personalised parameters from *sinus rhythm* BSPMs were used to predict the activation maps of different pacing situations. On some patients we found that the RV was activated without ventricular pacing, probably from the atrial pacing (100 to 200ms before) via the AV node. For these patients (#1, #2 6M, #4, #7, #9, #12, #13) we modelled an AV node activation after the ventricular pacings. We triggered the earliest activated zones estimated in the *sinus rhythm* result. Because no recording of atrial stimulation and AV delay were available, the triggering time was arbitrarily set to 40ms.

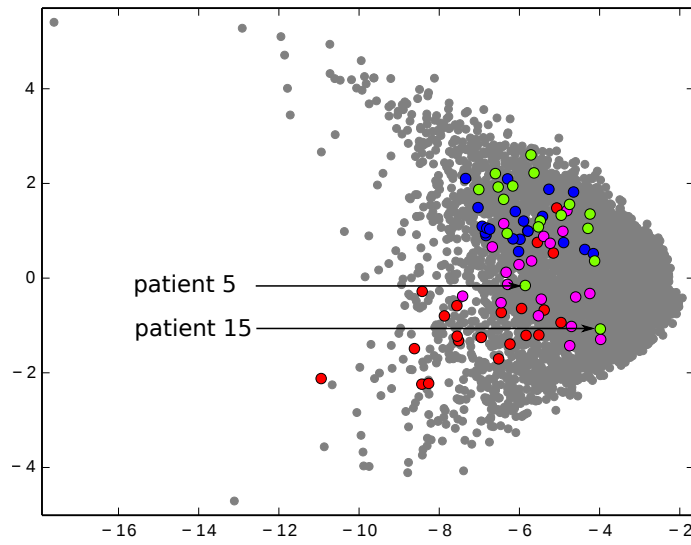
### 4.3 Personalisation Results and Pacing Predictions

#### 4.3.1 Projections on the Reduced Shape Space

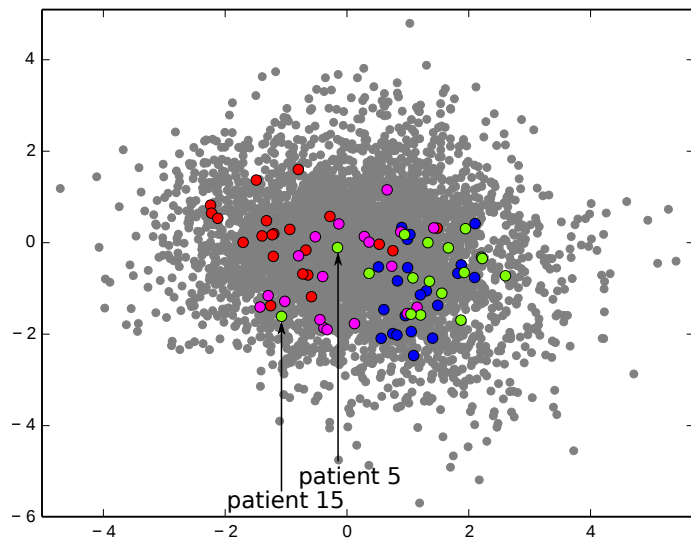
In Figure 4.7 we showed the RVR results of each real BSPM sequence on the reduced shape space. Because the modes of this space are related to modes of vibration, the results projected on the larger modes allow us to easily compare the BSPM sequences. Each grey point represents one simulated activation map used for training. The real sequences of the 20 patients are shown with colours representing the type of sequence. All the results from the real BSPM data lie inside the training set point cloud, which is important for the RVR to perform well. We can also see that the 3 different pacing sequences are separated in clusters, with the *simultaneous* between the *RV pacing* and the *LV pacing*. The *sinus rhythm* results in green are almost all situated near the *RV pacing* cluster, which is to be expected for LBBB patients. Interestingly, we can notice that the two *sinus rhythm* exceptions that are closer to the *LV pacing* group in blue correspond to the two RBBB patients of the cohort (patients #5 and #15).

#### 4.3.2 Estimated Sinus Rhythm Activation Maps

The RVR results of the *sinus rhythm* sequences in terms of activation map were used to estimate the local conduction velocity parameter of each patient. In Figure 4.8 is represented the mean solution as a transmural activation map (4.8a) that



(a) projection on modes 1 and 2



(b) projection on modes 2 and 3

- sinus rhythm
- LV only
- RV only
- simultaneous
- simulations for training set

Figure 4.7: RVR results on the reduced shape space from real BSPM sequences of the 20 patients. Grey dots: projection of the 5000 simulated activation maps used for training.

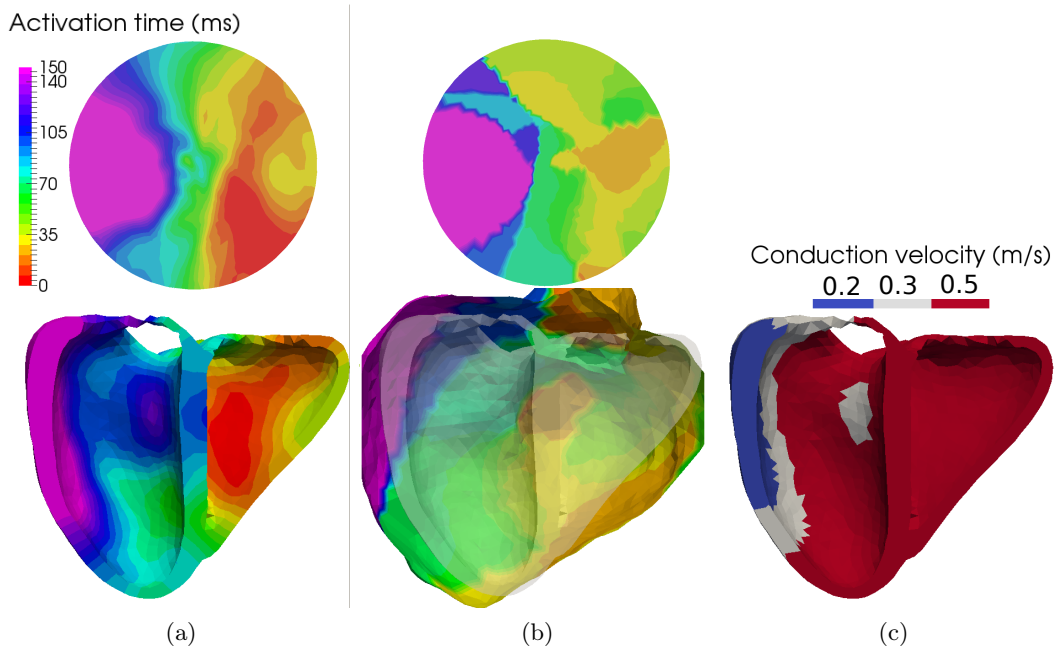


Figure 4.8: *Sinus rhythm* of patient #9 (a) estimated activation map from RVR method. *up*: flattening view of the epicardial surface. (b) CardioInsight epicardial inverse solution. (c) Personalised conduction velocity from thresholding the estimated activation map.

was compared with the CardioInsight epicardial inverse solution [Ramanathan 2003] (4.8b). The CardioInsight solution is interesting for comparison even if it is only an epicardial surface reconstruction. On top are flat representations of the epicardial surface [Soto-Iglesias 2016]. The wave shape are similar, with a large late activated zone on the lateral LV wall with probable scar tissue. In Figure 4.8c are shown the retained zones for healthy, diseased and scar tissues from thresholding of Figure 4.8a. Finally, because the RVR regression provided the result as a Gaussian probability distribution in the reduced shape space, the estimated standard deviation across each mode were projected on the myocardial mesh. The zones with a high estimated standard deviation were found near the valves where the mesh is thin, and the median standard deviation was 0.037s.

### 4.3.3 Pacing Predictions Results

#### 4.3.3.1 Predicted Activation Maps

From the CV parameters estimated using the RVR solution of the *sinus rhythm* BSPMs, we ran again our cardiac Mitchell-Schaeffer model with known pacing conditions and locations (*RV only*, *LV only*, *simultaneous*, *LV 40ms*, *RV 40ms*) and compared its output to the actual pacing recordings. We recall that in our predictions the pacing BSPMs were not used. In Figure 4.9 is represented the predicted

*LV 40ms* activation map for patient #9 (Figure 4.9a), the prediction if we used a model with a homogeneous myocardial CV (Figure 4.9a) and the CardioInsight solution (Figure 4.9b). The flat representation allows for a better comparison even if the projection of the epicardium may differ between two cardiac geometries. We can see that the homogeneous CV prediction missed the scar while with the personalised CV the wave shape and timings globally correspond to CardioInsight. The damaged tissue zone on the LV lateral wall (on the left) was well estimated as also visible on the CardioInsight map.

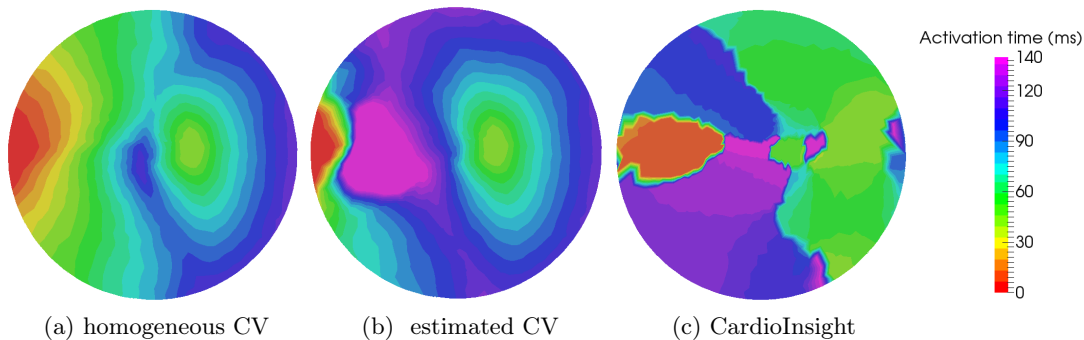


Figure 4.9: *LV 40ms* pacing prediction of patient #9, flattening epicardial representations of the activation maps (a) pacing prediction using homogeneous conduction velocity ;(b) using the personalised parameters from *sinus rhythm*; (c) CardioInsight inverse solution of the actual pacing.

The prediction of *LV only* pacing of patient 9 is shown on Figure 4.10a. The predicted propagation was completely blocked by the scar zone, while an RV activation is visible on the CardioInsight solution Figure 4.10c. With the AV activation model (see section 4.2.4.6), the resulting activation map (Figure 4.10b) is closer to the CardioInsight solution. In Figure 4.7, we could see some *LV only* projections (red) inside the *RV only* point cloud: they correspond to patients 1, 9 and 12 all showing a separate RV activation and also an important LV late activated near the LV pacing lead.

As a quantitative comparison, Figure 4.11 shows the activation times differences on the flat epicardium, between our predictions and the CardioInsight inverse solutions on 20 patients. The total median difference is 23.8ms. It indicates some similar activation patterns even if few points have an important difference (higher than 50ms). A perfect match is difficult because of the epicardial projections difference, the piece-wise constant CardioInsight solution and the approximation in the pacing electrodes locations. We can notice that the *LV only* seems to be the more difficult to predict.

#### 4.3.3.2 BSPM predictions

We also predicted the corresponding pacing BSPM signals and compared them with the true signals. Some signal examples of pacing predictions from patient #3 (Figure

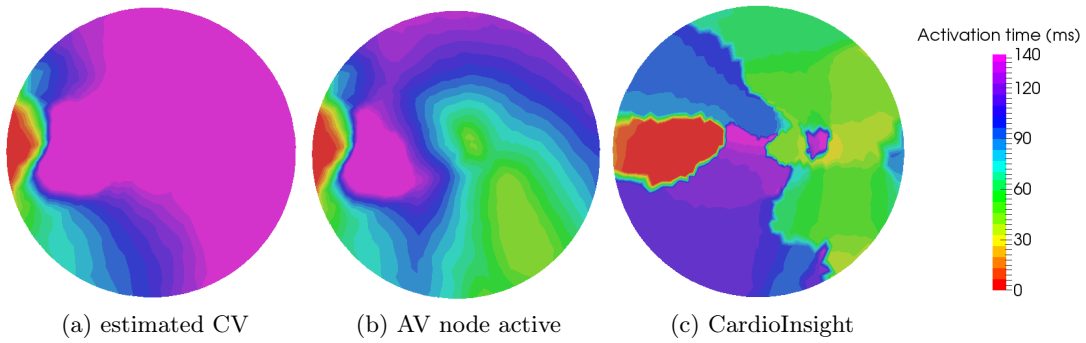


Figure 4.10: *LV only* pacing prediction of patient #9, flattening epicardial representations. (a) using the personalised parameters from *sinus rhythm*; (b) adding the modelled activation of the AV node after 40ms; (c) CardioInsight inverse solution from actual recordings of the pacing.

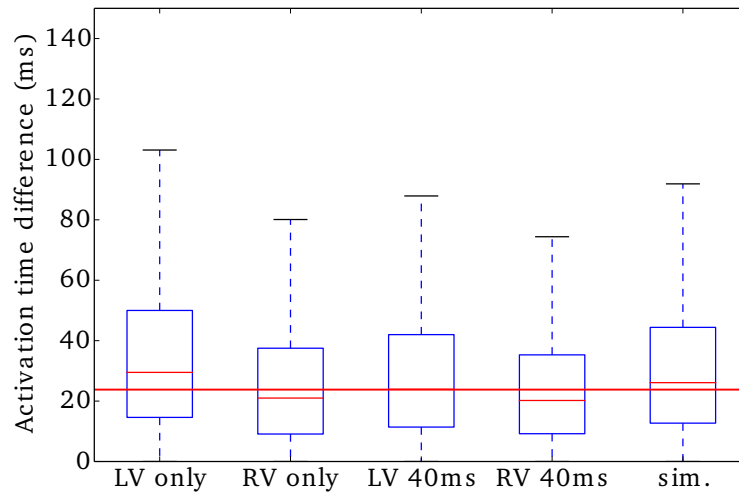


Figure 4.11: Prediction of pacing activation maps (20 patients): activation times differences on the flattened epicardial points, between our prediction and the CardioInsight inverse solution. Median difference (red line): 23.8ms.

4.12) showed a clear improvement when using the personalised CV for the *LV only*, while the homogeneous CV shows already a good agreement for the *RV only*. In Figure 4.13 we can see the averaged correlation coefficients ( $\overline{CC}$ ) between measured and predicted BSPM signals. Because the cardiac geometry was generic and the pacing locations not accurate, we cannot expect a perfect match between BSPMs. However, we can see that the mean  $\overline{CC}$  of every pacing type increases when the local CV was personalised from *sinus rhythm*. In particular, the effects on the *LV only* prediction are highest because the LV damaged tissues can have higher impacts on the wave propagation. We can still see some outliers having low  $\overline{CC}$  values. The lowest one (from patient #16) corresponds to the *LV only* outlier (red) in the projected modes of Figure 4.7a, in a zone where the training simulations are sparse.

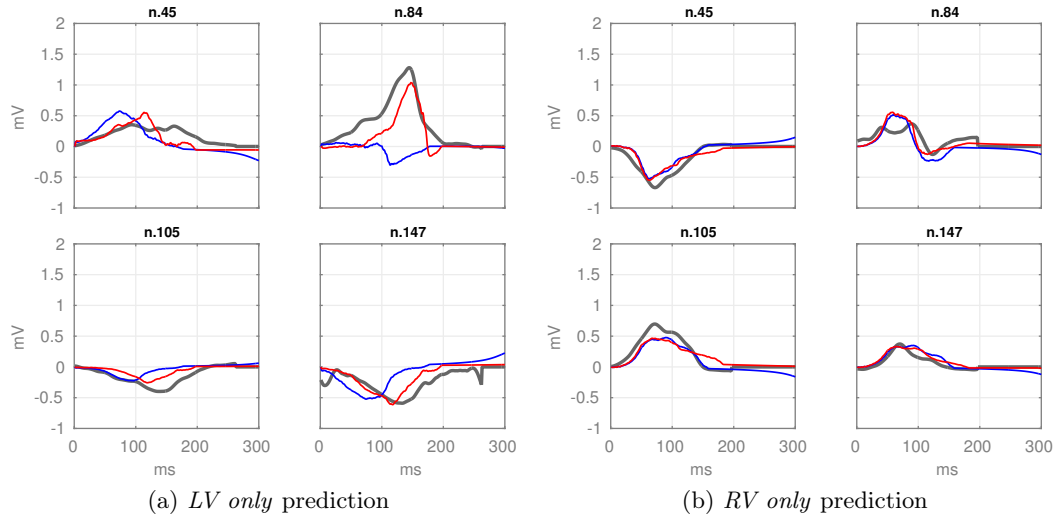


Figure 4.12: Pacing predictions of patient #3, example of BSPM signals. *Grey*: Ground truth signal; *blue*: pacing prediction with a homogeneous myocardial CV; *red*: pacing prediction with a personalised CV from *sinus rhythm*.

It might indicate that our training set did not cover properly this region of the parameter space.

## 4.4 Discussion

### 4.4.1 Reference Anatomy

The interpatient study could be a useful tool for different applications, as it also allows some comparison between patients. However, it is not universal because our template has a large number of electrodes on both sides of the torso. A new dataset composed of only frontal electrodes would not be correctly projected on the back. The use of a simpler reference with fewer electrodes could be a more general alternative.

We used a reference cardiac geometry, where the size of the heart was fixed. We evaluated the impact of the cardiac scaling on the simulated resulting BSPM signals. Two cardiac scalings of ratios 0.8 and 1.7 to the original size were tested (corresponding to extreme sizes). The center of mass of the myocardium was taken as origin. The resulting normalized BSPM signals showed a relative mean signal difference of 0.1% for the 0.8 scaling ratio and 0.2% for the 1.7 scaling ratio. We can deduce that the size of the heart can be neglected if an appropriate origin is chosen.

In our setting, the heart location and orientation was segmented from CT scan images. We think that this ionising and computational procedure could be replaced by an estimation of the position and orientation parameters, either by statistical prediction from easy patient characteristics [Odille 2017] or by simultaneous EP

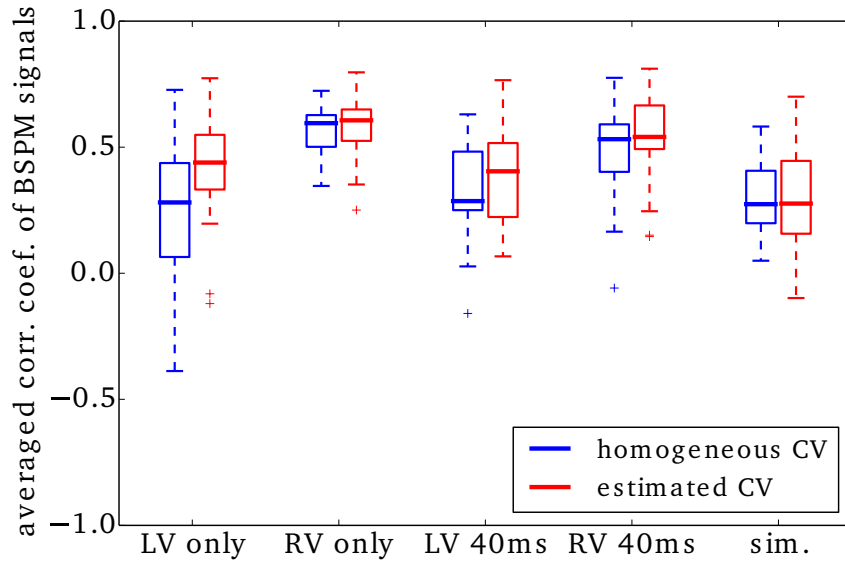


Figure 4.13: Prediction of pacing activation maps (20 patients): averaged correlation coefficient ( $\overline{CC}$ ) between measured and predicted BSPM signals. In blue, the prediction was performed with a homogeneous myocardial conduction velocity. In red is the result with the CV personalised from *sinus rhythm* (and with the AV activation in patients 1, 2 6M, 4, 7, 9, 12, 13).

inverse optimization [Rodrigo 2017, Coll-Font 2016a].

#### 4.4.2 Estimating conduction velocity from activation times

In this work we personalised the local conduction velocity parameter by assigning low values on late activated zones. The direct estimation of local velocity from an activation map raises many challenges (because of the mesh, the anisotropy, the direction of the wave), even though some recent studies are proposing new approaches [Doshi 2015, Duchateau 2017, Dallet 2015]. Their use could improve our estimation and thus the predictions.

#### 4.4.3 Estimating the uncertainty

The RVR standard deviation is a by-product of the regression and can be a way to interpret the regression uncertainty. However, a proper posterior distribution would be useful for a better accuracy and for identifying the stability of the solution. The use of surrogate modelling into a Metropolis Hasting sampling was recently proposed [Dhamala 2017b]. We could then also integrate the other sources of uncertainty as the mean torso sensor distance to the template..

#### 4.4.4 AV node Activation

We have seen that some patients were activated also from an atrial pacing via the AV node. We have modelled it with an arbitrary time delay, but we think it would be possible to integrate it with more complete data (if the atrial stimulation was recorded). Moreover, the integration of the atria in the ventricular model (for example as a thin layer [Schenone 2014]) and a study of the whole heart beat ECG could be beneficial for a precise and global personalisation.

### 4.5 Conclusion

In this chapter we have developed a methodology for solving the ECG inverse problem and estimating local cardiac conductivity parameters using a physiological model-based regression on a reference anatomy. The data matching to the template anatomy allowed us to use a large offline simulated database of EP forward models for the regression of the BSPM signals from 20 patients with a CRT indication. We used a sparse Bayesian kernel-based regression for the estimation of cardiac activation maps with the use of specific BSPM descriptors and a reduced space for the myocardial geometry. From the CV parameters estimated with the *sinus rhythm* BSPM sequence, we predicted the responses to different pacing conditions. We compared them with the true pacing BSPMs and with a commercially available epicardial inverse solution (median activation time difference: 24ms). While a validation with intracardiac recordings is still necessary, we believe that the small patient-specific computational time (less than 2 minutes) can be crucial for a clinical use.

## Part II

# Applications and Translation to Clinics



# From BSPM to 12-lead ECG : Personalisation Using Routinely Available Data

---

## Contents

---

<b>5.1</b>	<b>Introduction</b>	<b>80</b>
<b>5.2</b>	<b>Estimation of Purkinje Activation from 12-lead ECG</b>	<b>80</b>
5.2.1	Purkinje System and General Context	80
5.2.2	Materials and Methods	81
5.2.3	Intermittent Left Bundle Branch Block Study	83
5.2.4	Cardiac Resynchronization Therapy Study	85
5.2.5	Electrode Location Perturbation	86
5.2.6	Conclusion of the Purkinje Estimation	86
<b>5.3</b>	<b>Activation Onset Localisation from 12-lead ECG</b>	<b>88</b>
5.3.1	Clinical Data	88
5.3.2	Results on Activation Onset Localisation	88
5.3.3	Conclusion of the Activation Onset Localisation	88
<b>5.4</b>	<b>Conclusion</b>	<b>89</b>

---

This chapter is based on different contributions.

Section 5.2 is based on the following paper (except the unpublished CRT application, part 5.2.4): **Estimation of Purkinje Activation from ECG: an Intermittent Left Bundle Branch Block Study**, *Sophie Giffard-Roisin, Lauren Fovargue, Jessica Webb, Roch Molléro, Jack Lee, Hervé Delingette, Nicholas Ayache, Reza Razavi, and Maxime Sermesant*. In 7th International Statistical Atlases and Computational Modeling of the Heart (STACOM) Workshop, Held in Conjunction with MICCAI, Lecture Notes in Computer Science, Athens, Greece, October 2016.

Section 5.3 is based on the following paper (thus completing Chapter 2): **Non-Invasive Personalisation of a Cardiac Electrophysiology Model from Body Surface Potential Mapping**, *Sophie Giffard-Roisin, Thomas Jackson, Lauren Fovargue, Jack Lee, Hervé Delingette, Reza Razavi, Nicholas Ayache, and Maxime Sermesant*. IEEE Transactions on Biomedical Engineering, 2016.

## 5.1 Introduction

In Part I we presented some methodologies to estimate cardiac electrophysiological (EP) parameters from body surface potential mapping (BSPM) data, using between 170 to 250 torso electrodes. However, the ECG vest is not routinely used in clinical practice. For the analysis of the cardiac electrical activation, the 12-lead ECG (using only 9 torso electrodes) is widely used because of its efficiency and reduced cost. The 12 standard Einthoven, Goldberger and Wilson leads (12-lead ECG) measure the potential differences between selected electrodes (see Figure 5.5).

In this chapter, we will investigate how to personalise the EP cardiac model using only 12-lead ECG data. First, we propose a framework for the evaluation of 3 conduction parameters (linked to the fast conduction or Purkinje system) from the 12-lead ECG in the case of bundle branch block patients. Second, we show an adaptation of the method presented in Chapter 2 for the onset activation estimation using only the 12-lead ECG. Both studies were evaluated on real datasets.

## 5.2 Estimation of Purkinje Activation from 12-lead ECG

### 5.2.1 Purkinje System and General Context

Modelling the cardiac electrophysiology (EP) can help understanding pathologies and predicting the response to therapies such as cardiac resynchronization therapies (CRT). To this end, estimating patient-specific model parameters is crucial. In the case of patients with bundle branch blocks (BBB), part of the Purkinje system is often affected. The Purkinje fibers are located just beneath the endocardium and are able to conduct cardiac action potentials quickly and efficiently: typical conduction velocity (CV) ranges from 2 to  $3m/s$  while it ranges from 0.3 to  $0.4m/s$  for myocardial cells [Durrer 1970]. Stimulus arrives from the atrioventricular node through the His bundle which separates the network in two branches, the left bundle and the right bundle. When a block occurs in a bundle (LBBB for left, RBBB for right), the Purkinje system is not as efficient and the contraction of the ventricles isn't synchronized.

Some studies have been focusing on the understanding of LBBB patterns by simulating ECGs with different parameters from precise cardiac and torso models [Lorange 1993, Potse 2012]. Because of their complexity, we defined a simpler model for the estimation of patient-specific parameters. A study has also recently proposed an EP parameters estimation from ECG data [Zettinig 2014]. It uses two features from the 12-lead ECG to recover 3 electrical diffusivity parameters using a boundary element method forward model and a polynomial regression. As it is difficult to differentiate the contribution of the Purkinje system, our work was evaluated on two particular datasets. The first is an intermittent LBBB case where both LBBB and absence of LBBB (ALBBB) are recorded on 12-lead ECGs. The second is a CRT candidate, where both pre- and post-CRT 12-lead ECGs were recorded. First, an efficient forward EP model is proposed by coupling a 3-parameter cardiac EP

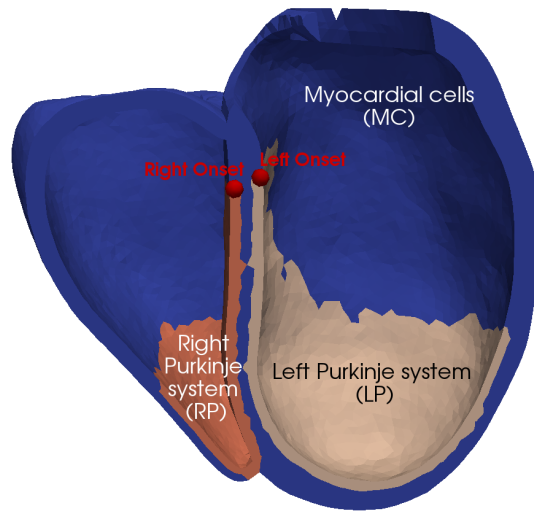


Figure 5.1: Long axis view of the cardiac mesh with delineated regions: Myocardial cells region (blue), right Purkinje system region (orange) and left Purkinje system region (beige). The red dots are the modeled right and left onset activation locations.

model based on the Mitchell-Schaeffer model with a current dipole formulation. We used the covariance matrix adaptation-evolution strategy (CMA-ES) algorithm to optimize the 3 parameters by minimizing the error with the ECG signals.

## 5.2.2 Materials and Methods

### 5.2.2.1 Clinical Data

In this study, we considered cardiac imaging data from MRI and electrical data from the 12-lead ECG. The MRI acquisition allows a precise myocardial geometry at end diastole. The 12-lead ECG represents the cardiac electrical activity recorded from 9 body surface electrodes. Because the locations of the electrodes were not registered, we manually position them guided by the conventional ECG placement (Figure 5.5).

### 5.2.2.2 Pre-processing

The myocardial mesh was generated using the VP2HF platform [Groth 2012] and the VP2HF meshing pipeline<sup>1</sup> creating a tetrahedral mesh with roughly 90K tetrahedra. Rule-based fibre directions were estimated with an elevation angle between  $-70^\circ$  and  $70^\circ$ . The right and left Purkinje regions were manually delineated (Figure 5.1). The 12-lead ECG were digitized using the open-source Engauge Digitizer followed by a

<sup>1</sup>VP2HF is a European Seventh Framework Program, <http://www.vp2hf.eu/>. The VP2HF meshing pipeline is based on CGAL, VTK, ITK and VMTK open-sources libraries.

resampling at a rate of 1kHz. Only the 200ms following the Q wave were used (QRS window).

### 5.2.2.3 Forward EP Model

**Mitchell-Schaeffer Cardiac Model:** We simulated the electrical activation of the heart using the monodomain version of the Mitchell-Schaeffer’s EP model [Mitchell 2003], see section 1.3.1.2.

In this work, we considered 3 different domains with uniform conduction velocities: the myocardial cells (MC), the left Purkinje system (LP) and the right Purkinje system (RP). The MC was modelled as one single domain for simplification reasons. We modelled the LP and RP as a thin layer covering the endocardial surfaces. By considering that the Purkinje geometry is unknown, this simplification to a layer allows also a rapid computation. Concretely, the layer is composed of all the tetrahedra connected to the endocardial surface.

We manually selected the onset activation locations on the septum near the valves, see Figure 5.1. This was driven by the fact that the electrical wave arrives from the His bundle to the left and right bundles located on the septum.

**From Cardiac Simulations to ECG:** We computed simultaneously the cardiac electrical sources and body surface potentials. Our forward method is based on a simplified framework composed of sources and sensors in an infinite and homogeneous domain. As in [Chávez 2015], we modelled every myocardium volume element (tetrahedron) as a spatially fixed but time varying current dipole, see Chapter 2 for further details.

### 5.2.2.4 Parameters Estimation using CMA-ES Algorithm

We estimated the 3 conduction parameters using a Covariance Matrix Adaptation Evolution Strategy (CMA-ES) [Hansen 2006]. It is a derivative-free and stochastic algorithm that is suited for non-convex continuous optimization problems. At each iteration, new candidate solutions are sampled from a multivariate normal distribution whose covariance matrix is adapted according to the ranking between the candidate solutions of the previous iteration. We define the score of a simulation  $S$  as its error to the ground truth 12-lead ECGs  $\Psi_{GT}$ :

$$f(S) = \int_{t=0}^T \frac{1}{N} \sum_{i=1}^N \left| \Psi_{GT}(i, t) - \frac{\|\Psi_{GT}\|}{\|\Psi_S\|} \Psi_S(i, t) \right| \quad (5.1)$$

with  $N$  the number of leads ( $N = 12$ ),  $T$  the final time ( $T = 200ms$ ),  $\Psi_{GT}(i, t)$  the ground truth difference of potential of the lead  $i$  at time  $t$  and  $\Psi_S(i, t)$  the simulated difference of potential of the lead  $i$  at time  $t$ . We used a population of 100 simulations per generation and optimized over 20 generations. We initialized the algorithm by a multivariate distribution of mean  $x_0 = (0.6, 0.6, 0.6)m/s$  and standard deviation  $std = 0.1m/s$  in each direction. We fix the parameter searching range at  $[0.05, 2.5]m/s$  to avoid non-physical solutions. The best score vs. the number of iterations for a parameters estimation is plotted on Figure 5.2.

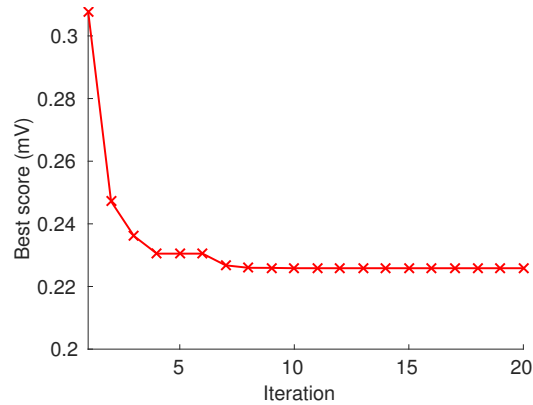


Figure 5.2: Best score versus the number of iterations of the CMA-ES algorithm. The score is identified as the mean error between the simulated and real 12-lead ECG, in mV.

### 5.2.3 Intermittent Left Bundle Branch Block Study

#### 5.2.3.1 Intermittent LBBB Patient Data

As a first evaluation of the proposed method, a patient with intermittent LBBB was selected. The data has been acquired at St Thomas Hospital (London) as part of the VP2HF project. Both LBBB pattern and absence of LBBB (ALBBB) were documented on two 12-lead ECG, the ALBBB being recorded after the LBBB. The parameters were estimated separately for the LBBB and ALBBB. Only the right onset location was activated for the LBBB whereas both right and left were activated for ALBBB because in an LBBB the left bundle is not active.

#### 5.2.3.2 Intermittent LBBB Results

Table 5.1 shows the CV before the parameters estimation, after the LBBB parameters estimation and after the ALBBB parameters estimation. First, all Purkinje CV are higher than myocardial CV which is to be expected. We can see that the myocardial cells CV and the right Purkinje CV are very similar between the LBBB and the ALBBB estimations. For the left Purkinje, we found  $0.49m/s$  for LBBB and  $1.32m/s$  for ALBBB, indicating that the model seems to identify the LBBB pathology (affected LP system). Moreover, the MC CV values lie in the myocardial CV range found in the literature [Durrer 1970]. The RP CV (as well as the LP CV for the ALBBB) is close to the Purkinje CV range found in the literature.

Figure 5.3 shows the simulation results after parameters estimation. Figure 5.3a represents the true (black) and simulated (blue) 12-lead ECG for the LBBB case and Figure 5.3b the corresponding cardiac activation map. We can see that the shape of the ECG is coherent with the ground truth and especially the clear notched R wave on leads V5 and V6, indicator of an LBBB pathology. Figures 5.3c and 5.3d depict the results for the ALBBB, where both QRS on ECG and activation times are

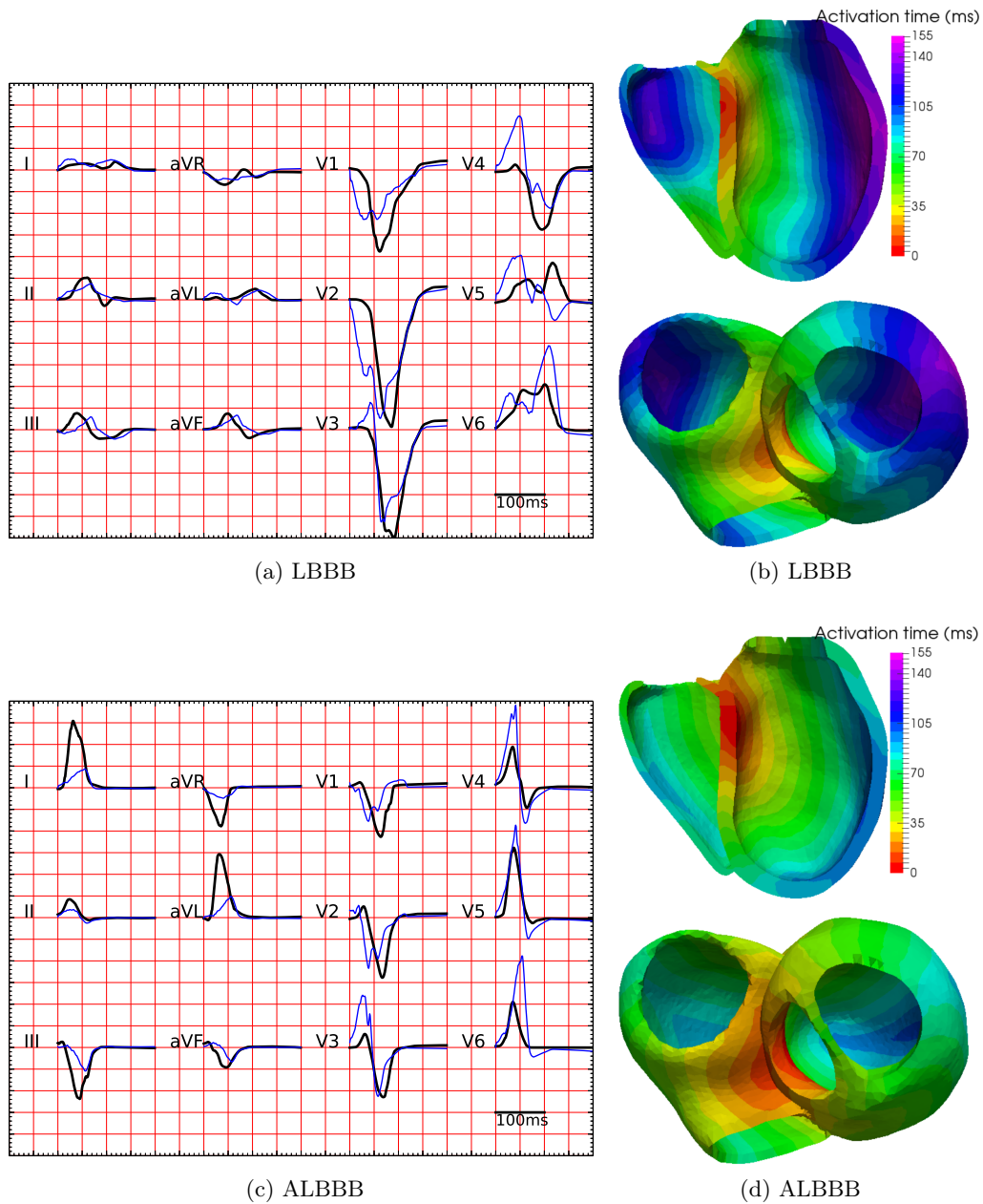


Figure 5.3: Simulation results after parameters estimation. *LBBB*: (a) Real 12-lead ECG (black) and estimated (blue) during the 200 ms after onset activation. (b) Estimated activation map. *ALBBB*: (c) Real 12-lead ECG (black) and estimated (blue) during the 200 ms after onset activation. (d) Estimated activation map.

Table 5.1: Estimated conduction velocities (CV) for LBBB and ALBBB.

$CV(m/s)$	myocardium	left Purkinje	right Purkinje
<b>Initially</b>	0.6	0.6	0.6
<b>LBBB</b>	0.39	0.49	0.95
<b>Absence of LBBB</b>	0.40	1.32	1.22

shorter than for the LBBB. The real and simulated ECG for ALBBB have similar shapes even though we can notice the notched V2 and V3 R waves (so RV and LV are not perfectly synchronous). It may indicate that our Purkinje zone delimitation could be improved.

The fact that the RP and LP conductions are smaller than the literature range may be because we model the Purkinje system as a layer and not a small fiber network. For consistency reasons, we initialized the LBBB with only the right onset. However, it leads to different initial settings between ALBBB and LBBB parameters estimation. That is why we also ran the ALBBB using only the right onset: we found a similar myocardial CV ( $0.39m/s$ ), a higher left Purkinje CV ( $2m/s$ ) and a smaller right Purkinje ( $0.17m/s$ ). It seems that the model is compensating the absence of left onset, while still showing a clear left Purkinje activation.

## 5.2.4 Cardiac Resynchronization Therapy Study

### 5.2.4.1 CRT Candidate Patient Data

We propose in this section to evaluate the Purkinje estimation on another LBBB patient being a CRT candidate, where both pre- and post-CRT 12-lead ECGs were recorded. The data has been acquired at St Thomas Hospital (London). For the post-CRT recording, the patient was under biventricular simultaneous pacing with an RV apex lead and an epicardial LV postero-lateral lead. The exact pacing locations were not recorded so they were manually placed on the cardiac mesh. This patient showed presence of scar tissue which was segmented from delayed contrast enhancement MRI. The conduction velocity in the myocardial scar regions was set to a low value ( $0.2m/s$ ) and the Mitchell-Schaeffer reaction term was set to 0 in these regions. For this case, we want to evaluate the predictive power of the method: we estimated the 3 conduction parameters from the pre-CRT 12-lead ECG, and used them to simulate the post-CRT 12-lead ECG (with pacing). We could finally compare the predicted ECG signals under pacing with the real post-CRT ECG signals.

### 5.2.4.2 CRT Candidate Results

The fitting of the 3 Purkinje parameters from the CMA-ES algorithm on the pre-CRT ECG signals gave the parameters of table 5.2. We can see that the myocardial and left Purkinje values are in the range of the LBBB values found for the inter-

Table 5.2: Estimated conduction velocities (CV) for the Pre-CRT data.

$CV(m/s)$	myocardium	left Purkinje	right Purkinje
<b>Initially</b>	0.6	0.6	0.6
<b>Pre-CRT</b>	0.36	0.40	0.68

mittent LBBB patient (see table 5.1). On this case the right Purkinje value is smaller even if it remains the higher CV. In Figure 5.4a are shown the simulation results after parameters estimation using the pre-CRT ECG signals. We can see that the shape, signs and QRS duration are globally well reproduced, even if some discrepancies are visible on V5 and V6.

On Figure 5.4c is shown the predicted 12-lead ECG with simulatenous pacing. We recall that the ground truth post-CRT 12-lead ECG is only used as validation and it was not used for the parameters estimation. We can see that here the shapes and timings are well reproduced. Particularly, the changes between pre- and post-signals are visible, such as the sign of II, III, aVL and aVF, the global reduction of QRS durations but also the time shift of the QRS extremum in V3 (from 100ms to 50ms). Again, some discrepancies between ground truth and prediction signals can be particularly visible on V5 and V6. Because the 9 ECG electrodes were manually placed, we think leads 5 and 6 might be misplaced. A better validation would consist in a dataset where the 9 electrodes are localized.

### 5.2.5 Electrode Location Perturbation

We have tested the sensitivity of our method to the locations of the 9 torso electrode by adding Gaussian noise on the intermittent LBBB estimation. After 5 tests with a perturbation mean of  $7.5mm$  in a random direction for each electrode, the relative differences to the estimated CVs have a mean of 3% ( $max = 10\%$ ). We can conclude that our method seems to be stable to small perturbations. However, as noted in section 5.2.4.2, some errors on the signals could be avoided by using a dataset where the 9 electrodes were localized.

### 5.2.6 Conclusion of the Purkinje Estimation

In this section, we showed a promising non-invasive parameters estimation for the identification of the Purkinje system activation using the CMA-ES algorithm. The method estimates 3 conduction parameters of the EP cardiac model based on the 12-lead ECG and was evaluated on 2 different applications.

For the intermittent LBBB patient, we identified the activation of the Purkinje system by independently estimating the parameters of the same patient with and without the LBBB pathology. The estimation of CV parameters for LBBB and absence of LBBB shows a good agreement for the myocardium CV ( $0.39m/s$  for

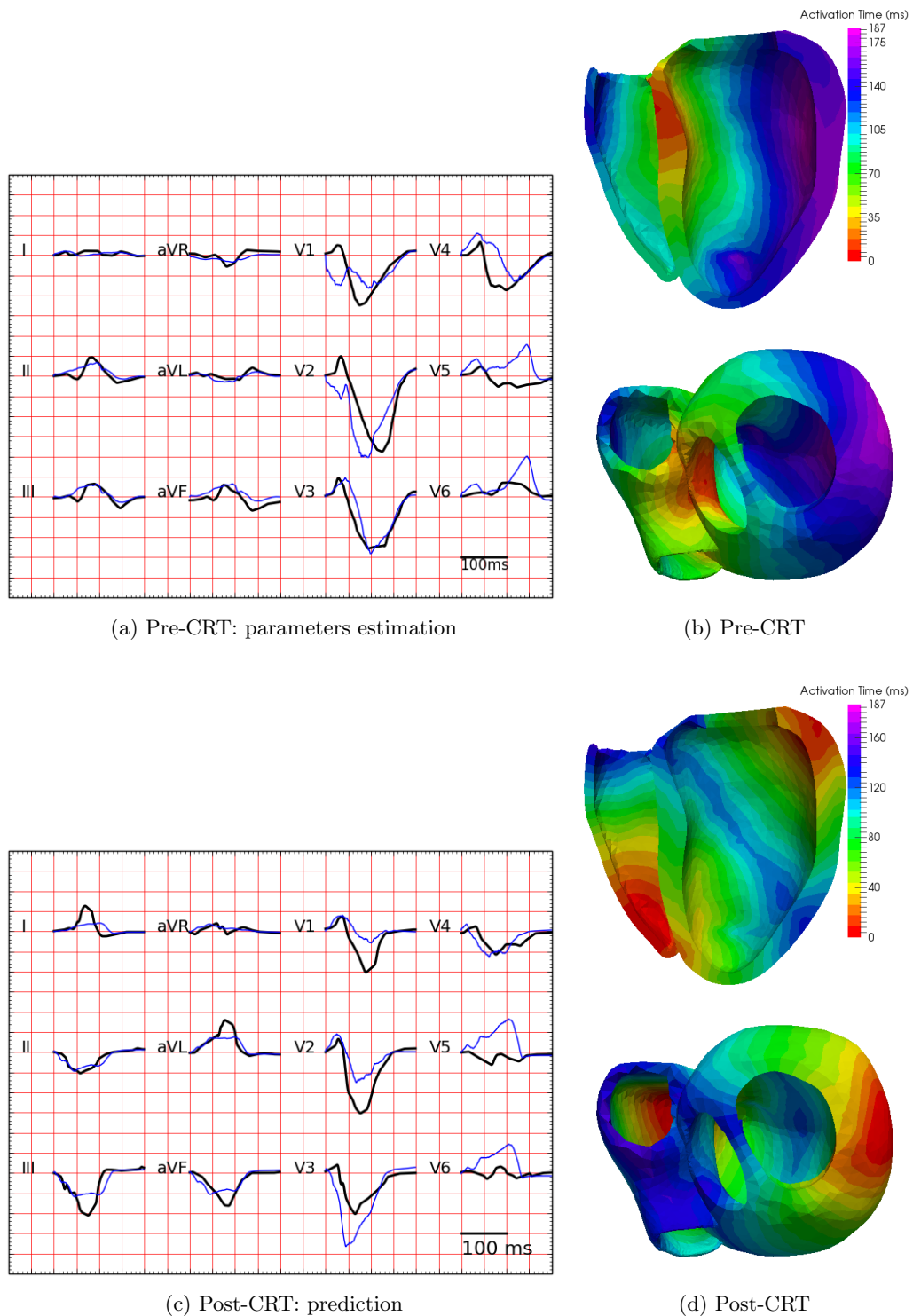


Figure 5.4: *Pre-CRT*: Simulation results after parameters estimation. (a) Real 12-lead ECG (black) and estimated (blue) during the 200 ms after onset activation. (b) Estimated activation map. *Post-CRT*: Prediction simulation results (using pre-CRT estimated parameters) (c) Real 12-lead ECG (black) and prediction (blue) during the 200 ms after onset activation. (d) Predicted activation map.

ABBB,  $0.40m/s$  for LBBB), while the estimation of the left Purkinje CV seems to identify the pathology ( $1.32m/s$  for ALBBB,  $0.49m/s$  for LBBB).

On the second dataset, we evaluated the predictive power of the method on a CRT candidate. We estimated the personalised parameters on a pre-CRT recording and showed that we were able to correctly predict the response to pacing.

In both studies, the plots of the simulated 12-lead ECGs and the real ECGs indicate similar shapes. We believe this work to be an interesting first step for understanding BBB pathology and selecting the CRT responders based on 12-lead ECG.

## 5.3 Activation Onset Localisation from 12-lead ECG

### 5.3.1 Clinical Data

The use of 12-lead ECG for onset location has been explored using ECGI methods, and in particular using the fastest route algorithm [van Dam 2013]. We want to study here the difference of the personalisation presented on Chapter 2 with BSPM data to standard 12-lead ECG data. The goal is to estimate the activation onset location from a simulated patient-specific database. As input we provide QRS shape-related descriptors and as output we provide an estimated cardiac activation map. We used a kernel ridge regression (see Chapter 2 for further details).

From the BSPM electrodes of the CRT dataset (5 patients), we extracted for each patient 9 electrodes roughly located at conventional ECG placements in order to derive the 12-lead ECG (Figure 5.5). The derivations were performed on the simulated and on the ground truth signals.

### 5.3.2 Results on Activation Onset Localisation

We applied our personalisation for the 12-lead ECG data to the 5 CRT patients. The MDE (mean distance error) between true and estimated activation onset was  $29.8mm$ , which is slightly higher than the BSPM personalisation ( $24.6mm$ ). However by looking closely at the results, the errors were particularly important on patient 2 (RV lead:  $57mm$ , LV lead:  $64mm$ ), while small errors were obtained on patient 5 (RV lead:  $10mm$ , LV lead:  $12mm$ ). Knowing that the data from patient 2 was of very poor quality and that patient 5 is the only one having a personalised geometry (see Chapter 2), the 12-lead ECG may be less robust than BSPM personalisation. The fact that the onset activation was well located on cases with correct data quality seems to show that our method is sufficiently constrained such as to work with few signals.

### 5.3.3 Conclusion of the Activation Onset Localisation

The extension of the BSPM personalisation to standard 12-lead ECG data seem to indicate that for correct quality data, the onset activation can be localized with only 12-lead ECG data. This would reduce considerably the complexity and the cost of

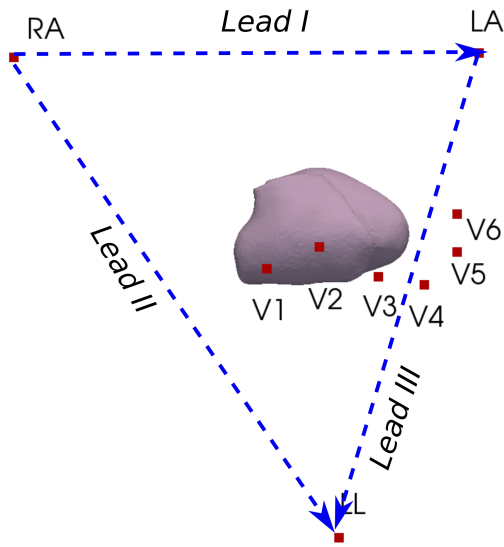


Figure 5.5: The 9 electrode locations used for the derivation of the 12-lead ECG and the cardiac mesh.

the procedure. However, for this study the electrodes used were selected from the BSPM vest and thus were precisely localized, which is not the case for the standard ECG routine. Moreover, a more refined study (for example by looking at errors in terms of epi/endo localisation) would be needed to fully compare the BSPM and the 12-lead ECG personalisations.

## 5.4 Conclusion

In this chapter, we investigated the personalisation of a cardiac EP model using only data from a 12-lead ECG. We first developed a specific methodology that is able to identify the Purkinje activation and we tested the predictive power of the approach on a CRT dataset. Then we showed in section 5.3 that using a satisfying data quality our personalisation method for onset activation localization is able to work with the 12-lead ECG with similar results. Because the 12-lead ECG is widely used and of small cost, we think this chapter to be of particular interest, showing how the cardiac EP personalisation is not restricted to particular and expensive research data.



# Personalisation in a CRT Clinical Prospective Study

---

## Contents

---

<b>6.1</b>	<b>Introduction</b>	<b>92</b>
<b>6.2</b>	<b>VP2HF Project</b>	<b>92</b>
6.2.1	Motivation	92
6.2.2	Goals	92
6.2.3	European Partners Involved	92
<b>6.3</b>	<b>CRT Clinical Prospective Study and Modelling Pipeline</b>	<b>93</b>
6.3.1	CRT Clinical Prospective	93
6.3.2	Modelling Pipeline	93
<b>6.4</b>	<b>Electrophysiological Personalisation as part of a Modelling Pipeline</b>	<b>94</b>
<b>6.5</b>	<b>First Results and Patients Modelling Reports</b>	<b>96</b>
<b>6.6</b>	<b>Discussion</b>	<b>97</b>
<b>6.7</b>	<b>Conclusion</b>	<b>97</b>

---

This chapter is partly based on the VP2HF deliverables and reports (freely available at <http://www.vp2hf.eu/>) and on the following VPH 2016 conference abstract:

**Personalised Cardiac Electromechanical Modelling in Clinical Time-frame**, Jack Lee, Lauren Fovargue, David Nordsletten, Liya Asner, Myria Hadjicharalambous, Sophie Giffard-Roisin, Maxime Sermesant, Jessica Webb, Nicolas Smith, Reza Razavi. Virtual Physiological Human Conference, Amsterdam, The Netherlands, September 2016.

## 6.1 Introduction

This PhD thesis is part of the European project entitled VP2HF and we mostly worked within the work-package entitled 'Non-invasive personalised electrophysiological modelling'. Moreover, we contributed to a clinical prospective study where mechanical and EP models were used to personalise and evaluate the chances of CRT response of new patients in a clinical time frame. Because BSPM data was not acquired in the prospective study, the personalisation was performed using simpler EP markers and a specific automatic pipeline was developed.

## 6.2 VP2HF Project

### 6.2.1 Motivation

Heart failure (HF) is a major health issue in Europe, currently affecting six million patients and growing substantially, but the poor short to medium term prognosis of these patients means that treatments such as cardiac re-synchronisation therapy (CRT) and mitral valve (MV) repair can have substantial impact. However, HF therapies are ineffective in up to 50% of treated patients and involve significant morbidity and substantial cost.

### 6.2.2 Goals

The European project VP2HF aims to bring together image and data processing tools, with statistical and integrated biophysical models, into a single clinical workflow to improve therapy selection and treatment optimisation in HF. This field was, and still is, an emerging field, in which few integrated products are available on the market. New tools were developed, and existing tools improved, to integrate into a single clinical HF software platform for intuitive, straightforward use by clinicians; and a prospective clinical study was run to demonstrate the successful translation of the platform into the clinical environment. By using a decision tree stratification approach, only the appropriate parts of the tool chain that would add maximum value to the predictions were used in individual patients, meaning that the more resource intensive parts were only used when they provided real value.

### 6.2.3 European Partners Involved

This 3-year project was funded by the European Union Seventh Framework Program for research, technological development and demonstration under grant agreement no 611823. It involves 9 European partners: 3 clinical centers (St-Thomas Hospital London, CHU Caen, Louvain Hospital), 5 public research teams (King's College London, Universtat Pompeu Fabra Barcelona, Inria Sophia-Antipolis, Inria Saclay, Simula Research Laboratory Oslo) and 2 industrial partners (Philips Research, Centron Diagnostics).

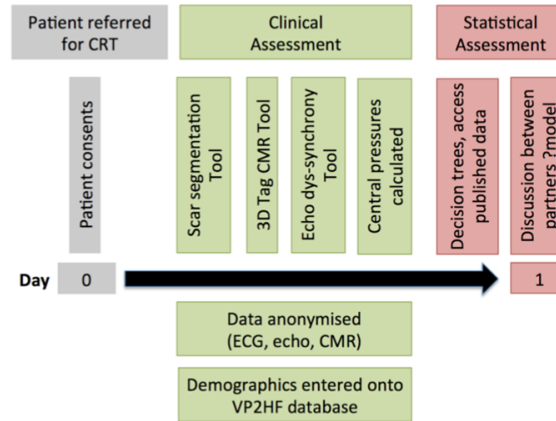


Figure 6.1: Overview of the clinical assessment process, beginning with the patient consenting to the research, then the clinical assessment and finally the statistical assessment.

## 6.3 CRT Clinical Prospective Study and Modelling Pipeline

### 6.3.1 CRT Clinical Prospective Study

A personalised patient selection requires the integration of multidimensional clinical data with a suitable decision support system. In the VP2HF project, we have tackled these challenges by combining image and data processing tools with statistical and biophysical modelling into a single hierarchical clinical work flow. In 2016, the project has entered a prospective observational trial phase, in which patients scheduled for CRT implantation were diagnosed using the pipeline in real clinical time. The principal goal is to use the non-invasive pre-assessment data to make patient-specific therapy outcome predictions. Figure 6.1 represents the overview of the clinical assessment process. After the non-invasive acquisitions and the calculation of the clinical biomarkers needed, the decision trees were used to propose a possible outcome after only one day.

### 6.3.2 Modelling Pipeline

Personalised electromechanical modelling represents the farthestmost stage in our assessment hierarchy, involving the highest level of complexity and data requirements, and is applied only for those patients regarded as borderline, by other clinical biomarkers. If the decision trees indicated modelling after day 1 (Figure 6.1), then the different partners involved in the modelling pipeline worked within a two-week window in order to provide a modelling report with a CRT indication (Figure 6.2). The modelling pipeline spans from combined image data processing, to inverse model parameterisation, finally leading to predictive simulation sweeps. The tool chain is largely automated, but is designed to be inspected by the operator at

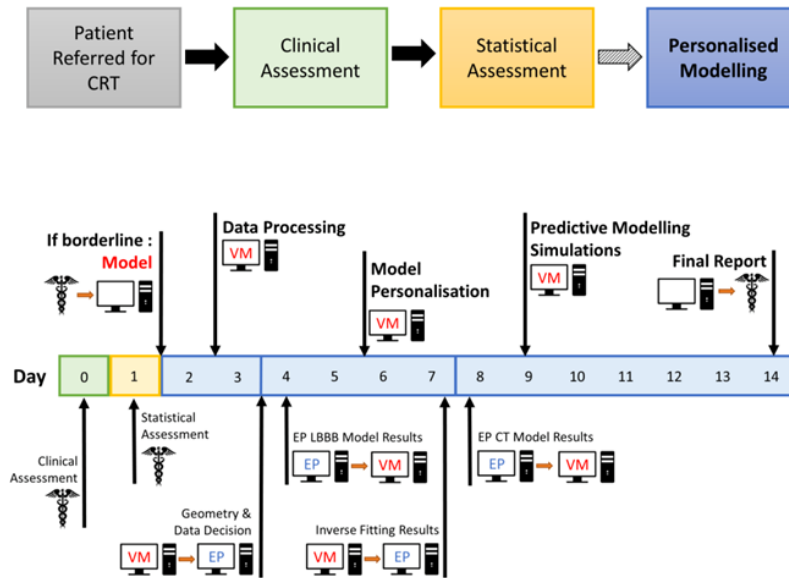


Figure 6.2: Overview of the patient assessment process (Top) and personalised modelling pipeline (Bottom). EP: electrophysiology, VM: Ventricular mechanics

pre-defined check points, allowing any necessary interventions and to optimise the modelling trajectory given the available data. The ventricular mechanics part was performed at KCL research by Lauren Fovargue, Jack Lee and Simone Rivolo.

## 6.4 Electrophysiological Personalisation as part of a Modelling Pipeline

The EP part of the modelling pipeline (Figure 6.2) was included in the PhD work. The EP personalisation is based on the patient-specific geometry, scar morphology, the presence of left or right bundle branch block and the ECG. As a more specific electrophysiological information is difficult to acquire non-invasively, the optimal activation pattern for the patient is estimated by incorporating the above information into a model to match the QRS duration, from a set of pre-selected pacing locations with additional clinical guidance.

For the EP simulations, a finite element discretisation of the monodomain equation is solved in conjunction with the Mitchell-Schaeffer model (see section 2.2.2.1) providing a spatially dependent depolarisation time map throughout the myocardium. Regional variation of tissue conduction was accounted for by creating distinction between healthy tissue, scar, and Purkinje fibres, as shown in Figure 6.3. To simulate LBBB, only right Purkinje fibres were given an accelerated conduction of 1.3m/s (for RBBB patients, only left Purkinje) The scar regions (segmented from late enhancement MRI) were fixed to a minimal value of 0.2m/s. The initial activation site, simulating the sinus rhythm, was taken from literature on the

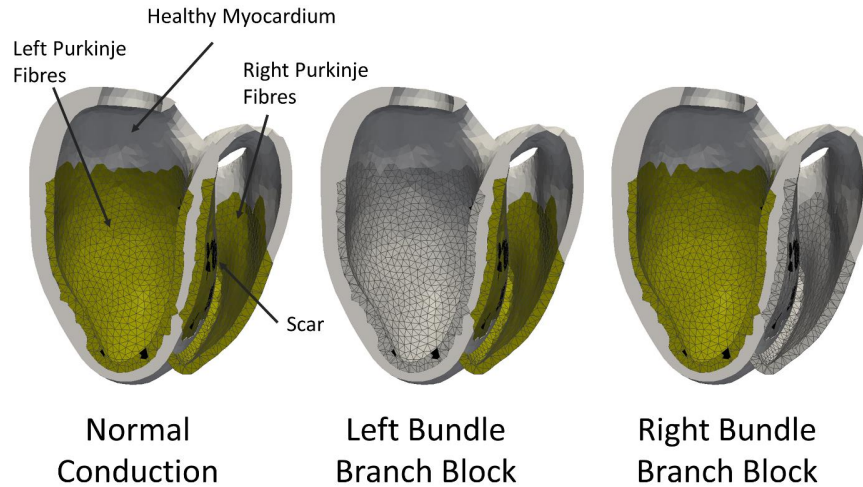


Figure 6.3: Regions defined in the electrophysiology (EP) model. Active Purkinje fibres, with fast conduction, are highlighted in gold. Deactivated Purkinje fibres are the basis of left and right bundle branch block, common forms of dyssynchrony. Here, these are modelled by using the same conduction velocity as the healthy myocardium

septum (Figure 6.4).

Fitting the healthy conduction velocity (CV) was achieved through a personalised training set of 100 simulations with random CV value between 0.15 and 0.8 m/s and nearest neighbor regression of the ECG QRS duration. Using the fitted sinus rhythm activation map, some mechanical parameters (passive stiffness and contractility of the myocardium) were also fitted from 2D echo, tagged MRI data and left ventricular end systolic pressure (for more details on the mechanical part, see the deliverable 6.4.1 freely available at <http://www.vp2hf.eu/>).

CRT pacing was induced by fixing the regional personalised conduction and moving initial activation points to the RV apex and LV lead for each pacing location (Figure 6.4). Two stimulating predictions were automatically performed using the Mitchell-Schaeffer cardiac model, corresponding to the most used in clinics: simultaneous pacing and left pacing ahead by 30 ms on the right pacing. On both, the QRS duration was estimated from the activation maps. The pacing activation maps were also used to predict the mechanical response to CRT by looking at the maximum LV pressure derivative  $\frac{dP}{dt}_{max}$  and the acute hemodynamic response (AHR, calculated by the percent increase in  $\frac{dP}{dt}_{max}$ ). A sensitivity analysis was performed on key parameters arising from susceptible data (such as the peak pressure estimate) giving an uncertainty quantification for the AHR.

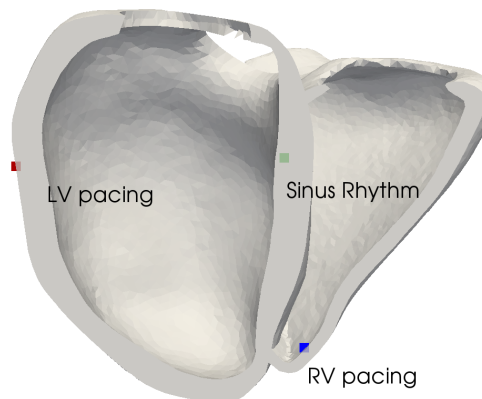


Figure 6.4: Onset activation locations manually selected. The sinus rhythm is on the septum (from literature). The left and right pacing sites correspond to the standard locations for the biventricular pacing device used in St Thomas Hospital, London.

## 6.5 First Results and Patients Modelling Reports

The HF platform and the decision trees have been used in all patients who have consented to VP2HF in the prospective study. At the time being, more than 50 patients were recruited and six entered into the biophysical modelling pipeline and obtaining results within a two-week window (see table 6.1). The final results are still being compiled since follow-up data from several patients is not available yet. Nevertheless we can already observe that 50% of the patients responded volumetrically to CRT at 6 months, in line with published literature. Also, more than 50% of the non-responders were identified by the decision trees, which could have had a large impact in the management of these patients if this information would have been used for clinician decisions.

The decision trees outcomes of the 6 modelled patients are visible in table 6.1. We can see that the different guidelines are not agreeing, which implied a modelling pipeline. After the whole electromechanical personalisation (2 weeks), a modelling report was delivered to the clinicians. The first 5 reports are reported in figures 6.5, 6.6, 6.7, 6.8, and 6.9. They include EP and mechanical responses to pacings. The first 4 patients were estimated to be CRT responders (even if patient n.3 was found limited responder), and the patient n.5 was estimated non-responder.

In the name of objectivity, the precise comparison with the true 6-months outcomes are not possible yet. However, we already know that for the modelled patients n.1, 2, 4 and 5 the outcome prediction of three out of four was correct.

Table 6.1: The six patients modelled in the prospective study (LVEF - left ventricular ejection fraction, LBBB - left bundle branch block). Reference published literature guidelines : European Society Cardiology (ESC) and National Institute Clinical Excellence (NICE). For every patient, the 3 guidelines are disagreeing.

Patient	Etiology	LVEF	QRSd, LBBB	ESC guidelines	NICE guidelines	Echo dyssynchrony
1	Ischaemic	31%	166 ms, LBBB	CRT indicated	CRT indicated	CRT not indicated: no septal flash, abnormal ventricular filling, long AV delay
2	Non ischaemic	30%	154 ms, LBBB	CRT indicated	CRT indicated	CRT not indicated: no septal flash, AF, no passive septal movement
3	Non ischaemic	36%	Intermittent (84 ms, LBBB)	CRT not indicated	Consider CRT	CRT indicated: no septal flash, abnormal ventricular filling, no long AV delay
4	Ischaemic	36%	168 ms, RBBB	CRT not indicated	Consider CRT	CRT not indicated: no septal flash, abnormal ventricular filling, long AV delay
5	Non ischaemic	31%	154 ms, LBBB	CRT not indicated	Consider CRT	Consider CRT: septal flash
6	Non ischaemic	40%	168 ms, LBBB	CRT not indicated	Consider CRT	Consider CRT: septal flash

## 6.6 Discussion

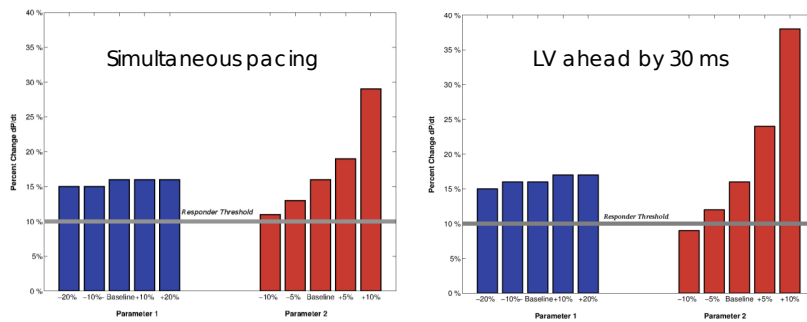
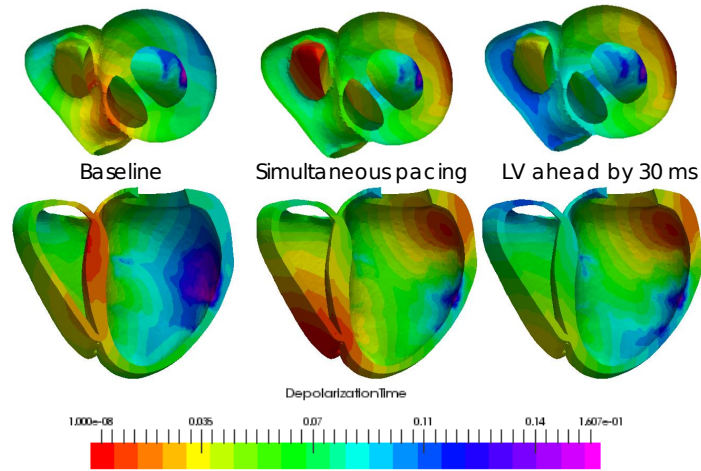
To our knowledge, this is the first time that an electromechanical cardiac modelling was performed in a non-invasive clinical study and in a reasonable time frame. Only the borderline cases were modelled (because of time demand) and we think that it would be interesting to include some other patients in order to properly validate the modelling. Moreover, the EP personalisation is only based on the geometry, the scar, the LBBB/RBBB pattern and the QRS duration matching. The complete 12-lead ECG was not used because the method presented in section 5.2 was not available at the beginning of the prospective study. We believe that it would be an important step forward. Finally, such a pipeline still needs an important number of non-automatic steps and was using the resources of 2 different centers. In the scope of an integration into a software for clinicians, some important efforts must still be done.

## 6.7 Conclusion

In this chapter, we used our EP personalisation into a CRT prospective study in a clinical time frame. Because less data and time was available, BSPM was not used and a simpler and automatic EP personalisation pipeline was performed to predict the activation maps under pacing from MRI imaging and sinus rhythm QRS duration and shape. The EP model was integrated in an electro-mechanical personalisation on 6 borderline patients, providing a modelling prediction of the CRT response to the clinicians.

### Modelling Report patient n.1

Report date: 27 Jan 2016  
 Study date: 12 Jan - 27 Jan 2016



#### Pre-implantation

dpdt <sub>max</sub>	901 ± 170 mmHg/s
EDP	12 mmHg
ESP	112 ± 8.8 mmHg
EDV	304 mL
ESV	235 ± 11 mL
EF	21.5 ± 4.8 %

#### Simultaneous Pacing

dpdt <sub>max</sub>	1120 ± 320 mmHg/s
Δdpdt	18.5 ± 7.9 %
EDP	12 mmHg
ESP	110 ± 8.6 mmHg
EDV	304 mL
ESV	236 ± 11 mL
EF	22.3 ± 3.7 %

#### LV ahead by 30ms

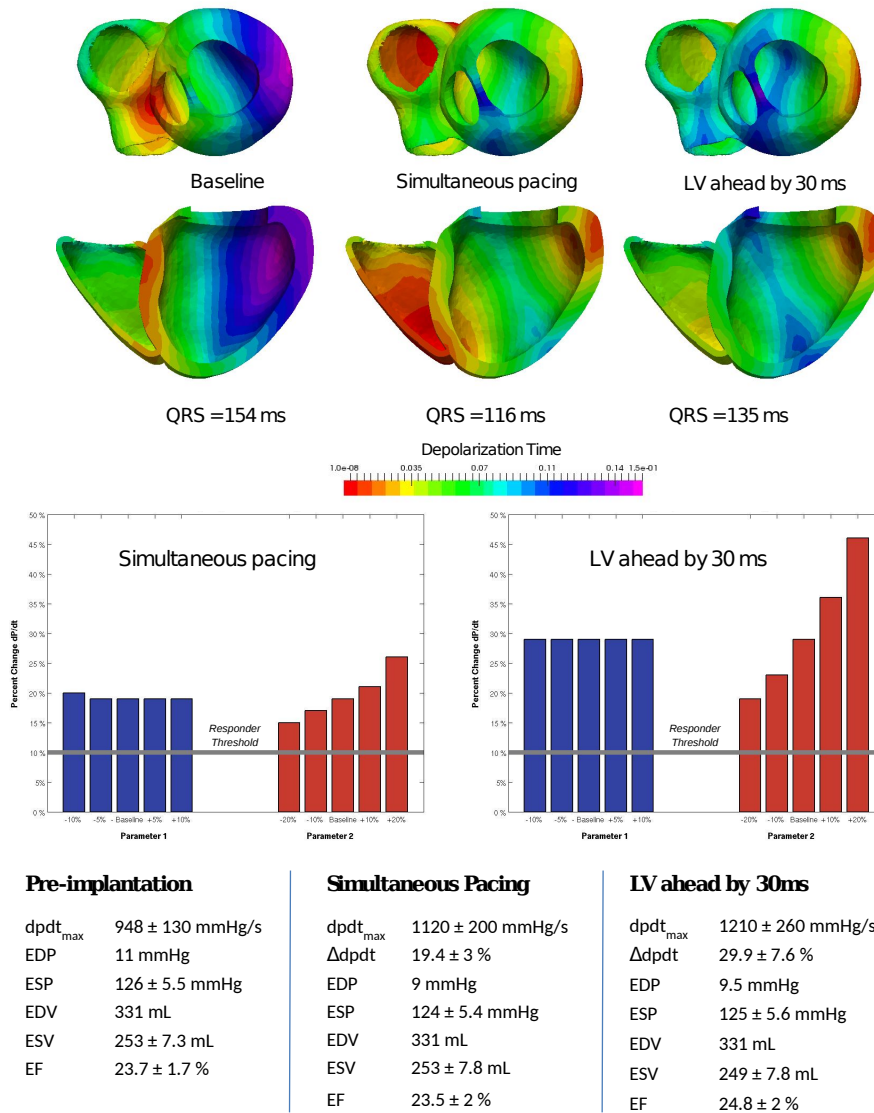
dpdt <sub>max</sub>	1140 ± 340 mmHg/s
Δdpdt	19.8 ± 9.7 %
EDP	12 mmHg
ESP	111 ± 8.8 mmHg
EDV	304 mL
ESV	232 ± 11 mL
EF	23.6 ± 3.6 %

### Modelling prediction: responder

Figure 6.5: Modelling report of patient n. 1. From this report, the patient was predicted as a CRT responder.

### Modelling Report patient n.2

Report date: 23 Feb 2016  
 Study date: 9 Feb - 23 Feb 2016

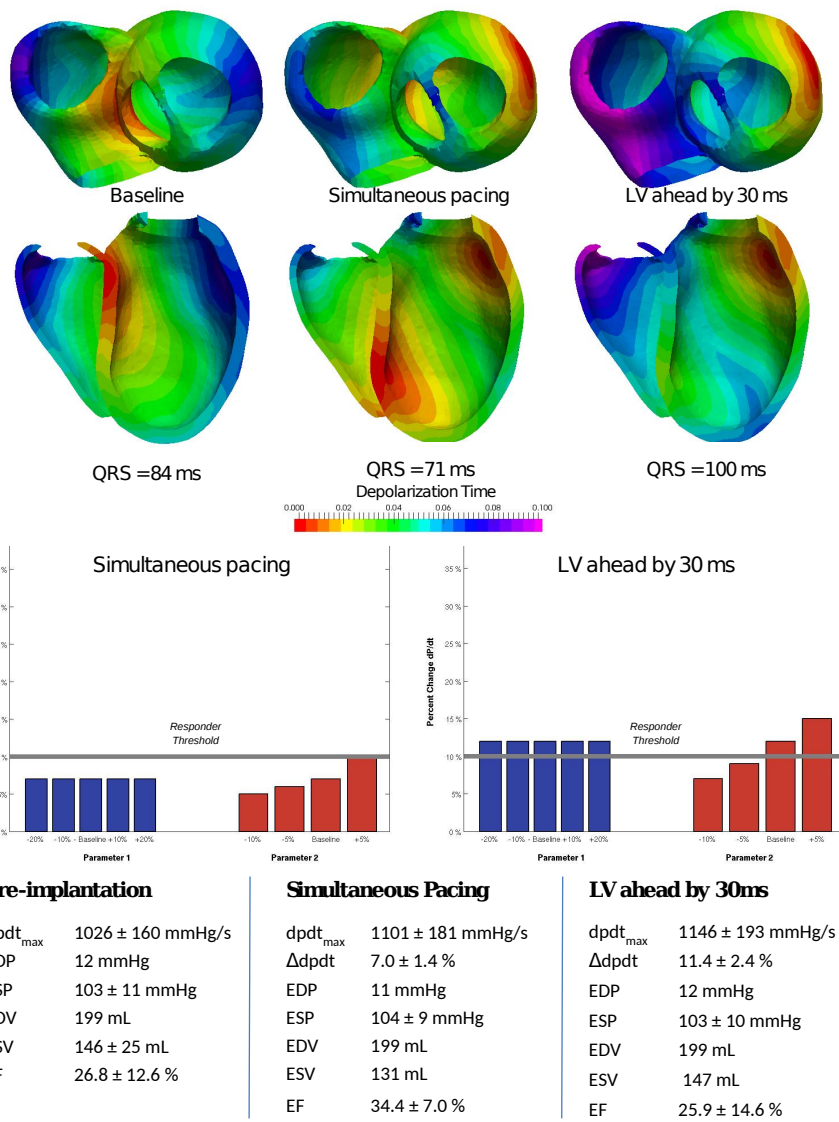


**Modelling Prediction : Responder**

Figure 6.6: Modelling report of patient n. 2. From this report, the patient was predicted as a CRT responder.

### Modelling Report patient n.3

Report date: 02 June 2016  
 Study date: 13 May 2016 - 02 June 2016



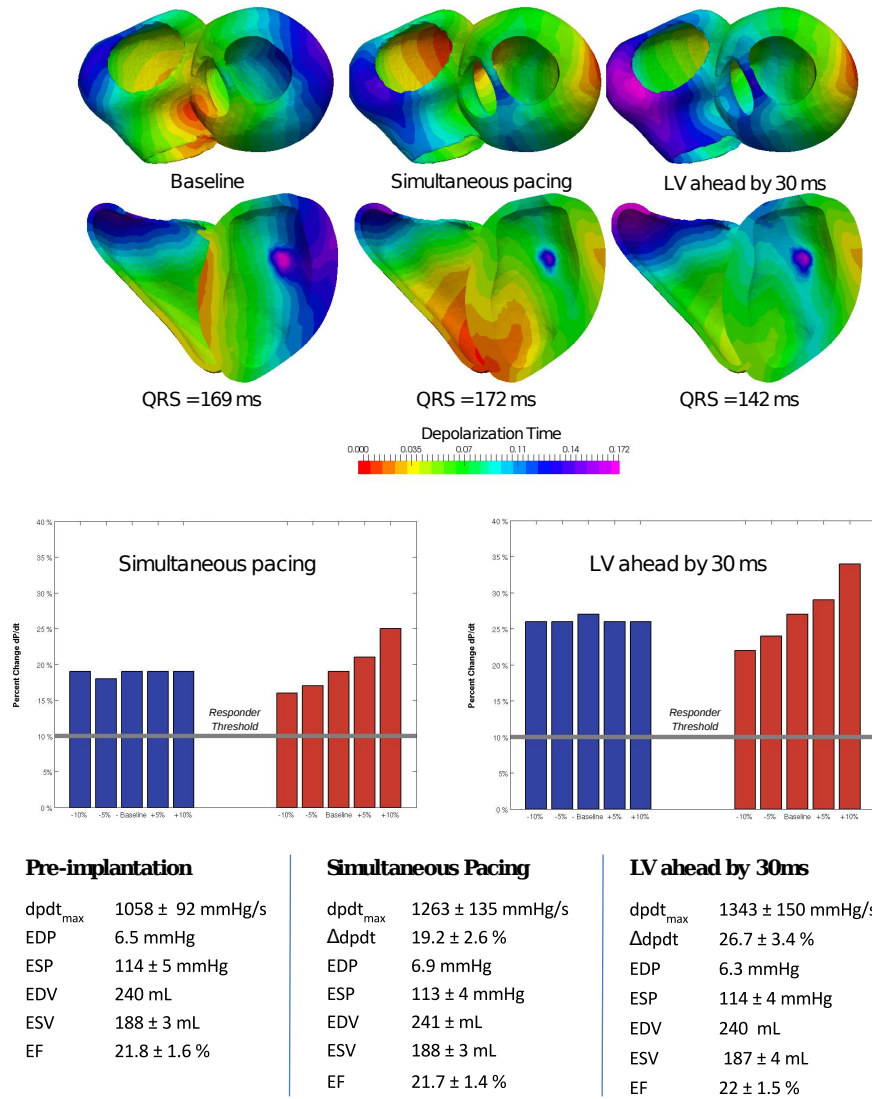
**Modelling Prediction : Responder (Limited)**

Figure 6.7: Modelling report of patient n. 3. From this report, the patient was predicted as a CRT responder. However, the threshold values are hardly reached so the modelling indicates a possibly limited response to CRT.

### Modelling Report patient n.4

Report date: 9 May 2016

Study date: 20 April - 9 May 2016



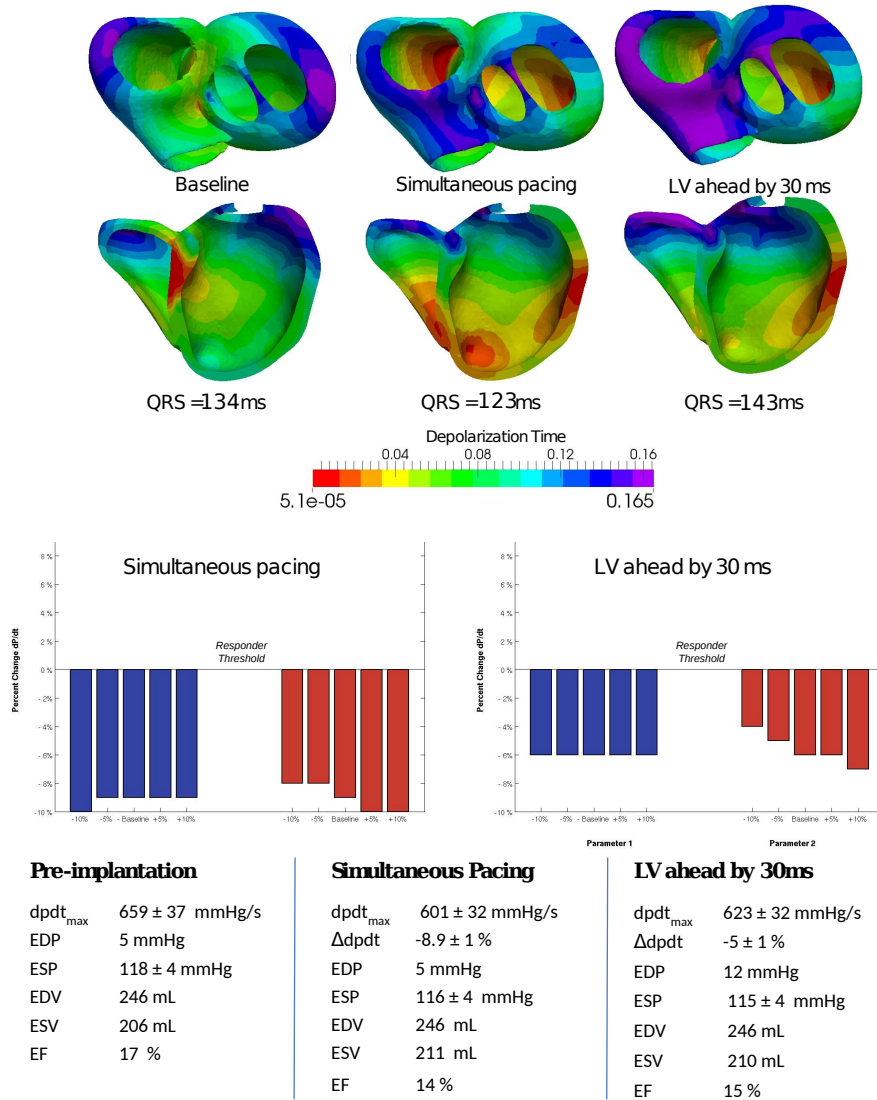
**Modelling Prediction : Responder**

Figure 6.8: Modelling report of patient n. 4. From this report, the patient was predicted as a CRT responder.

### Modelling Report patient n.5

Report date: 30 November 2016

Study date: 12 Sept - 30 November 2016



**Modelling Prediction : Non-Responder**

Figure 6.9: Modelling report of patient n. 5. From this report, the patient was predicted as a non-responder.

# Pre-clinical Electro-mechanical Model Personalisation on Canine Data

---

## Contents

---

<b>7.1</b>	<b>Introduction</b>	<b>104</b>
<b>7.2</b>	<b>Models and Methods</b>	<b>104</b>
7.2.1	Geometry Processing	105
7.2.2	Electro-Mechanical Modelling: SOFA Software	106
<b>7.3</b>	<b>Parameter Estimation</b>	<b>107</b>
7.3.1	Sensitivity Study	107
7.3.2	Mechanical Parameters Calibration: Unscented Transform Algorithm	108
<b>7.4</b>	<b>Results</b>	<b>108</b>
7.4.1	Clinical Data	108
7.4.2	Current Results	109
7.4.3	Discussion and Improvements	109
<b>7.5</b>	<b>Conclusion</b>	<b>111</b>

---

This chapter is based on the following paper:

**Evaluation of Personalised Canine Electromechanical Models**, *Sophie Giffard-Roisin, Stéphanie Marchesseau, Loïc Le Folgoc, Hervé Delingette, and Maxime Sermesant*. In Proceedings of the 5th international STACOM workshop (Boston, September 18, 2014), held in Conjunction with MICCAI 2014. Lecture Notes in Computer Science, Boston, September 2014.

## 7.1 Introduction

This work is part of a 2014 challenge on cardiac electromechanical (EM) modelling, where cardiac simulations were evaluated by comparing with the true cardiac movements recorded by tagged MRI. Several EM methods were finally compared in order to accelerate progress in the use of such models for clinical use.

Cardiac modelling aims at understanding cardiac diseases (such as heart failure, desynchronization or tachycardia) and predicting cardiac responses to treatment or therapies (as cardiac resynchronization therapy or radiofrequency ablation). The goal is to help cardiologists in detecting anomalies, planning interventions, and selecting suitable patients for a given therapy. Cardiac modelling is driven by the assumption that the electromechanical response of the heart can be simulated from anatomical and physiological data.

Heartbeat is initiated by an electrical wave that propagates through the myocardium, activating mechanical contraction at a microscopic scale. A suitable model needs to take into account the anatomical structure, the electrical propagation, as well as the mechanical function of the heart.

For an efficient EM modelling, this work is based on an Eikonal model [Serresant 2007] for the simulation of the electrophysiological system. The active and passive mechanical behavior is defined by the Bestel-Clement-Sorine modelling as formulated in [Chapelle 2012]. The latter ensures to take into account the microscopic scale phenomena of the contraction as well as laws of thermodynamics.

The coupled electro-mechanical simulation of the cardiac system is implemented within the SOFA platform<sup>1</sup>. The simulations were performed on healthy canine clinical data, provided by the STACOM'2014 challenge. They include left ventricular (LV) geometry, LV volume and LV pressure curves, as well as myocardial fibre directions.

## 7.2 Models and Methods

Canine and human hearts have close anatomical structures, that is why the canine heart is often used in pre-clinical studies. Both anatomies are composed of two ventricles, left (LV) and right (RV), and two atria. The heart function is mainly driven by the LV, acting like a pump to send the blood to the body. The system studied here is composed of a healthy canine left ventricle. In order to run the electrical and the mechanical cardiac models, input such as anatomical meshes and fibre directions have been processed.

---

<sup>1</sup>SOFA is an Open Source medical simulation software available at <http://www.sofa-framework.org>

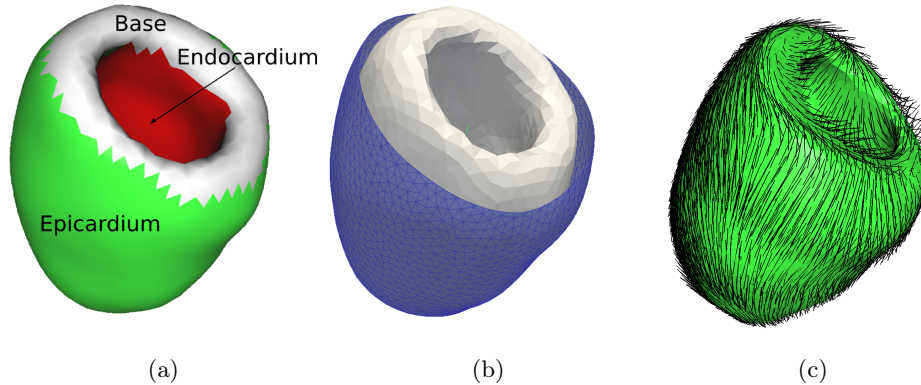


Figure 7.1: Geometry and fibres processing: Identification of the surface zones of the LV myocardium mesh (a), pericardium surface membrane (b) and fibre directions from DTI imaging (c).

## 7.2.1 Geometry Processing

### 7.2.1.1 Myocardial Mesh Generation.

The myocardium mesh is generated using CGAL<sup>2</sup> meshing software, to create a tetrahedral mesh from medical image segmentations. The geometry is computed at end diastole (ED). The number of elements is roughly 50K, so that the average edge length is close to 1.5mm. This refinement ensures to have enough elements in the thickness of the muscle to describe the anisotropy (at least 5 layers transmurally) while limiting computation time.

In addition to the volumetric mesh segmentation, endocardial (inner lining) and epicardial (outer layer) surface zones are manually delineated, as illustrated in Fig. 7.1a. These surface zones are useful for the electrical as well as for the mechanical simulations (Sec. 7.2.2).

For a single left ventricular model we consider that the contraction of the left ventricle does not depend on that of the RV as a first approximation. We depart from classic anatomical terminology in identifying the epicardium with the outer layer of the left ventricle segmentation.

### 7.2.1.2 Pericardium Surface Generation.

Our model incorporates boundary conditions that faithfully replicate anatomical constraints on the motion of the heart. Specifically, the pericardial membrane is modelled as a fixed surface around the epicardium as in [Marchesseau 2013], and was obtained by dilating the segmentation from the diastasis phase of 1.5 mm, see Fig. 7.1b). The SOFA simulation platform allows for realistic collision constraints between the myocardium and the surrounding pericardium, which limits radial mo-

<sup>2</sup>CGAL is a Computational Geometry Algorithms Library, available at [www.cgal.org](http://www.cgal.org).

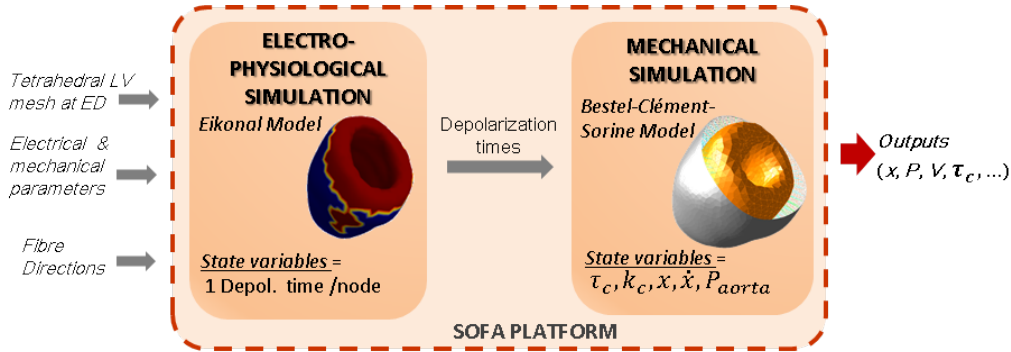


Figure 7.2: Complete electromechanical pipeline. A single simulation computes simultaneously the electrical and the mechanical modellings.

tion but also global translations. We model the presence of the RV as part of a pericardium membrane surrounding the LV. This is motivated by the fact that the pressure applied by the RV on the external wall of the LV could be approximated by a rigid constraint.

### 7.2.1.3 Fibre Directions.

The myocardium is organized in muscle fibres which govern the electric propagation as well as the anisotropic contraction. The anisotropic tensor at each position can be measured via DTI imaging, and the principal directions (from eigen value decomposition) generate an approximation of the fibre directions. They are displayed in Fig. 7.1c.

## 7.2.2 Electro-Mechanical Modelling: SOFA Software

The pipeline efficiently couples the simulation of the electrophysiology and mechanics of the heart in the SOFA platform. The electrical wave propagation is simulated in the ED configuration, during the first step of the cardiac cycle. The mechanical contraction and relaxation of the myocardium are simultaneously computed from the depolarization times output by the electrical simulation, taking into account the different forces and boundary conditions. The pipeline is summarized in Fig. 7.2.

### 7.2.2.1 Electrophysiological Simulation: Eikonal Model.

The electrophysiological pattern of activity is simulated using an Eikonal model, describing the depolarization front propagation. The depolarization times  $T_d$  at each node of the mesh are estimated by solving the Eikonal equation  $v\sqrt{\nabla T_d^t \mathbf{D} \nabla T_d} = 1$  using a Multi-Front Fast Marching Method [Sermesant 2007].  $v$  is the local conduction velocity, set here uniformly to 500 mm/s.  $D$  is the anisotropic tensor, with an anisotropic ratio of 0.1 between the fibre direction and the perpendicular directions, and with local fibre directions estimated according to section 7.2.1.3.

The initialization of the electric wave is set on the LV endocardial surface (see Fig. 7.1a), to simulate a simultaneous activation pattern of the endocardium from the extremities of the Purkinje network.

### 7.2.2.2 Mechanical Simulation: Bestel-Clement-Sorine Model.

Our study is based on Bestel-Clement-Sorine (BCS) mechanical modelling as formulated by [Chapelle 2012], improved and implemented on the SOFA platform by [Marchesseau 2013]. The BCS model is compatible with the laws of thermodynamics and it is based on the microscopic scale phenomena.

It is composed of a passive hyperelastic part described as a Mooney Rivlin material, that accounts for the elasticity. The stress along the cardiac fibres is decomposed into two parts. An active part models the contraction (binding/unbinding of actin-myosin filaments) together with an energy dissipation due to friction, and a parallel passive part corresponds to the elastic bound. The model is further improved by taking into account the circulation model representing the 4 phases of the cardiac cycle. Especially, the aortic pressure is modelled following a 2-parameter Winkessel model.

The BCS model is in particular able to capture the Starling effect (adaptation of the contraction enabling the stroke volume to compensate the end-diastolic volume) and the unbinding due to a too high relative speed between actin and myosin, with a constant  $\alpha$  related to the cross-bridge release. For more details on the mechanical model, refer to [Marchesseau 2013].

## 7.3 Parameter Estimation

We use the approach described in [Marchesseau 2013] to estimate the parameters on canine hearts. Note that [Marchesseau 2013] was used to estimate parameters on human data and therefore cannot be applied as it is since the geometry, the cardiac period and the mechanical materials are different. A complete sensitivity study and a personalized calibration of the most relevant parameters have been performed.

### 7.3.1 Sensitivity Study

The parameters of the model are summarized in Tab. 7.1. The electrophysiological model is governed by a simple law, and has therefore mainly three parameters (once fibre directions and initial conditions are set), the local conduction velocity  $v$ , the anisotropic ratio  $A$  and the action potential duration (*APDs*). For the mechanical part, the parameters can be separated in 3 groups: parameters related to the active contraction, parameters related to the passive material, and parameters related to the hemodynamic model.

Starting from the results of [Marchesseau 2013], a quantitative study has been performed in order to estimate the range of possible values of each parameter of Tab. 7.1. We used pressure and volume observations to control the simulation. Some

	Parameter Name	Unit	case 1	case 2	case 3	case 4
EP	$A$ (Anisotropic Ratio)		0.1	0.1	0.1	0.1
	$v$ (Local Cond. Velocity)	$mm.s^{-1}$	500	500	500	500
	$APD$ (Action Pot. Dur.)	$s$	0.18	0.18	0.20	0.24
Contraction	$\sigma_0$ (Max Contraction)	$MPa$	30	29	20	21
	$k_0$ (Max Stiffness)	$MPa$	6	6	6	6
	$k_{ATP}$ (Contraction Rate)	$s^{-1}$	40	40	40	40
	$k_{RS}$ (Relaxation Rate)	$s^{-1}$	90	90	90	90
	$E$ (Linear Modulus)	$MPa$	5	5	5	5
	$\alpha$ (Cross-bridges Rate)		0.8	0.8	0.8	0.8
	$\mu$ (Viscosity)	$MPa.s$	0.32	0.32	0.5	0.49
	$n_0$ (Red. factor, Starling)		0.5	0.5	0.5	0.5
Passive Mat.	$c1, c2$ (Mooney-R. Mod.)	$kPa$	50	50	50	50
	$K$ (Bulk Modulus)	$MPa$	1.7	1.7	2	1.9
Windkessel	$Rp$ (Wind. Resistance)	$MPa.m^{-3}s$	179	250	310	430
	$\tau$ (Wind. Charact. Time)	$s$	0.22	0.16	0.23	0.56

Table 7.1: Parameters of the electro-mechanical model for the 4 cases.

parameters do not impact significantly the simulation, as the maximum stiffness  $k_0$ . Others are easily calibrated, because they are visually perceptible, as the  $APD$ .

### 7.3.2 Mechanical Parameters Calibration: Unscented Transform Algorithm

The most influential and independent parameters identified as  $[\sigma, \mu, K]$  have been calibrated for each heart using the Unscented Transform Algorithm [Julier 1997]. The algorithm, derived from the Unscented Transform according to [Marchesseau 2013], calculates a set of  $n$  parameters of a nonlinear transformation that minimizes the difference between the measured observations and the predicted observations. Once having performed  $2n + 1$  simulations using some specific parameter values, the algorithm runs in one iteration. In our case, the observations are the minimal LV outgoing blood flow and the ejection fraction. LV outgoing flow is calculated as  $-dV/dt$ , with  $V$  the LV volume.

Independently, the Unscented Transform algorithm was used to calibrate the 2-parameter Windkessel model using the ground truth pressure curves.

## 7.4 Results

### 7.4.1 Clinical Data

The STACOM 2014 challenge revolves on data acquired on 4 healthy canine hearts. They include LV geometry and fibre directions. The 4 dogs were paced at 500ms

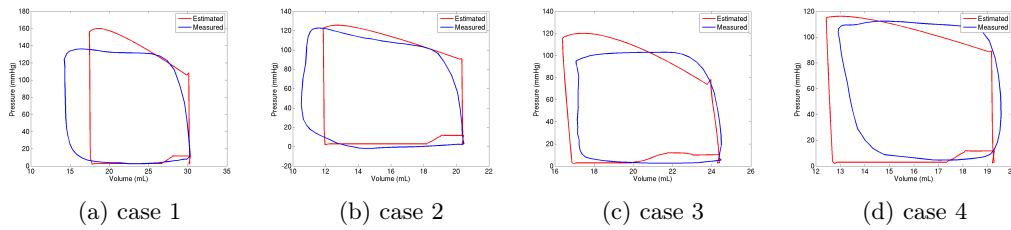


Figure 7.3: Comparison between LV pressure volume diagrams computed from simulations (red) and ground truth measures (blue).

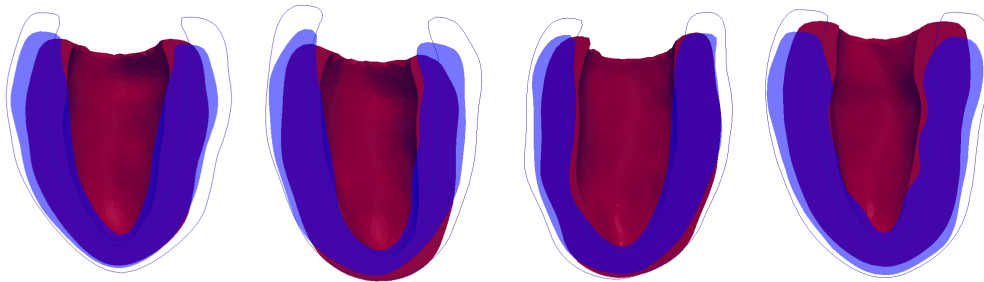


Figure 7.4: Simulated end-systolic geometry (red) of the LV of the 4 cases and ground truth (blue). The dark blue line represents the initial position (ED).

basic cycle length. The tetrahedral mesh is constructed from binary images of the LV at ED.

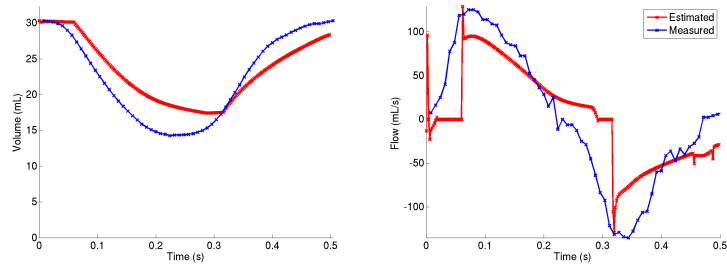
#### 7.4.2 Current Results

We give the results of the 4 canine simulations in terms of LV pressure volume diagrams (Fig. 7.3), LV volume, LV outgoing flow curves (Fig. 7.5) and ejection fractions (Tab.7.2). Comparison is made with the ground truth data, as LV volume and LV pressure curves were provided by the STACOM'2014 challenge for a complete cycle. We are displaying here the second cycle of the simulation, in order to avoid the wrong initial conditions.

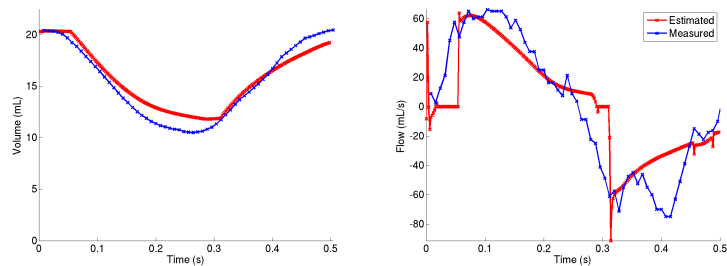
The simulated geometry of the 4 cases at ES is shown in Fig. 7.4. The ground truth end-systolic position is shown in blue while red is the simulation. The dark blue line represents the initial position (ED).

#### 7.4.3 Discussion and Improvements

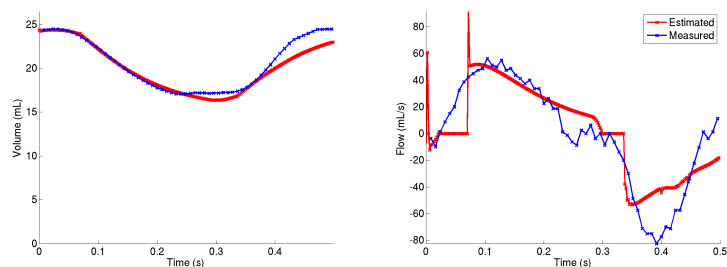
This first study shows promising results: the LV pressure volume diagrams and volume variations comparison indicate a realistic response of the model. Furthermore, the large variability of ejection fraction is reproduced in our results. We can also see from the slices of Fig. 7.4 that the modelled ventricle has a realistic movement



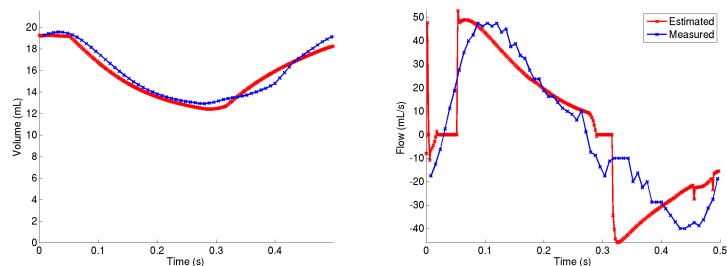
(a) case 1



(b) case 2



(c) case 3



(d) case 4

Figure 7.5: Comparison between LV volume and outgoing flow (as  $-dV/dt$ ) variations over one cardiac cycle computed from simulations (red) and ground truth measures (blue).

Ejection fraction	case 1	case 2	case 3	case 4
Measured (%)	53	49	30	34
Estimated (%)	43	42	33	36

Table 7.2: Comparison between ejection fractions computed from the simulations and the ground truth measures.

(note the correct apico-basal shortening). However, the myocardium wall thickness variation is not completely reproduced, corresponding to a simulated muscle not incompressible enough.

The calibration of a model of a standard case is the first step towards the prediction of its response to treatments and therapies. Since our model is driven by faithful anatomical constraints and mechanical laws, we are confident in the fact that such a model will be able to realistically simulate pathology cases and predict their responses to treatments.

## 7.5 Conclusion

In this chapter we have adapted an electro-mechanical cardiac modelling to canine hearts. From the geometry of the left ventricle in end diastole and the heart period and the fibre directions, we are able to simulate heart movement over the whole cardiac cycle. The quantitative validation (results of the STACOM'2014 challenge) is comforting the tendency of the global indicators: the displacement fields obtained with the simulations and the displacement fields obtained by tagged MRI provided by the STACOM'2014 challenge are in good agreement.

In the scope of electrophysiological models, it is essential to also evaluate the resulting cardiac movement. These pre-clinical studies with very precise data are essential for building accurate methods. We can see that for this study on healthy canine hearts, a simple Eikonal electrical model was able to capture the EP dynamics. However, more complex pathologies might need a more physiological EP model.



# Conclusion

---

## Contents

<b>8.1 Contributions Summary</b>	<b>113</b>
<b>8.2 Publications and Awards</b>	<b>114</b>
8.2.1 Publications	114
8.2.2 Awards	116
<b>8.3 Perspectives</b>	<b>116</b>
8.3.1 Clinical Perspectives	116
8.3.2 Methodological Perspectives	117

---

In this thesis, we explored the non-invasive EP cardiac model personalisation. We will now summarize the main contributions and propose some perspectives of the work.

## 8.1 Contributions Summary

We developed non-invasive methods for the personalisation of some parameters of the cardiac EP model, filling the gap between ECG imaging and model personalisation. Even if these new techniques are still exploratory approaches we focused our work to their clinical relevance by a constant evaluation on real data. Moreover, we concretely worked on specific methods using routinely available data and on an integration in a clinical time-frame.

We summarize here the main achievements of this PhD work.

- We proposed a fast physiological simulation of the cardiac EP propagation together with BSPM signals on the torso using the SOFA platform. The efficient forward model is based on the cardiac Mitchell-Schaeffer model and a current dipole formulation on an infinite domain, allowing to simultaneously calculate transmural cardiac potentials and BSPMs. We compared our results with a boundary element method simulation showing only small signal amplitude differences.
- We proposed a non-invasive estimation of patient-specific ventricular EP parameters from a large simulated training set, including multiple onset localisation and inhomogeneous ventricular conduction velocity. We developed a QRS

shape-related feature description of the BSPMs and we used machine learning and variational approaches to estimate parameters and cardiac activation maps. Different algorithms were used depending on the type of parameters to estimate: kernel ridge regression, relevance vector regression, covariance matrix adaptation and k-nearest neighbor regression. The evaluation on various clinical datasets (composed of CRT candidates and a premature ventricular contraction patient) showed a good estimation of onset activation locations together with realistic transmural cardiac activation maps. Moreover, the simulated torso signals using the estimated parameters were in good agreement with the real signals.

- We proposed a reference ventricle-torso anatomy able to easily represent every patient with preserved heart orientation and position. We were thus able to perform a model EP personalisation on clinical data with poor cardiac image quality. Moreover, we showed that a reference anatomy can be applied to many patients leading to a substantially reduced computational time (thanks to the common simulated dataset and common regression fitting) and to an easier classification and comparison of EP patterns between patients.
- We proposed a simulated prediction of different pacing configurations for the CRT candidates. We estimated the cardiac response to particular pacing configurations from the personalised model. We showed that the inclusion of patient-specific parameters lowers the torso signal difference with respect to the real paced signals. To our knowledge, this is the first non-invasive patient-specific prediction of pacing configurations.
- We proposed some applications using simplified and routinely available data such as 12-lead ECG and QRS duration. We showed that for CRT selection and CRT planning the cardiac EP model personalisation was not restricted to BSPM data. As part of an electro-mechanical modelling pipeline, we experienced in a clinical time-frame the prediction of CRT candidates outcomes.

## 8.2 Publications and Awards

### 8.2.1 Publications

This thesis has led to several publications in international peer-reviewed journals and conferences.

#### Journal publications

- Non-Invasive Personalisation of a Cardiac Electrophysiology Model from Body Surface Potential Mapping.  
*Sophie Giffard-Roisin, Thomas Jackson, Lauren Fovargue, Jack Lee, Hervé Delingette, Reza Razavi, Nicholas Ayache, and Maxime Sermesant.* IEEE Transactions on Biomedical Engineering, 2017.

- Learning Relevant ECGI Simulations on a Reference Anatomy for Personalised Predictions of Cardiac Resynchronisation Therapy.  
*Sophie Giffard-Roisin, Hervé Delingette, Thomas Jackson, Jessica Webb, Lauren Fovargue, Jack Lee, Christopher A. Rinaldi, Reza Razavi, Nicholas Ayache, Maxime Sermesant.* To be published.

### Conference publications

- Evaluation of Personalised Canine Electromechanical Models.  
*Sophie Giffard-Roisin, Stéphanie Marchesseau, Loïc Le Folgoc, Hervé Delingette, and Maxime Sermesant.* In Proceedings of the 5th international STACOM workshop (Boston, September 18, 2014), held in Conjunction with MICCAI 2014. Lecture Notes in Computer Science, Boston, September 2014.
- Estimation of Purkinje Activation from ECG: an Intermittent Left Bundle Branch Block Study.  
*Sophie Giffard-Roisin, Lauren Fovargue, Jessica Webb, Roch Molléro, Jack Lee, Hervé Delingette, Nicholas Ayache, Reza Razavi, and Maxime Sermesant.* In 7th International Statistical Atlases and Computational Modeling of the Heart (STACOM) Workshop, Held in Conjunction with MICCAI, Lecture Notes in Computer Science, Athens, Greece, October 2016.
- Sparse Bayesian Non-linear Regression for Multiple Onsets Estimation in Non-invasive Cardiac Electrophysiology.  
*Sophie Giffard-Roisin, Hervé Delingette, Thomas Jackson, Lauren Fovargue, Jack Lee, Aldo Rinaldi, Nicholas Ayache, Reza Razavi, and Maxime Sermesant.* In Functional imaging and modelling of the heart (FIMH) 2017 Proceedings, Toronto, Canada, June 2017.

### Co-author Publications

Some other collaborations during the thesis also lead to the following publications in international journals and conferences. We invite the reader to read the appendices [A](#) and [B](#) for more details on these collaborative works.

- A Pipeline for the Generation of Realistic 3D Synthetic Echocardiographic Sequences: Methodology and Open-Access Database.  
*Martino Alessandrini, Mathieu De Craene, Olivier Bernard, Sophie Giffard-Roisin, Pascal Allain, Irina Waechter-Stehle, Jürgen Weese, Eric Saloux, Hervé Delingette, Maxime Sermesant and Jan D’Hooge* IEEE Transactions on Medical Imaging, 2015.
- A Framework for the Generation of Realistic Synthetic Cardiac Ultrasound and Magnetic Resonance Imaging Sequences from the same Virtual Patients.  
*Yitian Zhou, Sophie Giffard-Roisin, Mathieu De Craene, Jan D’hooge, Martino Alessandrini, Denis Friboulet, Maxime Sermesant and Olivier Bernard,* IEEE Transactions on Medical Imaging, 2017.

- Generation of Ultra-realistic Synthetic Echocardiographic Sequences to Facilitate Standardization of Deformation Imaging.  
*Martino Alessandrini, and Brecht Heyde, **Sophie Giffard-Roisin**, Hervé Delingette, Maxime Sermesant, Pascal Allain, Olivier Bernard, Mathieu De Craene, Jan D’hooge*, 12th International Symposium on Biomedical Imaging (ISBI), 2015.
- Smoothed Particle Hydrodynamics for Electrophysiological Modeling: an Alternative to Finite Element Methods.  
*Éric Lluch Alvarez, Rubén Doste, **Sophie Giffard-Roisin**, Alexandre This, Maxime Sermesant, Oscar Camara, Mathieu De Craene and Hernán G. Morales*, Functional imaging and modelling of the heart (FIMH) conference, 2017.
- A Rule-Based Method to Model Myocardial Fiber Orientation for Simulating Ventricular Outflow Tract Arrhythmias.  
*Rubén Doste, David Soto-Iglesias, Gabriel Bernardino, Rafael Sebastian, **Sophie Giffard-Roisin**, Rocío Cabrera-Lozoya, Maxime Sermesant, Antonio Berruezo, Damián Sánchez-Quintana and Oscar Camara*, Functional imaging and modelling of the heart (FIMH) conference, 2017.

## 8.2.2 Awards

The oral presentation of the paper [Giffard-Roisin 2017a] received a *Best Paper Award* in the electrophysiology category at the 2017 FIMH conference in Toronto. Finally, the journal paper [Giffard-Roisin 2017b] was selected for the *TBME Highlights* of the TBME journal in September 2017.

## 8.3 Perspectives

### 8.3.1 Clinical Perspectives

#### 8.3.1.1 CRT Patient Selection

Because we were part of the VP2HF European project, our work was mainly focused on dyssynchrony patients and CRT patient selection. We hope that the developed tools could in the future help clinicians for understanding and also for predicting the patient CRT response. Because we rely on non-invasive data, the gain for the patient is maximized. Moreover, we believe that the predicted activation maps could be very helpful in pre-operatively identifying the best pacing locations. The CRT prospective study in the VP2HF project also showed that a cardiac EM modelling can fit in a clinical time-frame. However we were not able to test our methods relying on BSPM data during this study, and we think it would increase the modelling accuracy needed for a precise outcome prediction.

### 8.3.1.2 Atrio-Ventricular Personalisation

We have seen that an atrial pacing also activate the ventricles, however we encounter difficulties in modelling the atrio-ventricular coupling in our biventricular model. Moreover, some very recent studies have proposed to use a similar machine learning model-based personalisation for localizing the atrial ectopic beats [Ferrer-Albero 2017]. The integration of the atria in the ventricular model (for example as a thin layer [Schenone 2014]) and a study of the whole ECG heart beat could be beneficial for a precise and global personalisation.

### 8.3.1.3 Non-invasive Personalisation of Cardiac Arrhythmias

Cardiac electrophysiology is also an important tool for arrhythmia diagnostic and treatments. Some machine learning and model-based tools are for example locating local abnormal ventricular abnormalities (LAVA) from invasive procedures [Cabrera-Lozoya 2015]. A non-invasive personalisation for cardiac arrhythmia would be very useful because of the time gain and the smaller risk for the patient. However, such complex pathologies (involving very local changes of tissue properties and an abnormal wave propagation) may be more difficult to apprehend from non-invasive measures. One way could be to gather invasive and non-invasive data in order to integrate precise information into our framework.

### 8.3.1.4 Personalisation from 12-lead ECG Data

Finally, we have also explored the effectiveness of the methods relying only on 12-lead ECGs. Recently, [Potyagaylo 2016] showed that the ECGI results from 12-lead and 99-lead ECGs were comparable in many of the tested settings, while [Loewe 2011] was even able to detect ischemia from only 3 electrodes in optimal positions. We think that the major issue in using the common 12 leads for ECG imaging is not the number of leads but the lack of 3D localization. However, this localization could be recorded [Alioui 2011] or estimated from a learned distribution of previous recorded datasets. Because the 12-lead ECG is widely used and of small cost, we think it is of particular interest as cardiac EP personalisation should not be restricted to particular and expensive research data.

## 8.3.2 Methodological Perspectives

### 8.3.2.1 Variational vs. Sequential Approaches

We have used machine learning or variational data assimilation methods for our personalisations. As discussed in section 1.3.5, the sequential data assimilation is another possible approach. We have tested at the beginning of the PhD a sequential approach for the personalisation of local conductivity parameters. We coupled our forward model with a Reduced Order Unscented Kalman Filter (ROUKF), a data assimilation technique derived from the Kalman Filter and adapted to non-linear models with a large number of state variables. To achieve this, the simulation

software SOFA was driven by the Open Source generic library for data assimilation called Verdandi. The conductivity parameters were modified at each time step of the simulation. While being time efficient, in this case this method suffered from the too large number of state variables (the transmembrane potentials of all the nodes) and the high dependence on the previous states, which would have required the development of a more detailed reduction technique. Moreover, parameters such as onset activation locations cannot be re-adjusted once the EP simulation has began. As already mentioned, [Collin 2015] has developed a new sequential estimation method for making an atrial EP model patient-specific from simulated invasive measures. They have tackled the problem of complex EP wave shapes such as fibrillation by incorporating a correction term based on topological gradients. This way, it is possible to act only in active regions on the propagation front. This method could be applied for ventricular fibrillation patterns, and also maybe improve methods based on non-invasive data.

### 8.3.2.2 Cardiac Reduced Shape Space

In Chapter 3 and Chapter 4 we have used a dimensionality reduction of the myocardial shape based on the eigenmodes of a structural matrix, linked to modes of vibration of the tetrahedral mesh. We showed that the reconstruction errors was small for 400 modes and we also showed that the first modes were useful for visualizing the spread of simulated and real activation maps. However the small variations, contained in the last modes, are not spatially localized. For some applications such as the local CV estimation, it could be useful to work with a spatial reduced shape space, such as wavelet transform. Identifying the CV of simulated neighbors in each dimension could help in providing a direct local parameter estimation.

### 8.3.2.3 Transfer Learning

The use of a simulated database was driven by the fact that too few real data exists and by the fact that the simulated data can be large and patient-specific at the same time. However, simulated data and real data do not belong to the same domain (due to noise, geometrical errors or model simplifications). The correct framework would consist in transferring the knowledge between the source domain (large database with labeled data) to the target domain (smaller database, here real data) where the 2 domains are different but related. The transfer learning methods are solving these types of problems, and it has been applied for example in an ultrasound transducer localization in fluoroscopy images [Heimann 2014]. Because only unlabeled real images were available, they generated a simulated training data with an automatic labeling. The transfer learning was useful in order to adapt the simulated learning system to the real data by correcting the sample selection bias. In our case, the problem is harder as in the real data domain we usually have only one or very few samples. In fact in a patient-specific personalisation the only available data are the BSPM sequences from the patient itself, where only

few pacings are available. Moreover, the CV parameters are identical in all the sequences, so the transfer learning could not be applied to this task. By the use of a common heart/torso model, we can have more real data samples so we might consider it. A recent study on porcine MRI LV segmentation proposes to use transfer learning by fine tuning a deep learning network previously trained on a public human cine MRI dataset [Chen 2017a]. This could be a way to use a reference anatomical training and efficiently refine our learning to a specific patient.

#### 8.3.2.4 Unsupervised Interpatient Study

In Chapter 4 we have seen that a common heart-torso model was useful for the use of an offline and common simulated database. We also believe that it could be way to characterize a new patient by looking at its similarity with the patients previously recorded in the database. With a large real database of BSPM signals from different patients, we could determine clusters as groups of patients using unsupervised machine learning tools. A recent study proposes a similar approach for the characterization of myocardial motion patterns and identified some measures to differentiate healthy, breathless and heart failure with preserved ejection fraction (HFPEF) patients [Sanchez-Martinez 2017].

#### 8.3.2.5 Non-invasive Electro-mechanical Personalisation

Chapter 6 and Chapter 7 are dealing with electro-mechanical personalisations. These coupled E/M studies are essential for revealing the final cardiac outcome by the evaluation the resulting cardiac movement. However Chapter 7 is not using any EP data and Chapter 6 is only using simpler EP markers. We encounter difficulties in gathering good quality data both in non-invasive EP measures and in cardiac motion images. This coupling would be a necessary validation to non-invasive EP personalisations. Moreover, it can also be a very promising pacing prediction perspective, improving the method of the Chapter 6 by using BSPM data.



# Electro-Mechanical Personalisation for Image Simulations

---

## Contents

---

<b>A.1 A Pipeline for the Generation of Realistic 3D Synthetic Echocardiographic Sequences: Methodology and Open-Access Database . . . . .</b>	<b>122</b>
<b>A.2 Generation of Ultra-realistic Synthetic Echocardiographic Sequences To Facilitate Standardization Of Deformation Imaging . . . . .</b>	<b>123</b>
<b>A.3 A Framework for the Generation of Realistic Synthetic Cardiac US and MRI Sequences from the same Virtual Patients . . . . .</b>	<b>124</b>

---

This PhD has also lead to other collaborations that are partly linked to the thesis subject. This first appendix collects the electro-mechanical personalisation applications to image simulations, leading to 3 papers. We are showing in the following sections the papers summaries and our contributions.

## A.1 A Pipeline for the Generation of Realistic 3D Synthetic Echocardiographic Sequences: Methodology and Open-Access Database

Based on a collaboration with Martino Alessandrini, we contributed to the following work leading to a paper accepted to the Transactions on Medical Imaging journal.

**A Pipeline for the Generation of Realistic 3D Synthetic Echocardiographic Sequences: Methodology and Open-Access Database**, *Martino Alessandrini, Mathieu De Craene, Olivier Bernard, Sophie Giffard-Roisin, Pascal Allain, Irina Waechter-Stehle, Jürgen Weese, Eric Saloux, Hervé Delingette, Maxime Sermesant and Jan D’Hooge* IEEE Transactions on Medical Imaging, 2015. [10.1109/TMI.2015.2396632](https://doi.org/10.1109/TMI.2015.2396632)

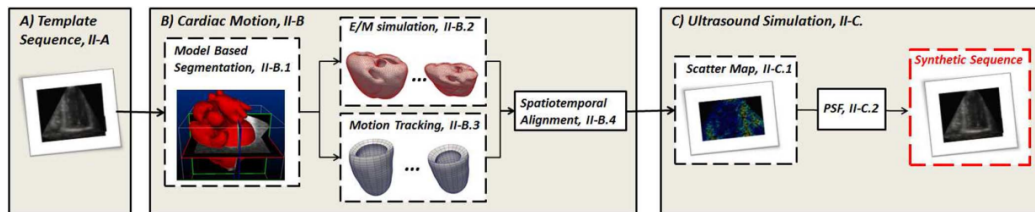


Figure A.1: Proposed pipeline for the simulation of ultra realistic cardiac ultrasound sequences: (A) a clinical recording works as a template for speckle texture and anatomy definition; (B) an electromechanical model controls the synthetic heart motion; (C) an ultrasound simulation environment merging information from the template image sequence and the electromechanical model accounts for the image formation process. In the simulated sequence the cardiac motion is fully controlled by the electromechanical model while the visual appearance is very similar to the one of a real acquisition.

**Abstract.** Quantification of cardiac deformation and strain with 3D ultrasound takes considerable research efforts. Nevertheless, a widespread use of these techniques in clinical practice is still held back due to the lack of a solid verification process to quantify and compare performance. In this context, the use of fully synthetic sequences has become an established tool for initial in silico evaluation. Nevertheless, the realism of existing simulation techniques is still too limited to represent reliable benchmarking data. Moreover, the fact that different centers typically make use of in-house developed simulation pipelines makes a fair comparison difficult. In this context, this paper introduces a novel pipeline for the generation of synthetic 3D cardiac ultrasound image sequences. State-of-the art solutions in the fields of electromechanical modeling and ultrasound simulation are combined within an original framework that exploits a real ultrasound recording to learn and simulate realistic speckle textures. The simulated images show typical artifacts that make motion tracking in ultrasound challenging. The ground-truth displacement

field is available voxelwise and is fully controlled by the electromechanical model. By progressively modifying mechanical and ultrasound parameters, the sensitivity of 3D strain algorithms to pathology and image properties can be evaluated. The proposed pipeline is used to generate an initial library of 8 sequences including healthy and pathological cases, which is made freely accessible to the research community via our project web-page.

**Personal contributions.** We collaborated with Martino Alssandrini in order to personalise human cardiac motions from real data imaging and then simulated different pathological conditions. We used the EM model presented in Chapter 7.

## A.2 Generation of Ultra-realistic Synthetic Echocardiographic Sequences To Facilitate Standardization Of Deformation Imaging

Based on a second collaboration with Martino Alessandrini, we contributed to the following work leading to a paper accepted to the International Symposium on Biomedical Imaging.

**Generation of Ultra-realistic Synthetic Echocardiographic Sequences to Facilitate Standardization of Deformation Imaging**, *Martino Alessandrini, and Brecht Heyde, Sophie Giffard-Roisin, Hervé Delingette, Maxime Sermesant, Pascal Allain, Olivier Bernard, Mathieu De Craene, Jan D’hooge*, 12th International Symposium on Biomedical Imaging (ISBI), 2015. 10.1109/ISBI.2015.7163982

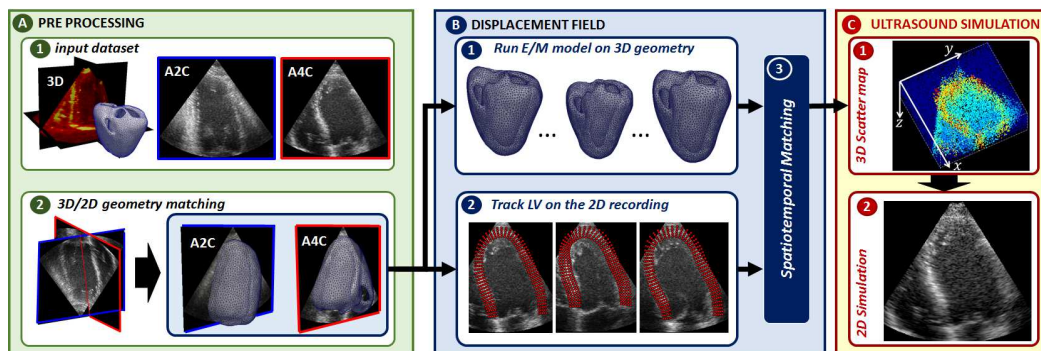


Figure A.2: Proposed simulation pipeline.

**Abstract.** Despite the overwhelming availability of techniques for computation of cardiac deformation and strain with 2D echocardiography, their widespread dissemination in clinical practice is still held back by the reported low reproducibility between different solutions. This can in part be attributed to the lack of a solid and open quality assurance framework to assess and compare their

performance. Building upon our previous work, we present here a new pipeline for the benchmarking of such algorithms making use of realistic 2D synthetic sequences. While the synthetic motion is fully controlled by a computational heart model, the visual appearance is extremely similar to a real ultrasound recording. The pipeline is used to generate an initial library of four sequences.

**Personal contributions.** As in section A.1, we collaborated with Martino Alessandrini in order to personalise human cardiac motions from real data imaging and then simulated different pathological conditions.

### A.3 A Framework for the Generation of Realistic Synthetic Cardiac US and MRI Sequences from the same Virtual Patients

Based on a collaboration with Yitian Zhou, we contributed to the following work leading to a paper accepted to the Transactions on Medical Imaging journal.

**A Framework for the Generation of Realistic Synthetic Cardiac Ultrasound and Magnetic Resonance Imaging Sequences from the same Virtual Patients**, *Yitian Zhou, Sophie Giffard-Roisin, Mathieu De Craene, Jan D’hooge, Martino Alessandrini, Denis Friboulet, Maxime Sermesant and Olivier Bernard*, IEEE Transactions on Medical Imaging, 2017. [10.1109/TMI.2017.2708159](https://doi.org/10.1109/TMI.2017.2708159)

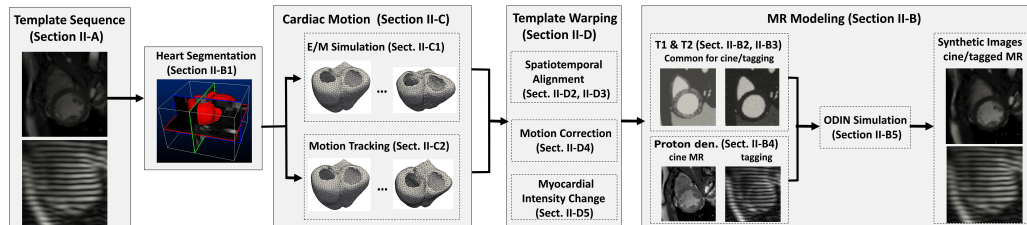


Figure A.3: Proposed pipeline for the simulation of realistic cardiac cine and tagged MR sequences.

**Abstract.** The use of synthetic sequences is one of the most promising tools for advanced in silico evaluation of the quantification of cardiac deformation and strain through 3D ultrasound (US) and magnetic resonance (MR) imaging. In this paper, we propose the first simulation framework which allows the generation of realistic 3D synthetic cardiac US and MR (both cine and tagging) image sequences from the same virtual patient. A state-of-the-art electromechanical (E/M) model was exploited for simulating groundtruth cardiac motion fields ranging from healthy to various pathological cases including both ventricular dyssynchrony and myocardial ischemia. The E/M groundtruth along with template MR/US images and physical

simulators were combined in a unified framework for generating synthetic data. We efficiently merged several warping strategies to keep full control of myocardial deformations while preserving realistic image texture. In total, we generated 18 virtual patients, each with synthetic 3D US, cine MR and tagged MR sequences. The simulated images were evaluated both qualitatively by showing realistic textures and quantitatively by observing myocardial intensity distributions similar to real data. In particular, the US simulation showed a smoother myocardium/background interface than the state-of-the-art. We also assessed the mechanical properties. The pathological subjects were discriminated from the healthy ones by both global indexes (ejection fraction and the global circumferential strain) and regional strain curves. The synthetic database is comprehensive in terms of both pathology and modality, and has a level of realism sufficient for validation purposes. All the 90 sequences are made publicly available to the research community via an open-access database.

**Personal contributions.** We worked with Yitian Zhou on the generation of a synthetic database composed of ultrasound and MRI sequences from the same virtual patients. In this work too we first personalise the EM cardiac model to some real cardiac images and then simulated realistic pathological motions.



# Applications of the Mitchell-Schaeffer Electrical Cardiac Model

---

## Contents

---

**B.1 Smoothed Particle Hydrodynamics for Electrocardiography Modeling: an Alternative to Finite Element Methods . 128**

**B.2 A Rule-Based Method to Model Myocardial Fiber Orientation for Simulating Ventricular Outflow Tract Arrhythmias 129**

---

This second appendix collects some applications of our Mitchell-Schaeffer electrical cardiac model. We are showing in the following sections the papers summaries and our contributions.

## B.1 Smoothed Particle Hydrodynamics for Electrocardiography Modeling: an Alternative to Finite Element Methods

Based on a collaboration with Èric Lluch Alvarez, we contributed to this work leading to a paper accepted to the functional imaging and modelling of the heart (FIMH) conference.

**Smoothed Particle Hydrodynamics for Electrophysiological Modeling: an Alternative to Finite Element Methods**, Èric Lluch Alvarez, Rubén Doste, Sophie Giffard-Roisin, Alexandre This, Maxime Sermesant, Oscar Camara, Mathieu De Craene and Hernán G. Morales, Functional imaging and modelling of the heart (FIMH) conference, 2017. [10.1007/978-3-319-59448-4\\_32](https://doi.org/10.1007/978-3-319-59448-4_32)

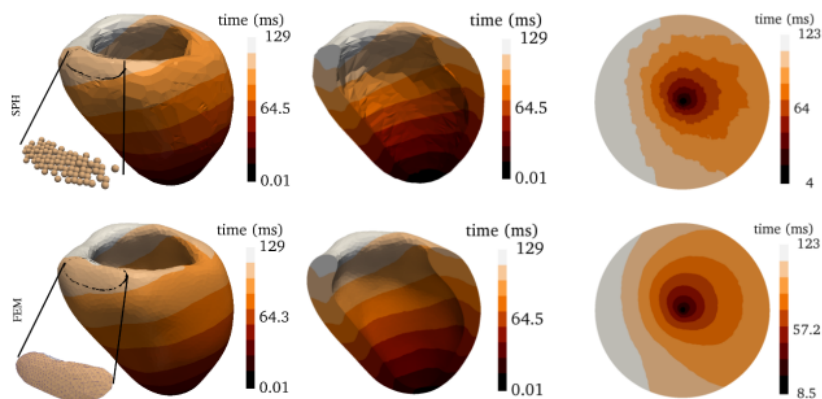


Figure B.1: Left: Contour color map of depolarization times for the left ventricle model. Middle: a longitudinal cross section of the ventricle. Right: projected endocardium onto a disk for both SPH and FEM simulations.

**Abstract.** Finite element methods (FEM) are generally used in cardiac 3D-electromechanical modeling. For FEM modeling, a step of a suitable mesh construction is required, which is non-trivial and time-consuming for complex geometries. A meshless method is proposed to avoid meshing. The smoothed particle hydrodynamics (SPH) method was used to solve an electrophysiological model on a left ventricle extracted from medical imaging straightforwardly, without any need of a complex mesh. The proposed method was compared against FEM in the same left-ventricular model. Both FEM and SPH methods provide similar solutions of the models in terms of depolarization times. Main differences were up to 10.9% at the apex. Finally, a pathological application of SPH is shown on the same ventricular geometry with an added scar on the heart wall.

**Personal contributions.** We collaborated here for a comparison of our finite

element method of the Mitchell-Schaeffer model to a new mesh-free model. After a pre-processing of the data, we simulated the electrical propagation for different conditions, where the depolarization times were compared to the proposed mesh-free computation.

## B.2 A Rule-Based Method to Model Myocardial Fiber Orientation for Simulating Ventricular Outflow Tract Arrhythmias

Based on a collaboration with Rubén Doste, we contributed to this work leading to a paper accepted to the functional imaging and modelling of the heart (FIMH) conference.

**A Rule-Based Method to Model Myocardial Fiber Orientation for Simulating Ventricular Outflow Tract Arrhythmias**, *Rubén Doste, David Soto-Iglesias, Gabriel Bernardino, Rafael Sebastian, Sophie Giffard-Roisin, Rocio Cabrera-Lozoya, Maxime Sermesant, Antonio Berruezo, Damián Sánchez-Quintana and Oscar Camara*, Functional imaging and modelling of the heart (FIMH) conference, 2017. [10.1007/978-3-319-59448-4\\_33](https://doi.org/10.1007/978-3-319-59448-4_33)

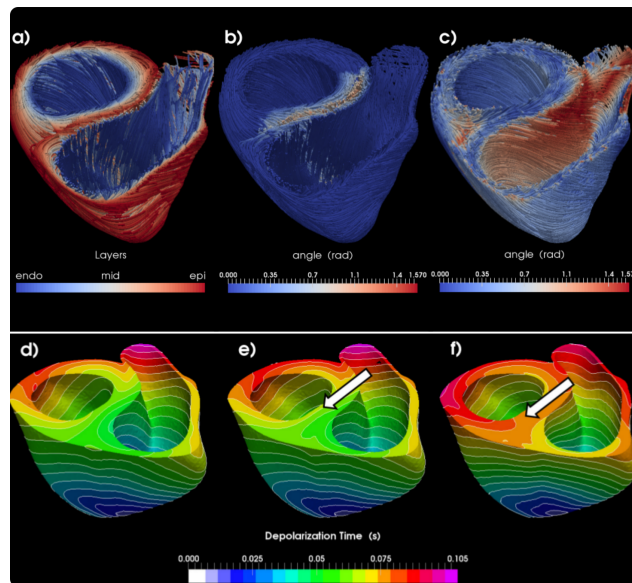


Figure B.2: Upper row:(a) Fiber orientation provided by the proposed RBM with a continuous septum; (b) angle differences (in radians) with fibers in a discontinuous septum; (c) and with Bayer RBM method. Lower row: Electrical activation isochrones (in seconds) provided by different models: the proposed RBM with a continuous (d) and discontinuous (e) septum; f) Bayer RBM. White arrows point towards the main differences found in the septal activation pattern.

**Abstract.** Myocardial fiber orientation determines the propagation of electrical waves in the heart and the contraction of cardiac tissue. One common approach for assigning fiber orientation to cardiac anatomical models are Rule-Based Methods (RBM). However, RBM have been developed to assimilate data mostly from the Left Ventricle. In consequence, fiber information from RBM does not match with histological data in other areas of the heart, having a negative impact in cardiac simulations beyond the LV. In this work, we present a RBM where fiber orientation is separately modeled in each ventricle following observations from histology. This allows to create detailed fiber orientation in specific regions such as the right ventricle endocardium, the interventricular septum and the outflow tracts. Electrophysiological simulations including these anatomical structures were then performed, with patient-specific data of outflow tract ventricular arrhythmias (OTVA) cases. A comparison between the obtained simulations and electro-anatomical data of these patients confirm the potential for in silico identification of the site of origin in OTVAs before the intervention.

**Personal contributions.** In this study, we provided the Mitchell-Schaeffer model and expertise in a cardiac fiber orientation study.

# Bibliography

- [Alessandrini 2015a] Martino Alessandrini, Mathieu De Craene, Olivier Bernard, Sophie Giffard-Roisin, Pascal Allain, Irina Waechter-Stehle, Jürgen Weese, Eric Saloux, Hervé Delingette, Maxime Sermesant and Jan D’hooge. *A pipeline for the generation of realistic 3D synthetic echocardiographic sequences: methodology and open-access database*. IEEE transactions on medical imaging, vol. 34, no. 7, pages 1436–1451, 2015. (Cited on page 5.)
- [Alessandrini 2015b] Martino Alessandrini, Brecht Heyde, Sophie Giffard-Roisin, Hervé Delingette, Maxime Sermesant, Pascal Allain, Olivier Bernard, Mathieu De Craene and Jan D’hooge. *Generation of ultra-realistic synthetic echocardiographic sequences to facilitate standardization of deformation imaging*. In Biomedical Imaging (ISBI), 2015 IEEE 12th International Symposium on, pages 756–759. IEEE, 2015. (Cited on page 5.)
- [Aliiev 1996] Rubin R Aliiev and Alexander V Panfilov. *A simple two-variable model of cardiac excitation*. Chaos, Solitons & Fractals, vol. 7, no. 3, pages 293–301, 1996. (Cited on page 13.)
- [Alioui 2011] Samir Alioui, Martim Kastelein, Eelco van Dam and Peter van Dam. *Automatic Registration of 3D Camera Recording to Model for Leads Localization*. In Computing in Cardiology, 2011, pages 741–744. IEEE, 2011. (Cited on page 117.)
- [Aras 2015] Kedar Aras, Wilson Good, Jess Tate, Brett Burton, Dana Brooks, Jaume Coll-Font, Olaf Doessel, Walther Schulze, Danila Potyagaylo, Linwei Wang et al. *Experimental Data and Geometric Analysis Repository EDGAR*. Journal of electrocardiology, vol. 48, no. 6, pages 975–981, 2015. (Cited on page 16.)
- [Bestel 2001] Julie Bestel, Frédérique Clément and Michel Sorine. *A biomechanical model of muscle contraction*. In International Conference on Medical Image Computing and Computer-Assisted Intervention, pages 1159–1161. Springer, 2001. (Cited on page 2.)
- [Bishop 2000] Christopher M Bishop and Michael E Tipping. *Variational relevance vector machines*. In Proceedings of the Sixteenth conference on Uncertainty in artificial intelligence, pages 46–53. Morgan Kaufmann Publishers Inc., 2000. (Cited on pages 22 and 68.)
- [Cabrera-Lozoya 2015] Rocío Cabrera-Lozoya. *Radiofrequency ablation planning for cardiac arrhythmia treatment using modeling and machine learning approaches*. PhD thesis, Université Nice Sophia Antipolis, 2015. (Cited on page 117.)

- [Cabrera-Lozoya 2017] Rocío Cabrera-Lozoya, Benjamin Berte, Hubert Cochet, Pierre Jaïs, Nicholas Ayache and Maxime Sermesant. *Image-based Biophysical Simulation of Intracardiac Abnormal Ventricular Electrograms*. IEEE Transactions on Biomedical Engineering, vol. 64, no. 7, pages 1446–1454, 2017. (Cited on page 17.)
- [Chapelle 2012] Dominique Chapelle, Patrick Le Tallec, Philippe Moireau and Michel Sorine. *Energy-preserving muscle tissue model: formulation and compatible discretizations*. International Journal for Multiscale Computational Engineering, vol. 10, no. 2, 2012. (Cited on pages 15, 104 and 107.)
- [Chávez 2015] Carlos Eduardo Chávez, Nejib Zenzemi, Yves Coudière, Felipe Alonso-Atienza and Diegó Alvarez. *Inverse problem of electrocardiography: Estimating the location of cardiac ischemia in a 3d realistic geometry*. In International Conference on Functional Imaging and Modeling of the Heart, pages 393–401. Springer, 2015. (Cited on pages 16, 27, 30 and 82.)
- [Chen 2016] Zhong Chen, Rocio Cabrera-Lozoya, Jatin Relan, Manav Sohal, Anoop Shetty, Rashed Karim, Hervé Delingette, Jaswinder Gill, Kawal Rhode, Nicholas Ayache, Maxime Sermesant and Reza Razavi. *Biophysical modeling predicts ventricular tachycardia inducibility and circuit morphology: a combined clinical validation and computer modeling approach*. Journal of cardiovascular electrophysiology, vol. 27, no. 7, pages 851–860, 2016. (Cited on page 28.)
- [Chen 2017a] Antong Chen, Tian Zhou, Sarayu Parimal, Belma Dogdas, Joseph Forbes, Smita Sampath, Ansuman Bagchi and Chih-Liang Chin. *Transfer learning for the fully automatic segmentation of left ventricle myocardium in porcine cardiac cine MR images*. In International Workshop on Statistical Atlases and Computational Models of the Heart (STACOM), held in conjunction with MICCAI. Springer, 2017. (Cited on page 119.)
- [Chen 2017b] Shuhang Chen, Prashna K Gyawali, Huafeng Liu, B Milan Horacek, John L Sapp and Linwei Wang. *Disentangling inter-subject variations: Automatic localization of ventricular tachycardia origin from 12-lead electrocardiograms*. In ISBI Conference, pages 616–619, 2017. (Cited on pages 18 and 59.)
- [Clifford 1990] Peter Clifford. *Markov random fields in statistics*. Disorder in physical systems: A volume in honour of John M. Hammersley, pages 19–32, 1990. (Cited on page 21.)
- [Coll-Font 2016a] Jaume Coll-Font. *Model Based Approaches to Incorporate Recordings of Multiple Heartbeats into the Inverse Problem of Electrocardiography*. PhD thesis, Northeastern University, 2016. (Cited on page 75.)

- [Coll-Font 2016b] Jaume Coll-Font, Jwala Dhamala, Danila Potyagaylo, Walther HW Schulze, Jess D Tate, Maria S Guillem, Peter Van Dam, Olaf Dossel, Dana H Brooks and Rob S Macleod. *The consortium for electrocardiographic imaging*. In Computing in Cardiology Conference (CinC), 2016, pages 325–328. IEEE, 2016. (Cited on page 16.)
- [Collin 2015] Annabelle Collin, Dominique Chapelle and Philippe Moireau. *Sequential State Estimation for Electrophysiology Models with Front Level-Set Data Using Topological Gradient Derivations*. In International Conference on Functional Imaging and Modeling of the Heart, pages 402–411. Springer, 2015. (Cited on pages 19 and 118.)
- [Dallet 2015] Corentin Dallet, Laura Bear, Josselin Duchateau, Mark Potse, Nejib Zemzemi, Valentin Meillet, Yves Coudière and Rémi Dubois. *Local conduction velocity mapping for electrocardiographic imaging*. In Computing in Cardiology Conference (CinC), 2015, pages 225–228. IEEE, 2015. (Cited on page 75.)
- [Dawoud 2016] Fady Dawoud, David D Spragg, Ronald D Berger, Alan Cheng, B Milan Horáček, Henry R Halperin and Albert C Lardo. *Non-invasive electromechanical activation imaging as a tool to study left ventricular dyssynchronous patients: implication for CRT therapy*. Journal of electrocardiology, vol. 49, no. 3, pages 375–382, 2016. (Cited on pages 16 and 28.)
- [Delingette 2004] Hervé Delingette and Nicholas Ayache. *Soft tissue modeling for surgery simulation*. Handbook of Numerical Analysis, vol. 12, pages 453–550, 2004. (Cited on page 31.)
- [Dhamala 2017a] Jwala Dhamala, Hermenegild Arevalo, John Sapp, Milan Horacek, Katherine Wu, Natalia Trayanova and Linwei Wang. *Spatially-Adaptive Multi-Scale Optimization for Local Parameter Estimation in Cardiac Electrophysiology*. IEEE Transactions on Medical Imaging, 2017. (Cited on pages 17, 21, 48 and 58.)
- [Dhamala 2017b] Jwala Dhamala, John L Sapp, Milan Horacek and Linwei Wang. *Quantifying the Uncertainty in Model Parameters Using Gaussian Process-Based Markov Chain Monte Carlo: An Application to Cardiac Electrophysiological Models*. In International Conference on Information Processing in Medical Imaging, pages 223–235. Springer, 2017. (Cited on pages 17, 21, 48 and 75.)
- [Doshi 2015] Ashish N Doshi, Richard D Walton, Sébastien P Krul, Joris R de Groot, Olivier Bernus, Igor R Efimov, Bastiaan J Boukens and Ruben Coronel. *Feasibility of a semi-automated method for cardiac conduction velocity analysis of high-resolution activation maps*. Computers in biology and medicine, vol. 65, pages 177–183, 2015. (Cited on page 75.)

- [Dössel 2000] O Dössel. *Inverse problem of electro-and magnetocardiography: Review and recent progress*. International Journal of Bioelectromagnetism, vol. 2, no. 2, 2000. (Cited on pages 16 and 27.)
- [Dössel 2011] Olaf Dössel, Martin W Krueger, Frank M Weber, Christopher Schilling, Walther HW Schulze and Gunnar Seemann. *A framework for personalization of computational models of the human atria*. In Engineering in Medicine and Biology Society, EMBC, 2011 Annual International Conference of the IEEE, pages 4324–4328. IEEE, 2011. (Cited on page 26.)
- [Doste 2017] Rubén Doste, David Soto-Iglesias, Gabriel Bernardino, Rafael Sebastian, Sophie Giffard-Roisin, Rocio Cabrera-Lozoya, Maxime Sermesant, Antonio Berruezo, Damián Sánchez-Quintana and Oscar Camara. *A Rule-Based Method to Model Myocardial Fiber Orientation for Simulating Ventricular Outflow Tract Arrhythmias*. Functional Imaging and Modelling of the Heart, page 344, 2017. (Cited on page 5.)
- [Dubois 2015] Rémi Dubois, Ashok J Shah, Mélèze Hocini, Arnaud Denis, Nicolas Derval, Hubert Cochet, Frédéric Sacher, Laura Bear, Josselin Duchateau, Pierre Jais and Michel Haissaguerre. *Non-invasive cardiac mapping in clinical practice: Application to the ablation of cardiac arrhythmias*. Journal of electrocardiology, vol. 48, no. 6, pages 966–974, 2015. (Cited on pages 16 and 28.)
- [Duchateau 2016] Nicolas Duchateau, Mathieu De Craene, Pascal Allain, Eric Saloux and Maxime Sermesant. *Infarct localization from myocardial deformation: prediction and uncertainty quantification by regression from a low-dimensional space*. IEEE Transactions on Medical Imaging, vol. 35, no. 10, pages 2340–2352, 2016. (Cited on page 65.)
- [Duchateau 2017] Josselin Duchateau, Mark Potse and Remi Dubois. *Spatially coherent activation maps for electrocardiographic imaging*. IEEE Transactions on Biomedical Engineering, vol. 64, no. 5, pages 1149–1156, 2017. (Cited on page 75.)
- [Durrer 1970] Dirk Durrer, R Th Van Dam, GE Freud, MJ Janse, FL Meijler and RC Arzbaecher. *Total excitation of the isolated human heart*. Circulation, vol. 41, no. 6, pages 899–912, 1970. (Cited on pages 8, 40, 80 and 83.)
- [Ferrer-Albero 2017] Ana Ferrer-Albero, Eduardo J Godoy, Miguel Lozano, Laura Martínez-Mateu, Felipe Atienza, Javier Saiz and Rafael Sebastian. *Non-invasive localization of atrial ectopic beats by using simulated body surface P-wave integral maps*. PloS one, vol. 12, no. 7, page e0181263, 2017. (Cited on page 117.)
- [FitzHugh 1961] Richard FitzHugh. *Impulses and physiological states in theoretical models of nerve membrane*. Biophysical journal, vol. 1, no. 6, pages 445–466, 1961. (Cited on pages 13 and 15.)

- [Ghosh 2009] Subham Ghosh and Yoram Rudy. *Application of L1-norm regularization to epicardial potential solution of the inverse electrocardiography problem*. *Annals of Biomedical Engineering*, vol. 37, no. 5, pages 902–912, 2009. (Cited on pages 16 and 27.)
- [Ghosh 2011] Subham Ghosh, Jennifer NA Silva, Russell M Canham, Tammy M Bowman, Junjie Zhang, Edward K Rhee, Pamela K Woodard and Yoram Rudy. *Electrophysiologic substrate and intraventricular left ventricular dyssynchrony in nonischemic heart failure patients undergoing cardiac resynchronization therapy*. *Heart Rhythm*, vol. 8, no. 5, pages 692–699, 2011. (Cited on pages 16 and 28.)
- [Giffard-Roisin 2014] Sophie Giffard-Roisin, Stéphanie Marchesseau, Loic Le Folgoc, Hervé Delingette and Maxime Sermesant. *Evaluation of Personalised Canine Electromechanical Models*. In *International Workshop on Statistical Atlases and Computational Models of the Heart*, pages 74–82. Springer, 2014. (Cited on pages 5 and 15.)
- [Giffard-Roisin 2016] Sophie Giffard-Roisin, Lauren Fovargue, Jessica Webb, Roch Molléro, Jack Lee, Hervé Delingette, Nicholas Ayache, Reza Razavi and Maxime Sermesant. *Estimation of Purkinje Activation from ECG: an Intermittent Left Bundle Branch Block Study*. In *International Workshop on Statistical Atlases and Computational Models of the Heart*, pages 135–142. Springer, 2016. (Cited on page 5.)
- [Giffard-Roisin 2017a] Sophie Giffard-Roisin, Hervé Delingette, Thomas Jackson, Lauren Fovargue, Jack Lee, Aldo Rinaldi, Nicholas Ayache, Reza Razavi and Maxime Sermesant. *Sparse Bayesian Non-linear Regression for Multiple Onsets Estimation in Non-invasive Cardiac Electrophysiology*. In *International Conference on Functional Imaging and Modeling of the Heart*, pages 230–238. Springer, 2017. (Cited on pages 5 and 116.)
- [Giffard-Roisin 2017b] Sophie Giffard-Roisin, Thomas Jackson, Lauren Fovargue, Jack Lee, Hervé Delingette, Reza Razavi, Nicholas Ayache and Maxime Sermesant. *Noninvasive Personalization of a Cardiac Electrophysiology Model From Body Surface Potential Mapping*. *IEEE Transactions on Biomedical Engineering*, vol. 64, no. 9, pages 2206–2218, 2017. (Cited on pages 4, 48, 58, 62 and 116.)
- [Groth 2012] A Groth, J Weese and H Lehmann. *Robust left ventricular myocardium segmentation for multi-protocol MR*. In *SPIE Medical Imaging*, page 83142S. International Society for Optics and Photonics, 2012. (Cited on pages 39 and 81.)
- [Han 2011] Chengzong Han, Steven M Pogwizd, Cheryl R Killingsworth and Bin He. *Noninvasive imaging of three-dimensional cardiac activation sequence*

- during pacing and ventricular tachycardia. *Heart Rhythm*, vol. 8, no. 8, pages 1266–1272, 2011. (Cited on pages 16 and 27.)
- [Han 2013] Chengzong Han, Steven M Pogwizd, Cheryl R Killingsworth, Zhaoye Zhou and Bin He. *Noninvasive cardiac activation imaging of ventricular arrhythmias during drug-induced QT prolongation in the rabbit heart*. *Heart Rhythm*, vol. 10, no. 10, pages 1509–1515, 2013. (Cited on pages 16 and 27.)
- [Han 2015] Chengzong Han, Steven M Pogwizd, Long Yu, Zhaoye Zhou, Cheryl R Killingsworth and Bin He. *Imaging cardiac activation sequence during ventricular tachycardia in a canine model of nonischemic heart failure*. *American Journal of Physiology-Heart and Circulatory Physiology*, vol. 308, no. 2, pages H108–H114, 2015. (Cited on pages 16 and 27.)
- [Hansen 2006] Nikolaus Hansen. *The CMA evolution strategy: a comparing review*. *Towards a new evolutionary computation*, pages 75–102, 2006. (Cited on pages 19 and 82.)
- [He 2002] Bin He, Guanglin Li and Xin Zhang. *Noninvasive three-dimensional activation time imaging of ventricular excitation by means of a heart-excitation model*. *Physics in medicine and biology*, vol. 47, no. 22, page 4063, 2002. (Cited on pages 16, 28 and 52.)
- [Heimann 2014] Tobias Heimann, Peter Mountney, Matthias John and Razvan Ionasec. *Real-time ultrasound transducer localization in fluoroscopy images by transfer learning from synthetic training data*. *Medical image analysis*, vol. 18, no. 8, pages 1320–1328, 2014. (Cited on page 118.)
- [Hoekema 1999] R Hoekema, GJH Uijen, L Van Erning and A Van Oosterom. *Interindividual variability of multilead electrocardiographic recordings: influence of heart position*. *Journal of electrocardiology*, vol. 32, no. 2, pages 137–148, 1999. (Cited on pages 17, 18 and 59.)
- [Huiskamp 1988] Geertjan Huiskamp and Adriaan Van Oosterom. *The depolarization sequence of the human heart surface computed from measured body surface potentials*. *Biomedical Engineering, IEEE Transactions on*, vol. 35, no. 12, pages 1047–1058, 1988. (Cited on pages 16 and 27.)
- [Huiskamp 1989] Geertjan Huiskamp and Adriaan van Oosterom. *Tailored versus realistic geometry in the inverse problem of electrocardiography*. *IEEE Transactions on Biomedical Engineering*, vol. 36, no. 8, pages 827–835, 1989. (Cited on pages 18, 59 and 62.)
- [Jiang 2009] Yuan Jiang, D Farina and Olaf Dössel. *Localization of the origin of ventricular premature beats by reconstruction of electrical sources using spatio-temporal MAP-based regularization*. In *4th European Conference of the International Federation for Medical and Biological Engineering*, pages 2511–2514. Springer, 2009. (Cited on pages 16 and 27.)

- [Julier 1997] Simon J Julier and Jeffrey K Uhlmann. *A new extension of the Kalman filter to nonlinear systems*. In Int. symp. aerospace/defense sensing, simul. and controls, volume 3, pages 182–193. Orlando, FL, 1997. (Cited on pages 18 and 108.)
- [Keener 1991] James P Keener. *The effects of discrete gap junction coupling on propagation in myocardium*. Journal of theoretical biology, vol. 148, no. 1, pages 49–82, 1991. (Cited on page 13.)
- [Keller 2010] David UJ Keller, Frank M Weber, Gunnar Seemann and Olaf Dössel. *Ranking the influence of tissue conductivities on forward-calculated ECGs*. IEEE Transactions on Biomedical Engineering, vol. 57, no. 7, pages 1568–1576, 2010. (Cited on pages 16 and 27.)
- [Konukoglu 2011] Ender Konukoglu, Jatin Relan, Ulas Cilingir, Bjoern H Menze, Phani Chinchapatnam, Amir Jadidi, Hubert Cochet, Meleze Hocini, Hervé Delingette, Pierre Jaïs, Michel Haissaguerre, Nicholas Ayache and Maxime Sermesant. *Efficient probabilistic model personalization integrating uncertainty on data and parameters: Application to eikonal-diffusion models in cardiac electrophysiology*. Progress in biophysics and molecular biology, vol. 107, no. 1, pages 134–146, 2011. (Cited on pages 17, 21, 26 and 27.)
- [Kybic 2005] Jan Kybic, Maureen Clerc, Touffic Abboud, Olivier Faugeras, Renaud Keriven and Théodore Papadopoulos. *A common formalism for the integral formulations of the forward EEG problem*. IEEE transactions on medical imaging, vol. 24, no. 1, pages 12–28, 2005. (Cited on page 31.)
- [Le Folgoc 2017] Loïc Le Folgoc, Hervé Delingette, Antonio Criminisi and Nicholas Ayache. *Sparse Bayesian registration of medical images for self-tuning of parameters and spatially adaptive parametrization of displacements*. Medical image analysis, vol. 36, pages 79–97, 2017. (Cited on pages 22 and 55.)
- [Lenkova 2012] Jana Lenkova, Jana Svehlikova and Milan Tysler. *Individualized model of torso surface for the inverse problem of electrocardiology*. Journal of electrocardiology, vol. 45, no. 3, pages 231–236, 2012. (Cited on pages 18 and 59.)
- [Li 2001] Guanglin Li and Bin He. *Localization of the site of origin of cardiac activation by means of a heart-model-based electrocardiographic imaging approach*. IEEE transactions on biomedical engineering, vol. 48, no. 6, pages 660–669, 2001. (Cited on pages 16, 27 and 58.)
- [Liu 2006] Zhongming Liu, Chenguang Liu and Bin He. *Noninvasive reconstruction of 3D ventricular activation sequence from the inverse solution of distributed equivalent current density*. IEEE transactions on medical imaging, vol. 25, no. 10, pages 1307–1318, 2006. (Cited on pages 16 and 27.)

- [Liu 2008] Chenguang Liu, Nicholas D Skadsberg, Sarah E Ahlberg, Cory M Swingen, Paul A Iaizzo and Bin He. *Estimation of Global Ventricular Activation Sequences by Noninvasive Three-Dimensional Electrical Imaging: Validation Studies in a Swine Model During Pacing*. Journal of cardiovascular electrophysiology, vol. 19, no. 5, pages 535–540, 2008. (Cited on pages 16, 28 and 58.)
- [Liu 2012] Chenguang Liu, Michael D Eggen, Cory M Swingen, Paul A Iaizzo and Bin He. *Noninvasive mapping of transmural potentials during activation in swine hearts from body surface electrocardiograms*. IEEE transactions on medical imaging, vol. 31, no. 9, pages 1777–1785, 2012. (Cited on pages 16 and 28.)
- [Lluch Alvarez 2017] Èric Lluch Alvarez, Rubén Doste, Sophie Giffard-Roisin, Alexandre This, Maxime Sermesant, Oscar Camara, Mathieu De Craene and Hernán G Morales. *Smoothed particle hydrodynamics for electrophysiological modeling: an alternative to finite element methods*. In Pop M, Wright GA, editors. Functional imaging and modelling of the heart. 9th International Conference, FIMH 2017; 2017 Jun 11-13; Toronto, Canada.[place unknown]: Springer; 2017. p. 333-43. Springer, 2017. (Cited on page 5.)
- [Loewe 2011] Axel Loewe, Walther HW Schulze, Yuan Jiang, Mathias Wilhelms and Olaf Dössel. *Determination of optimal electrode positions of a wearable ECG monitoring system for detection of myocardial ischemia: a simulation study*. In Computing in Cardiology, 2011, pages 741–744. IEEE, 2011. (Cited on page 117.)
- [Lorange 1993] Michel Lorange and Ramesh M Gulrajani. *A computer heart model incorporating anisotropic propagation: I. Model construction and simulation of normal activation*. Journal of electrocardiology, vol. 26, no. 4, pages 245–261, 1993. (Cited on page 80.)
- [Malmivuo 1995] Jaakko Malmivuo and Robert Plonsey. *Bioelectromagnetism: principles and applications of bioelectric and biomagnetic fields*. Oxford university press, 1995. (Cited on pages 30 and 62.)
- [Marchesseau 2013] Stéphanie Marchesseau, Hervé Delingette, Maxime Sermesant and Nicholas Ayache. *Fast parameter calibration of a cardiac electromechanical model from medical images based on the unscented transform*. Biomechanics and modeling in mechanobiology, pages 1–17, 2013. (Cited on pages 15, 105, 107 and 108.)
- [Messnarz 2004] Bernd Messnarz, Bernhard Tilg, Robert Modre, Gerald Fischer and Friedrich Hanser. *A new spatiotemporal regularization approach for reconstruction of cardiac transmembrane potential patterns*. IEEE transactions on Biomedical Engineering, vol. 51, no. 2, pages 273–281, 2004. (Cited on pages 16 and 27.)

- [Mitchell 2003] Colleen C Mitchell and David G Schaeffer. *A two-current model for the dynamics of cardiac membrane*. Bulletin of mathematical biology, vol. 65, no. 5, pages 767–793, 2003. (Cited on pages 13, 14, 26, 30, 64 and 82.)
- [Molléro 2016] Roch Molléro, Xavier Pennec, Hervé Delingette, Nicholas Ayache and Maxime Sermesant. *A multiscale cardiac model for fast personalisation and exploitation*. In International Conference on Medical Image Computing and Computer-Assisted Intervention, pages 174–182. Springer, 2016. (Cited on page 19.)
- [Odille 2017] Freddy Odille, Shufang Liu, Peter van Dam and Jacques Felblinger. *Statistical Variations of Heart Orientation in Healthy Adults*. In Computing in Cardiology Conference, Rennes. IEEE, 2017. (Cited on page 74.)
- [Oster 1992] Howard S Oster and Yoram Rudy. *The use of temporal information in the regularization of the inverse problem of electrocardiography*. Biomedical Engineering, IEEE Transactions on, vol. 39, no. 1, pages 65–75, 1992. (Cited on pages 16 and 27.)
- [Pollard 2003] Andrew E Pollard. *From myocardial cell models to action potential propagation*. Journal of electrocardiology, vol. 36, pages 43–49, 2003. (Cited on pages 2 and 26.)
- [Potse 2006] Mark Potse, Bruno Dubé, Jacques Richer, Alain Vinet and Ramesh M Gulrajani. *A comparison of monodomain and bidomain reaction-diffusion models for action potential propagation in the human heart*. IEEE Transactions on Biomedical Engineering, vol. 53, no. 12, pages 2425–2435, 2006. (Cited on page 30.)
- [Potse 2012] Mark Potse, Dorian Krause, Ljuba Bacharova, Rolf Krause, Frits W Prinzen and Angelo Auricchio. *Similarities and differences between electrocardiogram signs of left bundle-branch block and left-ventricular uncoupling*. Europace, vol. 14, no. suppl\_5, pages v33–v39, 2012. (Cited on page 80.)
- [Potyagaylo 2016] Danila Potyagaylo, Olaf Dössel and Peter van Dam. *Influence of modeling errors on the initial estimate for nonlinear myocardial activation times imaging calculated with fastest route algorithm*. IEEE Transactions on Biomedical Engineering, vol. 63, no. 12, pages 2576–2584, 2016. (Cited on page 117.)
- [Prakosa 2014] Adityo Prakosa, Maxime Sermesant, Pascal Allain, Nicolas Villain, C Aldo Rinaldi, Kawal Rhode, Reza Razavi, Hervé Delingette and Nicholas Ayache. *Cardiac electrophysiological activation pattern estimation from images using a patient-specific database of synthetic image sequences*. IEEE Transactions on Biomedical Engineering, vol. 61, no. 2, pages 235–245, 2014. (Cited on page 17.)

- [Pullan 2010] Andrew J Pullan. *The inverse problem of electrocardiography*. In Comprehensive Electrocardiology, pages 299–344. Springer London, 2010. (Cited on pages 2, 16, 27 and 58.)
- [Rahimi 2015] Azar Rahimi and Linwei Wang. *Sensitivity of noninvasive cardiac electrophysiological imaging to variations in personalized anatomical modeling*. IEEE Transactions on Biomedical Engineering, vol. 62, no. 6, pages 1563–1575, 2015. (Cited on pages 18 and 59.)
- [Rahimi 2016] Azar Rahimi, John Sapp, Jingjia Xu, Peter Bajorski, Milan Horacek and Linwei Wang. *Examining the impact of prior models in transmural electrophysiological imaging: A hierarchical multiple-model bayesian approach*. IEEE transactions on medical imaging, vol. 35, no. 1, pages 229–243, 2016. (Cited on pages 16, 27 and 58.)
- [Ramanathan 2001] Charulatha Ramanathan and Yoram Rudy. *Electrocardiographic imaging: Effect of torso inhomogeneities on noninvasive reconstruction of epicardial potentials, electrograms, and isochrones*. Journal of cardiovascular electrophysiology, vol. 12, no. 2, pages 241–252, 2001. (Cited on pages 16 and 27.)
- [Ramanathan 2003] Charulatha Ramanathan, Ping Jia, Raja Ghanem, Daniela Calvetti and Yoram Rudy. *Noninvasive electrocardiographic imaging (ECGI): application of the generalized minimal residual (GMRes) method*. Annals of biomedical engineering, vol. 31, no. 8, pages 981–994, 2003. (Cited on pages 16, 28, 39 and 71.)
- [Relan 2011a] Jatin Relan, Phani Chinchapatnam, Maxime Sermesant, Kawal Rhode, Matt Ginks, Hervé Delingette, C Aldo Rinaldi, Reza Razavi and Nicholas Ayache. *Coupled personalization of cardiac electrophysiology models for prediction of ischaemic ventricular tachycardia*. Interface Focus, vol. 1, no. 3, pages 396–407, 2011. (Cited on pages 17 and 26.)
- [Relan 2011b] Jatin Relan, Mihaela Pop, Hervé Delingette, Graham A Wright, Nicholas Ayache and Maxime Sermesant. *Personalization of a cardiac electrophysiology model using optical mapping and MRI for prediction of changes with pacing*. IEEE Transactions on Biomedical Engineering, vol. 58, no. 12, pages 3339–3349, 2011. (Cited on pages 17 and 26.)
- [Reuter 2005] Martin Reuter, Franz-Erich Wolter and Niklas Peinecke. *Laplace-spectra as fingerprints for shape matching*. In Proceedings of the 2005 ACM symposium on Solid and physical modeling, pages 101–106. ACM, 2005. (Cited on pages 49 and 66.)
- [Robert 2004] Christian P Robert. Monte carlo methods. Wiley Online Library, 2004. (Cited on page 21.)

- [Rodrigo 2017] Miguel Rodrigo, Andreu M Climent, Alejandro Liberos, Ismael Hernandez-Romero, Angel Arenal, Javier Bermejo, Francisco Fernandez-Aviles, Felipe Atienza and Maria S Guillem. *Solving inaccuracies in the heart position and orientation for inverse solution by using electric information*. In Computing in Cardiology Conference, Rennes. IEEE, 2017. (Cited on page 75.)
- [Sanchez-Martinez 2017] Sergio Sanchez-Martinez, Nicolas Duchateau, Tamas Erdei, Alan G Fraser, Bart H Bijnens and Gemma Piella. *Characterization of myocardial motion patterns by unsupervised multiple kernel learning*. Medical image analysis, vol. 35, pages 70–82, 2017. (Cited on page 119.)
- [Schenone 2014] Elisa Schenone. *Reduced order models, forward and inverse problems in cardiac electrophysiology*. PhD thesis, Université Pierre et Marie Curie-Paris VI, 2014. (Cited on pages 76 and 117.)
- [Schulze 2015] W. H. W. Schulze. *ECG imaging of ventricular activity in clinical applications*. PhD thesis, Karlsruhe, 2015. (Cited on pages 36 and 37.)
- [Sermesant 2006] Maxime Sermesant, Hervé Delingette and Nicholas Ayache. *An electromechanical model of the heart for image analysis and simulation*. IEEE transactions on medical imaging, vol. 25, no. 5, pages 612–625, 2006. (Cited on page 15.)
- [Sermesant 2007] Maxime Sermesant, Ender Konukoglu, Hervé Delingette, Yves Coudière, Phani Chinchapatnam, Kawal S Rhode, Reza Razavi and Nicholas Ayache. *An anisotropic multi-front fast marching method for real-time simulation of cardiac electrophysiology*. In International Conference on Functional Imaging and Modeling of the Heart, pages 160–169. Springer, 2007. (Cited on pages 104 and 106.)
- [Sermesant 2012] Maxime Sermesant, Radomir Chabiniok, Phani Chinchapatnam, Tommaso Mansi, Florence Billet, Philippe Moireau, Jean-Marc Peyrat, K Wong, Jatin Relan, Kawal Rhode, M. Ginks, P. Lambiase, H. Delingette, M. Sorine, C.A. Rinaldi, D. Chapelle, R. Razavi and N. Ayache. *Patient-specific electromechanical models of the heart for the prediction of pacing acute effects in CRT: a preliminary clinical validation*. Medical image analysis, vol. 16, no. 1, pages 201–215, 2012. (Cited on pages 2, 15, 26 and 58.)
- [Soto-Iglesias 2016] David Soto-Iglesias, Constantine Butakoff, David Andreu, Juan Fernández-Armenta, Antonio Berruezo and Oscar Camara. *Integration of electro-anatomical and imaging data of the left ventricle: an evaluation framework*. Medical image analysis, vol. 32, pages 131–144, 2016. (Cited on pages 53 and 71.)
- [Strumpf 1990] RK Strumpf, FCP Yin and JD Humphrey. *Determination of a constitutive relation for passive myocardium: I. A new functional form*.

- Journal of biomechanical engineering, vol. 112, page 333, 1990. (Cited on page 2.)
- [Sutton 2003] Martin G St John Sutton, Ted Plappert, William T Abraham, Andrew L Smith, David B DeLurgio, Angel R Leon, Evan Loh, Dusan Z Kocovic, Westby G Fisher, Myrvin Ellestad *et al.* *Effect of cardiac resynchronization therapy on left ventricular size and function in chronic heart failure*. *Circulation*, vol. 107, no. 15, pages 1985–1990, 2003. (Cited on pages 1 and 26.)
- [Swenson 2011] Darrell J Swenson, Sarah E Geneser, Jeroen G Stinstra, Robert M Kirby and Rob S MacLeod. *Cardiac position sensitivity study in the electrocardiographic forward problem using stochastic collocation and boundary element methods*. *Annals of biomedical engineering*, vol. 39, no. 12, page 2900, 2011. (Cited on pages 45 and 59.)
- [Talbot 2012] Hugo Talbot, Christian Duriez, Hadrien Courtecuisse, Jatin Relan, Maxime Sermesant, Stéphane Cotin and Hervé Delingette. *Towards real-time computation of cardiac electrophysiology for training simulator*. In *International Workshop on Statistical Atlases and Computational Models of the Heart*, pages 298–306. Springer, 2012. (Cited on page 31.)
- [Talbot 2013] Hugo Talbot, Stéphanie Marchesseau, Christian Duriez, Maxime Sermesant, Stéphane Cotin and Hervé Delingette. *Towards an interactive electromechanical model of the heart*. *Interface focus*, vol. 3, no. 2, page 20120091, 2013. (Cited on pages 13 and 15.)
- [Talbot 2015] Hugo Talbot, Stéphane Cotin, Reza Razavi, Christopher Rinaldi and Hervé Delingette. *Personalization of cardiac electrophysiology model using the unscented Kalman filtering*. In *Computer Assisted Radiology and Surgery (CARS 2015)*, 2015. (Cited on page 19.)
- [Ten Tusscher 2004] KHWJ Ten Tusscher, D Noble, PJ Noble and Alexander V Panfilov. *A model for human ventricular tissue*. *American Journal of Physiology-Heart and Circulatory Physiology*, vol. 286, no. 4, pages H1573–H1589, 2004. (Cited on page 13.)
- [Tereshchenko 2011] Larisa G Tereshchenko, Alan Cheng, Barry J Fetters, Barbara Butcher, Joseph E Marine, David D Spragg, Sunil Sinha, Darshan Dalal, Hugh Calkins, Gordon F Tomaselli and Ronald D Berger. *A new electrocardiogram marker to identify patients at low risk for ventricular tachyarrhythmias: sum magnitude of the absolute QRST integral*. *Journal of electrocardiology*, vol. 44, no. 2, pages 208–216, 2011. (Cited on page 33.)
- [Tipping 2003] Michael E Tipping, Anita C Faulstich *et al.* *Fast marginal likelihood maximisation for sparse Bayesian models*. In *AISTATS*, 2003. (Cited on pages 21, 51 and 66.)

- [Umeyama 1988] Shinji Umeyama. *An eigendecomposition approach to weighted graph matching problems*. IEEE transactions on pattern analysis and machine intelligence, vol. 10, no. 5, pages 695–703, 1988. (Cited on pages 49 and 66.)
- [Van Dam 2009] Peter M Van Dam, Thom F Oostendorp, André C Linnenbank and Adriaan Van Oosterom. *Non-invasive imaging of cardiac activation and recovery*. Annals of biomedical engineering, vol. 37, no. 9, pages 1739–1756, 2009. (Cited on page 16.)
- [van Dam 2013] Peter M van Dam, Roderick Tung, Kalyanam Shivkumar and Michael Laks. *Quantitative localization of premature ventricular contractions using myocardial activation ECGI from the standard 12-lead electrocardiogram*. Journal of electrocardiology, vol. 46, no. 6, pages 574–579, 2013. (Cited on pages 16 and 88.)
- [Varma 2007] Niraj Varma, Ping Jia and Yoram Rudy. *Electrocardiographic imaging of patients with heart failure with left bundle branch block and response to cardiac resynchronization therapy*. Journal of electrocardiology, vol. 40, no. 6, pages S174–S178, 2007. (Cited on pages 16 and 28.)
- [Wallman 2014] Mikael Wallman, Nicolas P Smith and Blanca Rodriguez. *Computational methods to reduce uncertainty in the estimation of cardiac conduction properties from electroanatomical recordings*. Medical image analysis, vol. 18, no. 1, pages 228–240, 2014. (Cited on pages 17, 21, 26 and 27.)
- [Wang 2010] Linwei Wang, Ken C. L. Wong, Heye Zhang, Huafeng Liu and Pengcheng Shi. *How Much Geometrical Detail Do We Need in Cardiac Electrophysiological Imaging? A Generic Heart-Torso Representation for Fast Subject-Specific Customization*. In STACOM Workshop, held in Conjunction with MICCAI Conference, pages 232–241, 2010. (Cited on pages 18 and 59.)
- [Wang 2011] Linwei Wang, Ken CL Wong, Heye Zhang, Huafeng Liu and Pengcheng Shi. *Noninvasive computational imaging of cardiac electrophysiology for 3-D infarct*. IEEE Transactions on Biomedical Engineering, vol. 58, no. 4, pages 1033–1043, 2011. (Cited on pages 16, 19, 27 and 58.)
- [Wiener 1938] Norbert Wiener. *The homogeneous chaos*. American Journal of Mathematics, vol. 60, no. 4, pages 897–936, 1938. (Cited on page 21.)
- [Yu 2015] Long Yu, Zhaoye Zhou and Bin He. *Temporal sparse promoting three dimensional imaging of cardiac activation*. IEEE transactions on medical imaging, vol. 34, no. 11, pages 2309–2319, 2015. (Cited on pages 16 and 27.)
- [Zettinig 2014] Oliver Zettinig, Tommaso Mansi, Dominik Neumann, Bogdan Georgescu, Saikiran Rapaka, Philipp Seegerer, Elham Kayvanpour, Farbod Sedaghat-Hamedani, Ali Amr, Jan Haas, Henning Steen, Hugo Katus, Benjamin Meder, Nassir Navab, Ali Kamen and Dorin Comaniciu. *Data-driven*

- estimation of cardiac electrical diffusivity from 12-lead ECG signals*. Medical image analysis, vol. 18, no. 8, pages 1361–1376, 2014. (Cited on pages 17, 20, 21, 26, 27 and 80.)
- [Zhang 2005] Xin Zhang, Indiresha Ramachandra, Zhongming Liu, Basharat Muneer, Steven M Pogwizd and Bin He. *Noninvasive three-dimensional electrocardiographic imaging of ventricular activation sequence*. American Journal of Physiology-Heart and Circulatory Physiology, vol. 289, no. 6, pages H2724–H2732, 2005. (Cited on pages 16 and 28.)
- [Zhou 2017] Yitian Zhou, Sophie Giffard-Roisin, Mathieu De Craene, Jan D’hooge, Martino Alessandrini, Denis Friboulet, Maxime Sermesant and Olivier Bernard. *A Framework for the Generation of Realistic Synthetic Cardiac Ultrasound and Magnetic Resonance Imaging Sequences from the same Virtual Patients*. IEEE Transactions on Medical Imaging, 2017. (Cited on page 5.)

---

## Non-invasive Personalisation of Cardiac Electrophysiological Models from Surface Electrograms

### Abstract:

The objective of this thesis is to use non-invasive data (body surface potential mapping, BSPM) to personalise the main parameters of a cardiac electrophysiological (EP) model for predicting the response to cardiac resynchronization therapy (CRT). CRT is a clinically proven treatment option for some heart failures. However, these therapies are ineffective in 30% of the treated patients and involve significant morbidity and substantial cost. The precise understanding of the patient-specific cardiac function can help to predict the response to therapy. Until now, such methods required to measure intra-cardiac electrical potentials through an invasive endovascular procedure which can be at risk for the patient.

We developed a non-invasive EP model personalisation based on a patient-specific simulated database and machine learning regressions. First, we estimated the onset activation location and a global conduction parameter. We extended this approach to multiple onsets and to ischemic patients by means of a sparse Bayesian regression. Moreover, we developed a reference ventricle-torso anatomy in order to perform a common offline regression and we predicted the response to different pacing conditions from the personalised model. In a second part, we studied the adaptation of the proposed method to the input of 12-lead electrocardiograms (ECG) and the integration in an electro-mechanical model for a clinical use. The evaluation of our work was performed on an important dataset (more than 25 patients and 150 cardiac cycles). Besides having comparable results with state-of-the-art ECG imaging methods, the predicted BSPMs show good correlation coefficients with the real BSPMs.

**Keywords:** ECG Imaging, Personalisation, Cardiac Electrophysiology Model, Machine learning, Simulated database, Inverse problem.

---